University of Denver

Digital Commons @ DU

2023

Identifying the Role of Phospholipase D1 and Phosphatidic Acid in Exocytosis

Broderick L. Bills

Identifying the Role of Phospholipase D1 and Phosphatidic Acid in Exocytosis

Abstract

Exocytosis is an essential process for intercellular communication in eukaryotic cells. This process involves significant changes in membrane curvature, and lipids and curvature-sensing proteins can assist these processes. One protein in particular, phospholipase D1 (PLD1), and its product, the lipid phosphatidic acid (PA), are involved in multiple exocytic processes. However, PLD1 and PA's role in this process has remained unclear. In this work, PLD1 and the production of PA were visualized during exocytosis, and PA localization to regions of membrane curvature was established. Together, these results support the hypothesis that PLD1 production of PA stabilizes negative curvature during membrane fusion.

We demonstrate the localization of PLD1 to multiple exocytic proteins during different forms of exocytosis. We investigate PLD1 localization to secretory exocytic machinery and cargo; using a pH-sensitive probe for secretory vesicles in PC12 cells, we observe this localization to sites of exocytosis. PLD1 is present on secretory vesicles throughout the process from trafficking, to docking and finally to fusion. A fluorescently tagged PA binding protein, PASS, was then used to visualize the change of PA localization or production during this process. With PLD inhibitors we identify that PLD1 specifically produces PA after vesicles dock and during fusion.

In parallel, PLD1 was observed during exosome secretion from multivesicular endosomes (MVEs) in A549 cells. PLD1 localizes to late endosomes, especially MVEs. PLD1 is also present on MVEs during the entire process, but it is only required to produce PA on docking MVEs. PLD1 inhibition also increases the density of lysosomes near the surface, indicating a role in late endosome fate.

Finally, to understand why PA is essential in these processes, we explored PA accumulation to curvature *in vitro.* A tubulated supported lipid bilayer assay was developed to identify curvature preference of lipids. PA was found to stabilize the formation of these regions of curvature and to localize to the inner, negatively curved leaflet of liposomes.

Document Type

Dissertation

Degree Name

Ph.D.

First Advisor

Michelle K. Knowles

Second Advisor

Schuyler van Engelenburg

Third Advisor

Yan Qin

Keywords

Exocytosis, Membranes, Multivesicular endosomes, Phosphatidic acid, Phospholipase D, Supported lipid bilayers

Subject Categories

Biochemistry, Biophysics, and Structural Biology | Biophysics | Cell and Developmental Biology | Cell Biology | Life Sciences | Molecular Biology

Publication Statement

Identifying the Role of Phospholipase D1 and Phosphatidic Acid in Exocytosis

_____

A Dissertation

Presented to

the Faculty of the College of Natural Sciences and Mathematics

University of Denver

_____

In Partial Fulfillment

of the Requirements for the Degree

Doctor of Philosophy

_____

by

Broderick L. Bills

August 2023

Advisor: Michelle K. Knowles, PhD

Author: Broderick L. Bills
Title: Identifying the Role of Phospholipase D1 and Phosphatidic Acid in Exocytosis
Advisor: Michelle K. Knowles, PhD
Degree Date: August 2023

Abstract

Exocytosis is an essential process for intercellular communication in eukaryotic cells. This process involves significant changes in membrane curvature, and lipids and curvature-sensing proteins can assist these processes. One protein in particular, phospholipase D1 (PLD1), and its product, the lipid phosphatidic acid (PA), are involved in multiple exocytic processes. However, PLD1 and PA's role in this process has remained unclear. In this work, PLD1 and the production of PA were visualized during exocytosis, and PA localization to regions of membrane curvature was established. Together, these results support the hypothesis that PLD1 production of PA stabilizes negative curvature during membrane fusion.

We demonstrate the localization of PLD1 to multiple exocytic proteins during different forms of exocytosis. We investigate PLD1 localization to secretory exocytic machinery and cargo; using a pH-sensitive probe for secretory vesicles in PC12 cells, we observe this localization to sites of exocytosis. PLD1 is present on secretory vesicles throughout the process from trafficking, to docking and finally to fusion. A fluorescently tagged PA binding protein, PASS, was then used to visualize the change of PA localization or production during this process. With PLD inhibitors we identify that PLD1 specifically produces PA after vesicles dock and during fusion.

In parallel, PLD1 was observed during exosome secretion from multivesicular endosomes (MVEs) in A549 cells. PLD1 localizes to late endosomes, especially MVEs.

PLD1 is also present on MVEs during the entire process, but it is only required to produce PA on docking MVEs. PLD1 inhibition also increases the density of lysosomes near the surface, indicating a role in late endosome fate.

Finally, to understand why PA is essential in these processes, we explored PA accumulation to curvature *in vitro*. A tubulated supported lipid bilayer assay was developed to identify curvature preference of lipids. PA was found to stabilize the formation of these regions of curvature and to localize to the inner, negatively curved leaflet of liposomes.

Acknowledgements

I would first like to thank Dr. Michelle Knowles for offering me a position in her lab over the last several years. Her mentorship has been pivotal for my development as a scientist. The other members of her lab have also provided support. Members of my thesis committee have also provided guidance throughout this process. In particular, I would like to thank Dr. Schuyler van Engelenburg and his PhD student Claire Jiang for helping us develop the CD63-pHmScarlet probe used throughout Chapter 3 and offering Brefeldin A for the same chapter. I would also like to thank our collaborator, Dr. Christina Coughlan, at the University of Colorado Anschutz, for allowing us to use her lab's NanoSight in Chapter 3.

My family and friends have also provided a support system over the last six years. My mother, Shari, and my brothers, Jack and Alex, have offered support during this program. Finally, my partner, Nat Timmens, who I would like to thank for being an incredibly supportive and patient partner as I have worked on this project.

Table of Contents

List of Figures

Chapter One: Introduction

1.1: Phospholipase D and Phosphatidic Acid

Cell membranes in mammalian cells are a mix of lipids and proteins that separate the interior of the cell from the extracellular matrix that surrounds the cell. The hydrophobic center of membranes prevents most molecules from passing through, which protects the cell. The lipid composition of cell membranes is controlled by several classes of proteins, which can move or modify lipids for curvature or signaling. One group of lipid-modifying proteins are phospholipases.

Phospholipases are a class of enzymes that cleave phospholipids at various sites [1]. In the case of phospholipase D (PLD), the headgroup of a lipid is cleaved, resulting in phosphatidic acid (PA) [1]. In mammals, there are 6 known PLDs, although only three have been shown to have enzymatic activity: PLD1, PLD2 and PLD6, with PLD1 and PLD2 cleaving choline from phosphatidylcholine [2]. However, all 6 human PLDs have been implicated in cancers [2]–[11]. PLDs conduct enzymatic activity via two highly conserved HxKxxxxD domains, where x is any amino acid [12]. In addition, both PLD1 and PLD2 have lipid-binding phox, pleckstrin homology (PH) and a phosphatidylinositol 4,5-bisphosphate domains [12]. PLD1 and PLD2 are both specific to phosphatidylcholine (PC) [12]. One main difference in structure is the presence of a loop domain unique to PLD1 and thought to be involved in regulation of activity. PLD1 is less basally active than PLD2,
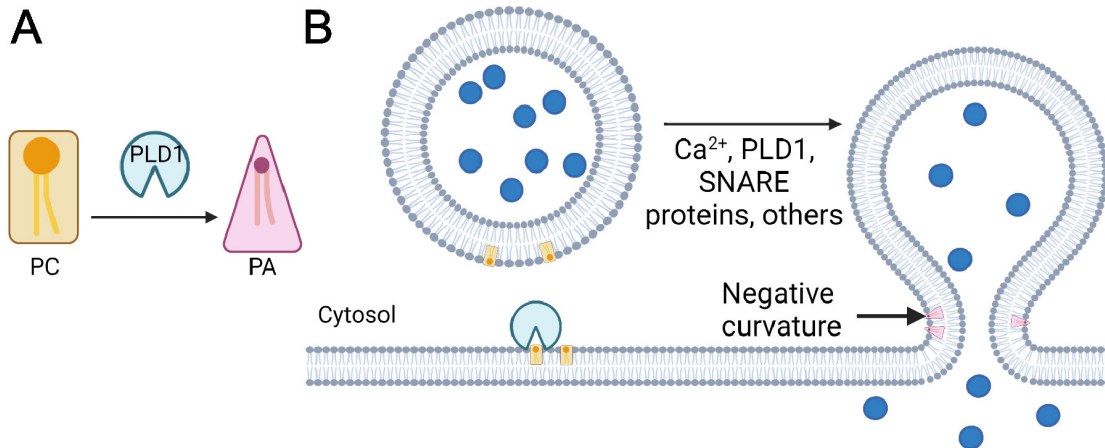
Figure 1.1: Cartoon Description of Hypothesis for Phospholipase D1 Activity During Exocytosis. A) PLD1 reaction. The headgroup of the cylindrical lipid, PC (yellow), is cleaved, producing PA (pink), an inverse conical lipid. B) Description of predicted PLD1 activity during exocytosis. Upon stimulation with Ca^{2+}, PLD1 is thought to produce PA on the plasma membrane to stabilize the fusion pore, assisting with the release of vesicular cargo (blue circles). Cartoon created with BioRender.com.

requiring activation via protein kinase C and small G proteins [13], [14]. Upon stimulation, PLD1 is activated and cleaves choline from PC (Figure 1A).

PLD1, but not PLD2, has been shown to be necessary for stimulated exocytosis [15]. One hypothesis for the role of PLD1 is that its product, PA, stabilizes the fusion pore during exocytosis due to its inverse conical shape and the significant negative curvature required at the site of the fusion pore (Figure 1.1). This is supported by the fact that introduction of the lipid lysoPC on the extracellular side of the leaflet, a lipid with positive curvature preference, rescues exocytosis in PLD1 knockdown experiments [15]. PLD1 is also involved in the Golgi apparatus, where it is also implicated in the formation and transport of vesicles from the Golgi [16]. Therefore, an alternate hypothesis for PLD1's role in exocytosis could be related to this role, where if vesicle formation is reduced that would indirectly reduce exocytosis. To test this hypothesis, we observed PLD1 localization

during exocytosis. Temporal mapping data of PLD1 during fusion was lacking, as was data regarding just how much PA stabilizes regions of curvature.

1.2: Exocytic Pathway of Secretory Vesicles

The exocytic pathway is vital for intercellular communication. Vesicles containing signaling molecules, such as neurotransmitters or hormones, dock at the plasma membrane. Upon stimulation, Ca^{2+} enters the cell, which signals for the release of secretory vesicles via Ca^{2+}-binding proteins. This process is controlled by many proteins. The hallmark proteins of exocytosis are the three SNARE proteins, Syntaxin (Syx1a), SNAP25 and vesicle associated membrane protein (VAMP2), which fold to fuse the membranes together [17]. While SNARE proteins are the most studied, and form the minimum machinery for exocytosis, it is known that there are other proteins involved in this process. In this work, we focus on PLD1; PLD1 has been shown to also be required for exocytosis, as knockdowns or inhibition of PLD1 but not PLD2 lead to a significant reduction of exocytosis [12], [18]–[21]. Because PLD1 produces a lipid with a negative curvature preference, it is thought that production of PA at the plasma membrane stabilizes the curvature at the fusion pore [15] (Figure 1.1). Syntaxins have also been shown to have PA-binding domains, which may have a role in this process [22], [23].

Like PA, other lipids and cholesterol have also been well-characterized in the exocytic process. Particularly, cholesterol and phosphatidylinositol-(4,5)-bisphosphate ($PI(4,5)P_2$) have been shown to be enriched at sites of fusion. $PI(4,5)P_2$ has been shown to be a lipid that binds to exocytic proteins, including Synaptotagmin and SNAREs.

3

Additionally, syntaxins have a polybasic region that binds to charged lipids, including PA and PIP$_2$ [22], [23]. This polybasic domain could drive recruitment of PA to the fusion pore, illuminating a second potential role of PLD1 during exocytosis. Additionally, PLD1 has both a PIP-binding PH domain and a specific PI(4,5)P$_2$ binding domain, so it is likely recruited to these lipid domains near docked vesicles, as well.

1.3: Multivesicular Endosomes and Exosome Secretion

Another method for intercellular communication lies in secretion of exosomes, a class of extracellular vesicles. Late endosomes can form intraluminal vesicles (ILVs), becoming multivesicular endosomes (MVEs). Once these MVEs fuse with the plasma membrane, the ILVs become exosomes, and may contain various biomolecules to deliver to other cells, such as proteins or RNAs. MVEs have been seen in many cell types by electron microscopy, with more exosomes are secreted in many cancers [24]–[27]. Although MVEs are known to play a role in intercellular communication and cancer, not much is currently known about MVE formation and secretion.

Exosomes are known to play a role in metastasis [24]–[27], and the secretion of exosomes is upregulated in advanced cancers [26]. Similarly, PLD1 and PLD2 overexpression is implicated in certain cancers [3]–[11]. PLD1 and PLD2 have been shown to localize to endosomes under basal conditions [28]–[33]. Some evidence already exists that suggests that both PLDs play a role during both ILV formation (PLD2) and exosome secretion (PLD1) [2], [34]–[36]. If PLD1/2 overexpression was related to exosome secretion, it could help identify the role these proteins play in cancer. Knockouts of either

PLD1 or PLD2 lead to a significant reduction of exosomes secreted [36], and PLD1 has

been specifically implicated in secretion, while PLD2 is implicated in MVE formation [2].

PLDs may be involved in this process due to the curvature of fusion, like in secretory

vesicles, or by stabilizing curvature during the formation of intraluminal vesicles in MVEs.

One protein exosomes are particularly enriched in is the tetraspanin CD63, which often

serves as markers for MVEs or exosomes. In Chapter 3, we used various CD63 probes to

observe MVEs, and we explored PLD1 and PA during these processes.

1.4: Lipid Geometry and Curvature-Based Sorting

Cells must regulate the shape of their membranes. This regulation is critical for

many cell processes, including maintaining important shapes of organelle membranes and

cell signaling. The fusion pore during exocytosis is an example of a highly curved

membrane (Figure 1.1B). Curvature can be regulated by proteins, whether by inserting in

the membrane or by scaffolding [37]. Alternatively, lipid geometry can affect membrane

curvature [37]–[40]. In this work, we focus on the role of lipids in membrane curvature.

There are two models for lipid-based regulation of membrane shape: lipid geometry

and defect sites. In the former case, lipid geometry is dependent on the size of the

headgroup compared to the acyl chains, and can be cylindrical, conical or inverse conical.

PC is a common example of a cylindrical lipid, with no preference for membrane curvature.

PA, one of the main focuses of this work, is an inverse conical lipid (Figure 1.1A). When

a high concentration of inverse conical lipids, like PA, are present, the membrane begins

to deform [39], [41]–[43]. The defect site model suggests that lipids will sort to already

present curvature instead of forming curvature themselves [40], [44]. These models are not mutually exclusive.

The headgroups of lipids, however, are not the only part of the lipid to play a role in curvature preference. Previous studies have shown that the number of carbons in the acyl chains also affects curvature preference, with lipids with longer chains having a higher preference [38], [40]. To understand curvature stabilization of PA, in Chapter 4 we explored the effects of lipid headgroups and tails to regions of curvature using a new curvature assay.

Chapter Two: Phospholipase D1 Produces Phosphatidic Acid at Sites of Secretory Vesicle Docking and Exocytosis

Phospholipase D1 (PLD1) activity is essential for the stimulated exocytosis of secretory vesicles where it acts as a lipid-modifying enzyme to produces phosphatidic acid (PA). PLD1 localizes to the plasma membrane and secretory vesicles, and PLD1 inhibition or knockdowns reduce the rate of fusion. However, temporal data resolving when and where PLD1 and PA are required during exocytosis is lacking. In this work, PLD1 and production of PA are measured during the trafficking, docking, and fusion of secretory vesicles in PC12 cells. Using fluorescently tagged PLD1 and a green fluorescent protein-tagged PA binding protein (GFP-PASS), cells were imaged using total internal reflection fluorescence microscopy to monitor the presence of PLD1 and the formation of PA throughout the stages of exocytosis. Single docking and fusion events were imaged at high speed to measure the recruitment of PLD1 and the formation of PA. PLD1 is present on mobile, docking, and fusing vesicles and also colocalizes with Syx1a clusters. Treatment of cells with PLD inhibitors significantly reduces fusion, but not PLD1 localization to secretory vesicles, however, the formation of PA is altered. When PLD1 is active, PA is produced slowly on docked vesicles in stimulated cells over the course of 10s of seconds and produced during fusion with a maximum PA occurring ~1.4 s after fusion. Production of PA during docking and fusion is eliminated in cells treated with PLD1 inhibitors,

7

indicating that PLD1 produces PA during exocytosis. PA formation is required for secretory vesicle exocytosis and potentially acts an essential regulator of fusion.

One of our undergraduate students, Megan Hulser, assisted with ~5% the data collection and analysis of this chapter, while I collected and analyzed the rest. Michelle Knowles assisted with revising the writing, ~30%.

2.1: Introduction

Regulated exocytosis is a tightly controlled process in neuroendocrine cells that is essential for the secretion of hormones and neurotransmitters. During exocytosis, the membrane of a docked vesicle fuses with the plasma membrane, a process with a high energy barrier. SNARE proteins have been shown to provide the minimal machinery for fusion [1] and a few copies, along with their accessory proteins, can provide the energy required [2], [3]. While SNARE proteins are vital for exocytosis, lipid rearrangement has been proposed to assist by recruiting protein clusters [4], recruiting vesicles [5], or stabilizing the highly curved fusion pore [6]–[8]. For example, phosphatidylinositol (4,5)-bisphosphate (PI(4,5)P$_2$) has been shown to inhibit fusion pore dilation [9] and cholesterol is involved with the clustering of Syntaxin1a, a plasma membrane associated SNARE protein essential to docking and fusion [4]. Lipid-modifying enzymes, such as phospholipase D1 (PLD1), have been implicated as essential in exocytosis [10]–[14] and its product, phosphatidic acid (PA), can stabilize negatively curved membranes [8], [15]–[17].

There are six PLD isoforms in mammals, with PLD1 and PLD2 acting as lipases positioned within to play a role in exocytosis [11], [12], [14], [18], [19]. PLD1 and PLD2 use the substrate phosphatidylcholine to produce PA [20]. PLD1 and PLD2 primarily differ in basal activity; PLD2 is constitutively active and PLD1 is stimulated [21]. Several studies have shown that inhibition and knockdowns of PLDs reduce exocytosis [10]–[14]. Specifically, PLD1 is essential for exocytosis in platelets, HL-60 cells, PC12 cells and chromaffin cells [13], [22]–[24], where the loss or inhibition of PLD1 diminishes secretion, demonstrating that that PLD1 or PA is required. However, PLD2 has also been shown to be involved in exocytosis, particularly in mast cells, where PLD1 and PLD2 are involved at different stages [25]. Overall, PLD1 is required for stimulated exocytosis in most secretory cells, and it is likely that the formation of PA is essential.

PLD1 localizes partially to the plasma membrane [18], [26], [27], and its activity increases during stimulation leading to the formation of PA at the plasma membrane [13], [28]. PA formation has typically been observed by the recruitment of the PA binding domain (PABD) of Spo20 to the plasma membrane [13], [23], [29]. However, new dyes have been designed to show where PA is newly formed, using click chemistry and relying on PLD activity [30]. One hypothesis for the role of PA is during the membrane fusion step of secretion, where PA could stabilize the highly curved fusion pore [8], [15]–[17]. PA is an inverse conical lipid containing a small, negatively charged headgroup with two fatty acid tails. PA has been established as preferring negative curvature in *in vitro* studies [15], [16], [31]. However, precisely when and where PA is formed during exocytosis is currently lacking.

To test if PLD1 is present at fusing vesicles and determine when and where the production of PA is required, a model secretory cell line (PC12) was used to express either GFP-PLD1 or GFP-PASS, a PA biosensor similar to PABD [32]. Cells were imaged using total internal reflection fluorescence microscopy and the presence of PLD1 and the formation of PA were compared with the location of secretory proteins: Syntaxin-1a (Syx1), vesicle associated membrane protein 2 (VAMP2) and neuropeptide Y (NPY). Single fusion events were imaged at high speed to measure the recruitment of PLD1 and the formation of PA as vesicles docked and fused with the plasma membrane. Colocalization under basal, stimulated, and inhibitory conditions demonstrate that PLD1 is present on docked, fusing, and moving vesicles and colocalizes with Syx1 clusters. However, PA is only produced after vesicles dock and during membrane fusion, and the production of PA requires PLD1.

2.2: Materials and Methods

Cell Culture:

PC12-GR5 cells were cultured in flasks in Dulbecco's modified eagle medium (DMEM, ThermoFisher, Waltham, MA, USA) supplemented with 5% fetal bovine serum (ThermoFisher, Waltham, MA, USA) and 5% equine serum (ThermoFisher, Waltham, MA, USA) and incubated at 37°C and 5% CO_2. For imaging, PC12 cells were plated in 8 well plates (Cellvis, Mountain View, CA, USA) treated with poly-L-lysine (Sigma Aldrich, St. Louis, MO, USA). Cells were transfected with Lipofectamine 2000 (ThermoFisher, Waltham, MA, USA) and plasmids (25-100 ng/well) for fluorescently tagged proteins. The

EGFP-PLD1 plasmid was a gift from Jeremy Baskin [30]. VAMP2-pHmScarlet was a gift from Pingyong Xu (Addgene plasmid # 166890). GFP-PASS was a gift from Guangwei Du (Addgene plasmid # 193970). Cells were tested for mycoplasma using MycoFluor (ThermoFisher, Waltham, MA, USA) according to manufacturer protocols.

To stimulate fusion, a stimulation buffer containing 3 mM NaCl, 140 mM KCl, 1 mM MgCl2, 3 mM CaCl2, 10 mM D-glucose and 10 mM HEPES, pH 7.4 (ThermoFisher, Waltham, MA, USA) was added to a final concentration (KCl) of 60 mM. In inhibitory experiments, cells were incubated with 0.013% DMSO with or without 100 nM pan-PLD inhibitor 5-fluoro-2-indolyl des-chlorohalopemide (PLD1/2i, Sigma Aldrich, St. Louis, MO, USA) or 500 nM PLD1-specific inhibitor VU0155069 (PLD1i, Sigma Aldrich, St. Louis, MO, USA) for 30 minutes at 37°C and then imaged immediately.

Calcium imaging was performed on a point-scanning confocal microscope (Olympus Fluoview 3000) with 488 and 640 laser excitation to observe a change in intensity post stimulation with high K+. Cells were treated with Fluo 4 AM (ThermoFisher, Waltham, MA, USA) and far-red CellMask (ThermoFisher, Waltham, MA, USA) to test the influx of Ca2+ upon addition of 3 mM NaCl, 140 mM KCl, 1 mM MgCl2, 3 mM CaCl2, 10 mM D-glucose and 10 mM HEPES, pH 7.4 (ThermoFisher, Waltham, MA, USA) to a final concentration (KCl) of 60 mM. CellMask and Fluo4-AM were used according to the manufacturer protocols.

To quantify slot blots, average intensities of each band were measured using Image J and a background intensity nearby was also measured. Values were corrected by

normalizing to actin, then divided by the value of wild type cell from the same day, described in Equation 2.1:

$$I_{Relative} = \frac{I_{O,PLD1} - I_{O,BG}}{I_{WT,PLD1} - I_{WT,BG}} * \frac{I_{WT,Actin} - I_{WT,BG}}{I_{O,Actin} - I_{O,BG}} \tag{2.1}$$

where O is overexpressed, WT is wild type, PLD1 is the PLD1 band, Actin is the actin band and BG is a nearby background intensity surrounding the adjacent band.

For immunostaining, PC12 cells expressing VAMP2-pHluorin were fixed in 3.2% paraformaldehyde (Electron Microscopy Sciences, Hatfield, PA, USA) for 30 minutes and immediately permeabilized with 0.1% Triton-X 100 (Sigma Aldrich, St. Louis, MO, USA) for 10 minutes. Cells were then blocked in 0.5 mg/mL BSA (ThermoFisher, Waltham, MA, USA) for 4 hours at 4°C and treated with mouse anti-PLD1 (Santa Cruz Biotechnology, Santa Cruz, CA, USA) overnight. Cells were then treated with Alexa-594 conjugated rabbit anti-mouse (ThermoFisher, Waltham, MA, USA) for 4 hours. Transfection efficiency was 25-30% based on the number of cells observed to be transfected.

Total Internal Reflection Fluorescence Microscopy:

PC12 cells were imaged in Fluobrite DMEM (ThermoFisher, Waltham, MA, USA) using a TIRF microscope (Nikon Ti-U) equipped with 491 nm and 561 nm lasers, as described previously [33]. A 60x 1.49 NA objective, a 2.5x magnifying lens, and an EMCCD (Andor iXon897, Abingdon, UK) were used in combination with a DualView (Optical Insights, Suwanee, GA, USA) to split the red and green fluorescence channels onto the camera via a 565LP dichroic with 525/50 and 605/75 emission filters (Chroma

Technologies, Bellows Falls, VT, USA). Both color channels were taken simultaneously, and images were collected by MicroManager at 0.109 µm/pixel and 136 ms/frame [34]. For tracking and inhibition studies, cells were imaged on a stage heater at 37°C. Otherwise temperature is noted in the figure captions for all data.

Image Analysis:

Image analysis was conducted using MATLAB (v. R2021b, Natick, MA, USA) To measure the colocalization of static images, $\Delta F/S$ was calculated using Equation 2.2

$$\frac{\Delta F}{S} = \frac{C - A}{A - bg} \tag{2.2}$$

where C is the intensity of a 7 pixel circle in the GFP-PLD1 channel at a spot found in the red channel, A is a 1 pixel wide concentric ring with one pixel gap from the circle, and bg is the average intensity of the background surrounding the cell. Movies were corrected for photobleaching by a home-built code to correct to a constant cell intensity. Visiting, docking and fusing vesicles were found using a previously established algorithm [33]. Here, a difference movie was calculated, max projected, bandpass filtered and a peak finding algorithm identify spots where a rapid increase of intensity occurs. Locations of intensity changes in the red channel were identified and cropped from the photobleach corrected movies (both green and red). From these cropped movies, intensity plots, calculated as:

$$\frac{\Delta F}{F} = \frac{C_t - C_0}{C_{max} - C_0} \tag{2.3}$$

where C is the intensity of a 7 pixel circle as described in Figure 1 at frame t (C_t) or the frame with the brightest intensity (C_{max}), and C_i is the average initial intensity of a circle for 5 frames prior to onset of intensity increase. From the traces, data is manually binned

into visiting, docking and fusing vesicles. If the trace is not clear, the cropped movie is viewed to determine the fate of the vesicle. Fusion is verified in the movie by an outward expansion of fluorescence post fusion. For average images of events, only events with at least 50 frames prior to event onset and 100 frames after were included. The bar graphs relating the $\Delta F/F$ for PLD1 or PASS intensity were measured at the time corresponding to the peak in intensity for each event for fusion and visiting vesicles. For the docking events, 80% to the plateau of the VAMP2 intensity was used instead of the peak intensity.

To determine the relative PASS intensity for the different stages of fusion the PASS intensity within a circular region divided by the average cell intensity was measured. This corrects for GFP-PASS protein expression levels. To obtain the relative PASS intensity for the visiting (orange), docking (pink) and fusion (blue), the PASS$_{initial}$ intensity for visiting vesicles was subtracted. The formation or accumulation of PA (via PASS intensity) at fusion, docking and visiting sites is noted by an increase above 0 in the relative intensity and is compared to the PASS$_{initial}$ intensity prior to vesicles visiting.

To determine the mobility of vesicles, tracking of SVs was done on VAMP2-pHmScarlet vesicles following a previously published analysis [35]. A position list of peaks was created for each frame, then a tracking algorithm determines tracks from those points. After tracking, the intensity ($\Delta F/S$) of the PLD or PA in the vesicle's position was measured in time using home-built code. The diffusion coefficient (D) is calculated from individual tracks by calculating the mean squared displacement. Significance testing and plotting were conducted using GraphPad Prism (v. 9.5.1, San Diego, CA, USA). The MATLAB code to locate and crop fusion, visiting and docking events is available on

GitHub (https://github.com/michelleknowles/membrane-fusion) and previously published [33].

2.3: Results

PLD1 localizes to secretory vesicles and Syx1 clusters

To determine the role of PLD1 in SV secretion, PC12 cells were transiently transfected with GFP-PLD1 and either VAMP2-pHmScarlet, NPY-mCherry or Syx1-mCherry. GFP-PLD1 visually colocalizes to all three proteins (Figure 2.1A-C). To quantify the extent of colocalization, the GFP-PLD1 intensity within a circle centered around the vesicle or Syx1 cluster location was measured relative to the local surrounding background (ΔF = circle – annulus, shown in Figure 2.1D). This was normalized by the expression level (S = annulus – background outside of the cell). A positive value indicates that GFP-PLD1 is present at VAMP2 containing vesicles, NPY vesicles, or Syx1 clusters. GFP-PLD1 significantly localizes to all three compared to a negative control: cytosolic GFP. Upon stimulation with high K^+ buffer, Ca^{2+} enters PC12 cells and fluorescence from a calcium indicator increases (Figure 2.2). All cells were labeled with CellMask (Figure 2.2A) and Fluo4-AM (Figure 2.2B-C). The only cells that did not show a change indicating the influx of Ca^{2+} were cells that were part of a larger cluster of cells (Figure 2.2D-E), therefore, single cells or pairs of cells were measured for the remaining experiments. No increase in colocalization was observed for PLD1 at VAMP2 positions after 2 minutes of stimulation (Figure 2.1D). Overall, PLD1 is positioned to play a role in is exocytosis, in line with what
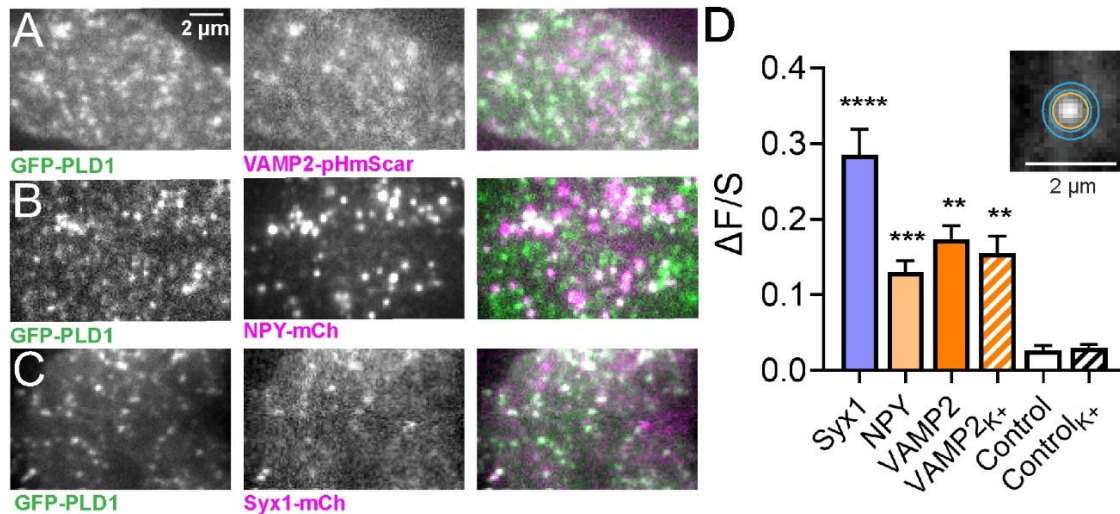
Figure 2.1: Phospholipase D1 Colocalizes with Secretory Vesicle Markers and Syntaxin Clusters. A-C) PC12 cells were transfected with GFP-PLD1 (left) and A) VAMP2-pHmScarlet, B) NPY-mCherry or C) Syx1-mCherry (middle) and imaged at room temperature using TIRF microscopy. The overlays (right) are white where colocalization occurs. Scale bar: 2 μm. D) The extent of GFP-PLD1 accumulation, ΔF/S, at VAMP2 spots (dark orange), NPY (light orange) or Syx1 (blue). As a control, ΔF/S was measured for cytosolic GFP at VAMP2 spots (white). Striped bars represent ΔF/S of PLD1 or cytosolic GFP in cells stimulated with 60 mM KCl. Significance represents comparison to the cytosolic GFP control (** $p < 0.005$, *** $p < 0.0005$). The KCl stimulated cells are compared to the KCl stimulated control. *Inset*: description of ΔF/S measurements, where $\frac{\Delta F}{S} = \frac{C-A}{A-bg}$. The circle, C, is represented by the orange circle, while annulus A is the space between the cyan circles and bg is the average intensity surrounding the cell.

others have shown [11], [14], [18], [19], and stimulation does not alter the position of PLD1 over a short period of time.

One limitation of using GFP-PLD1 is that some studies suggest that overexpression of PLD1 leads to mislocalization [27]. By eye, GFP-PLD1 is extremely low expressing as noted by how dim cells were on the microscope, suggesting that transient expression in PC12 cells is low. To quantify the amount of overexpression a slot blot of PLD1 from transiently transfected cells was compared to endogenous PLD1 expression (Figure 2.3A).
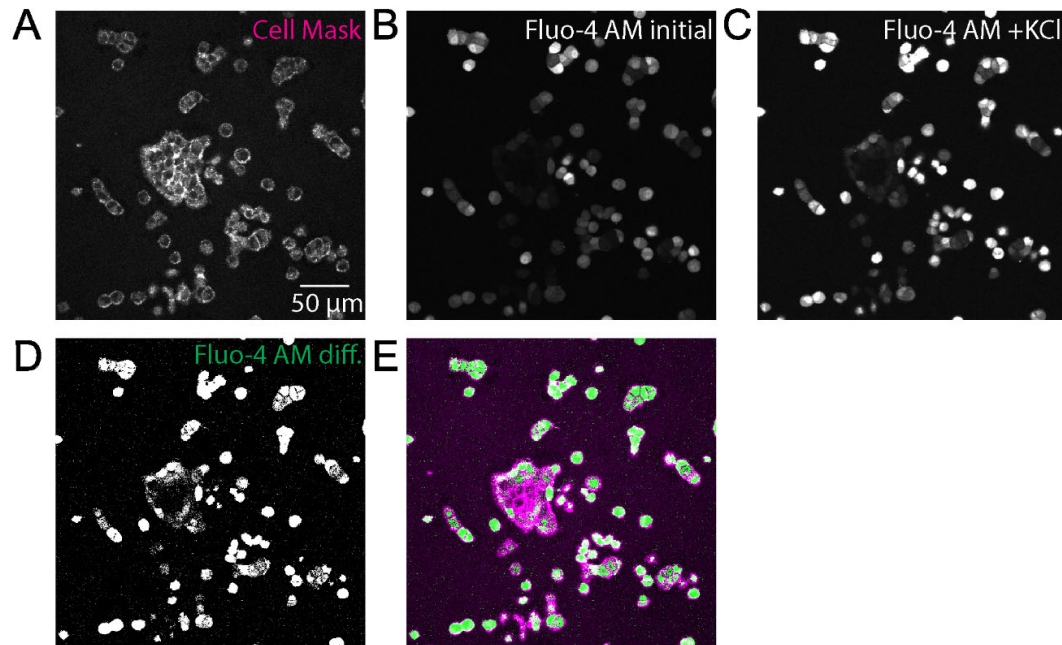
Figure 2.2: Calcium Influx in KCl Stimulated PC12 Cells. PC12 cells were treated with Deep Red CellMask and the Ca^{2+} dye Fluo-4 AM and imaged on a confocal microscope. Images were taken before and after the addition of stimulation buffer to a final KCl concentration of 60 mM. A) Average of 50 frames at 2.17 s/frame in CellMask channel. B-D) average of 5 frames prior to (B) or after (C) KCl stimulation and the difference between the images (D). B and C are contrasted identically. E) Composite image of the difference image shown in D (green) and the CellMask image shown in A (magenta).

PLD1 is increased by 4.3% overall and about 25% of cells are transfected (Figure 2.3), therefore it is overexpressed by approximately 17% in transfected cells. To determine if the colocalization observed with GFP-PLD1 (Figure 2.1) was also present with endogenous PLD1, immunofluorescence was performed on fixed cells; anti-PLD1 is present at sites of VAMP2-pHluorin (Figure 2.3D).
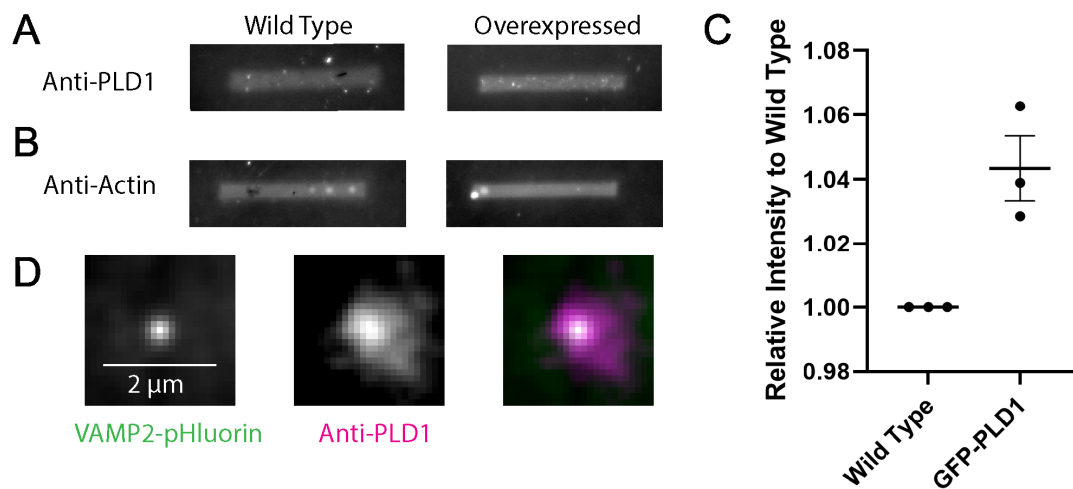
Figure 2.3: Blotting Overexpression of PLD1 and Staining for Localization. A) Example Slot Blot of PLD1 and actin in wild type PC12 cells and PC12 cells transfected with GFP-PLD1. C) Normalized and corrected intensity of bands for PLD1. Values were corrected by normalizing to actin, then divided by the value of wild type cell from the same day. Lines are average, error bars are SEM (n = 3 days). C) Cells expressing VAMP2-pHluorin (left) were fixed, permeabilized and stained with anti-PLD1 and Alexa594-labeled anti-mouse (middle). On overlay of the two is also shown.

GFP-PLD1 is present on mobile VAMP2 vesicles and during docking, fusion

To assess whether PLD1 is recruited as vesicles traffic to the plasma membrane, dock and then fuse, cells expressing GFP-PLD1 and VAMP2-pHmScarlet were imaged in time using TIRF microscopy. VAMP2-pHmScarlet is visible prior to fusion and also increases in fluorescence due to the large pH change that occurs upon fusion [36], making it an excellent probe for visualizing moving, docking, and fusing vesicles in a single-color channel. VAMP2-pHmScarlet vesicles were located using a previously established method [33], then divided into three classes: visiting, docking, or fusing vesicles based on whether they move through a cropped movie (Figure 2.4A), appear and remain static (Figure 2.4B), or appear, increase quickly in intensity and spread out from the center (Figure 2.4C). To quantify the data, the intensity within a circular region (Figure 2.1D, inset orange) was

measured in time and the average of five frames prior to the event onset (-0.5 to -0.1 s) was subtracted and normalized (see Methods). Note that the annulus was not used in this measurement because it changes in intensity when fusion occurs asfluorescence radially expands. The whole trace was then normalized by the maximum intensity. To visualize this change, events were averaged into one movie and then 5-frames at fusion and visitor onset (-0.5 to -0.1 s, "initial") and VAMP2 peaks or plateaus ("final") were averaged (Figure 2.4D-F, top row). To highlight the change that occurs in the PLD1 concentration during the events, the initial image was subtracted from the final image to create a difference image ("Δ"). All GFP-PLD1 difference images show spots in the center. As a control, cytosolic GFP was expressed in place of GFP-PLD1 (Figure 2.4D-F, bottom row). The intensity in time is shown for both the vesicle (Figure 2.4G-I, purple) and PLD1 (Figure 2.4G-I, green) such that 0 s is the beginning of the rise in VAMP2 intensity. In all three types of events, the intensity of GFP-PLD1 significantly increases after the onset of visiting, docking or fusion (Figure 2.4D-I), suggesting that PLD1 is carried on VAMP2 vesicles. Cytosolic GFP was used as a control, and an increase is not observed (Figure
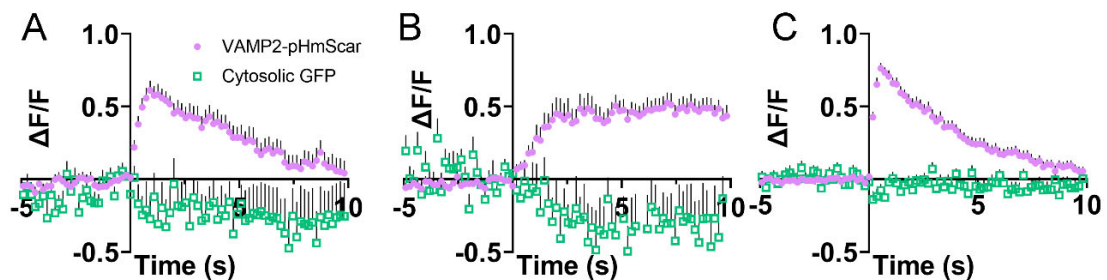
Figure 2.5: Cytosolic GFP does not change during moving, docking or fusion events. The normalized intensity of VAMP2-pHmScarlet (purple circles) and cytosolic GFP (green squares) during A) Visiting, B) Docking and C) Fusion events. Error is SEM.
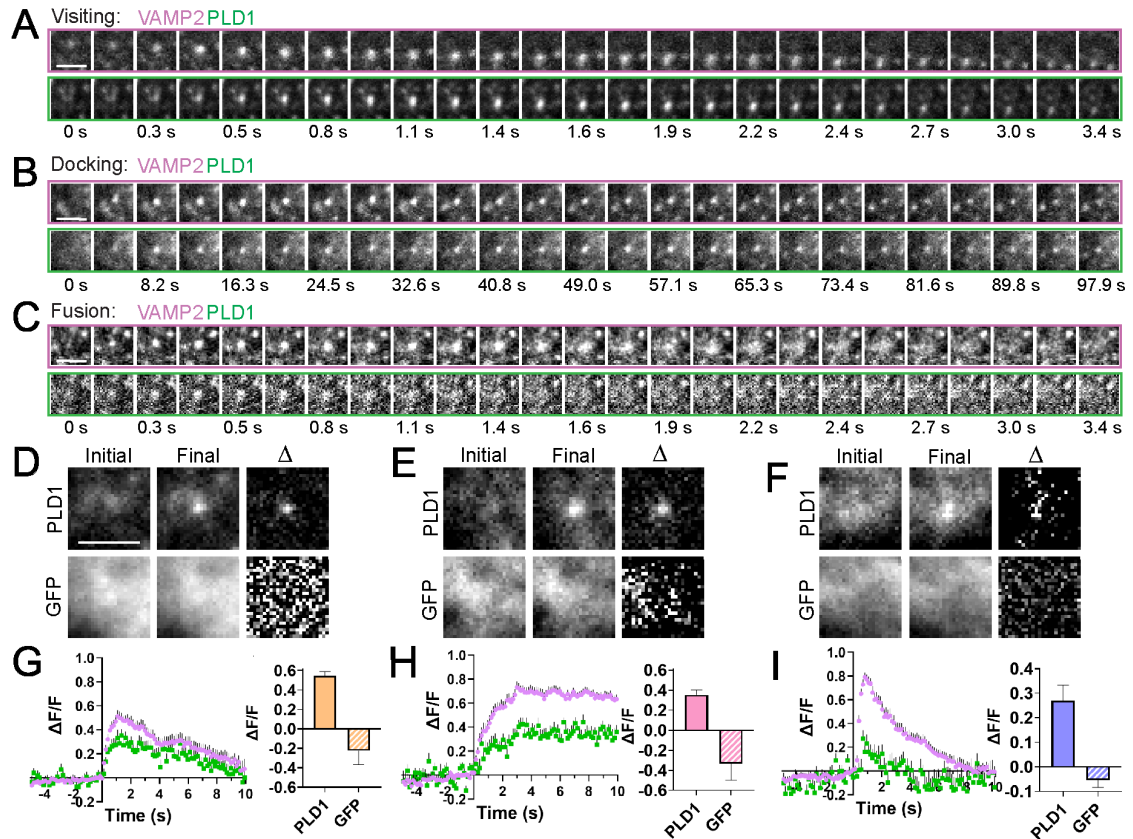
Figure 2.4: GFP-PLD1 Localizes to Visiting, Docking, and Fusing VAMP2 Vesicles. PC12 cells expressing GFP-PLD1 and VAMP2-pHmScarlet were imaged at 136 ms/frame at room temperature. A-C: Single vesicle events were located using an automated algorithm that identifies three types of events: visiting (A), docking (B) or fusing (C) vesicles Top rows: montages of VAMP2-pHmScarlet. Bottom rows: corresponding montages of GFP-PLD1, where each image is a 5-frame average. Scale bars: 2 μm. A-C are examples of a single event. D-F) Average images of many events prior to visiting (D, 17 PLD1 and 22 GFP events), docking (E, 18 and 10 events) or fusion (F, 22 and 25 events) at the onset (left) and peak/plateau VAMP2 intensity (middle) for PLD1 (top) or cytosolic GFP (bottom). A difference image, Δ, of each is shown to highlight changes (right). Initial and final images are contrasted the same. Scale bar: 2 μm. G-I) Left: Traces of G) visiting (n = 37), H) docking (n = 20) and I) fusing (n = 32) vesicles for GFP-PLD1 (green) and VAMP2-pHmScarlet (purple). The intensity, ΔF/F, was normalized to 1.0 for each event prior to averaging. Bar graphs depicting ΔF/F values of GFP-PLD1 (solid) and cytosolic GFP (striped) at the peak of the VAMP2 traces or at 80% of the plateau. Error bars are SEM.

2.4G-I, Figure 2.5). This suggests that PLD1 is present on moving VAMP2 vesicles and more may be recruited during docking and fusion.

Inhibition of PLD1 reduces the fusion of VAMP2 vesicles and vesicle mobility but does not alter PLD1 localization

One key feature of PLD1 is its ability to convert PC into PA, where the lipid PA is then involved trafficking [29], [37], [38] and fusion [10]–[14]. To explore the activity of PLD1, PC12 cells expressing GFP-PLD1 and VAMP2-pHmScarlet were treated with 100 nM FIPI, a pan-PLD inhibitor or 500 nM VU0155069, a PLD1 specific inhibitor. To verify if fusion is blocked in the presence of inhibitors, the rate of fusion was measured. The frequency of fusion was reduced in both unstimulated and K^+ stimulated cells when cells were treated with either inhibitor (Figure 2.6A-B), but the localization of GFP-PLD1 to sites of fusion was not significantly affected (Figure 2.6C). The inhibition of PLDs also altered the rate vesicles near the plasma membrane moved. VAMP2 vesicles were tracked in time and the rate of motion was measured. Diffusion coefficients of VAMP2+ vesicles in cells treated with inhibitors were slightly slower (Figure 2.6D). However, when only mobile vesicles (D > 0.0055 μm^2/s) were counted (Figure 2.6E), the reduction in motion vanishes, suggesting that the reduction observed is due to a change in the number of mobile vesicles. Interestingly, the fraction of mobile vesicles per cell does not significantly decrease upon treatment with either inhibitor (Figure 2.6F). Therefore, the activity of PLD1 is essential for the mobility and fusion of VAMP+ vesicles but does not contribute to the location of PLD1.
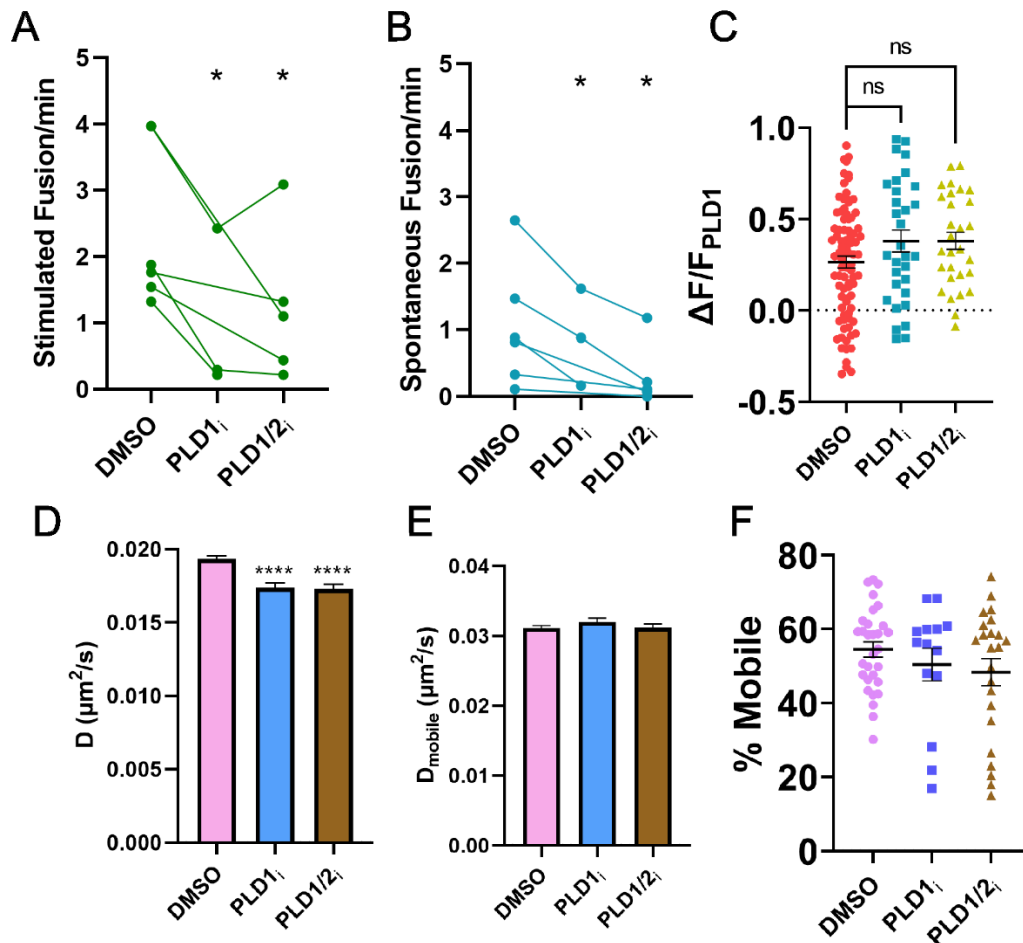
Figure 2.6: PLD Inhibition Reduces Fusion Rates and Mobility. PC12 cells were treated with inhibitors for PLD1 (VU0155069, 500 nM), PLD1 and 2 (FIPI, 100 nM), or a similar amount of DMSO (control). Cells were incubated 30 m prior to imaging and imaged at 37°C. A) The frequency of VAMP2 fusion events that are A) stimulated or B) spontaneous decreases with inhibition. Each triplet of points represents the average of 2 or more cells from one day. C) The intensity (ΔF/F) of PLD1 at peak VAMP2 intensity during fusion in DMSO, PLD1i or PLD1/2i treated cells. D) Diffusion coefficients of single, tracked VAMP2 vesicles (n > 9500 tracks) decreases slightly, but significantly in the presence of inhibitors. E) Average diffusion coefficients of the mobile VAMP2 vesicles, where mobility is defined as $D > 0.0055\ \mu m^2/s$. F) Percent of vesicles that are mobile in a given cell. Each point represents one cell. Each point is one vesicle event. Data is not significantly different with treatment in E and F. Lines are averages, error bars are SEM. * $p < 0.05$, **** $p < 0.0001$ compared to DMSO.

PA accumulates at fusion sites, and this depends on PLD1 activity

If PLD1 activity is essential to fusion, the formation of PA should occur and the timing of PA formation during the fusion process can be determined by imaging single fusion events. To test this, fusion events were located in cells expressing VAMP2-pHmScarlet and GFP-PASS analogous to the approach shown for GFP-PLD1 (Figure 2.4). GFP-PASS is a PA binding protein tagged to mGFP and marks regions of the cell that are enriched in PA [32]. Visiting, docking and fusion events were identified, and average GFP-PASS images were calculated from events prior to visiting (Figure 2.7A), docking (Figure 2.7B) or fusing (Figure 2.7C) vesicles. A difference image visualizes the change in PA via the GFP-PASS intensity in all three classes of events (Figure 2.7A-C). To quantify the intensity change, the $\Delta F/F$ of PASS during visiting, docking and fusion were calculated (Figure 2.7D-F). Unlike PLD1, PASS does not significantly increase immediately upon visiting or docking but does increase during fusion (Figure 2.7G), reaching a maximum 1.4s after the peak of the VAMP2 fusion event (Figure 2.7H).

PA has been hypothesized to accumulate at negatively curved regions within the fusion pore, which suggests that the amount of PA could possibly affect the release rate of content post-fusion. To probe whether the presence of PA affects the fusion kinetics, the slope of the decay of VAMP2 from the peak fluorescence to 1 s later and the GFP-PASS intensity ($\Delta F/S$) was measured for single fusion events. It is useful to note that the measurement $\Delta F/S$ is normalized by the local background (S) and conveys enrichment at the vesicle position, and this is insensitive to the expression level within a range [39]. The
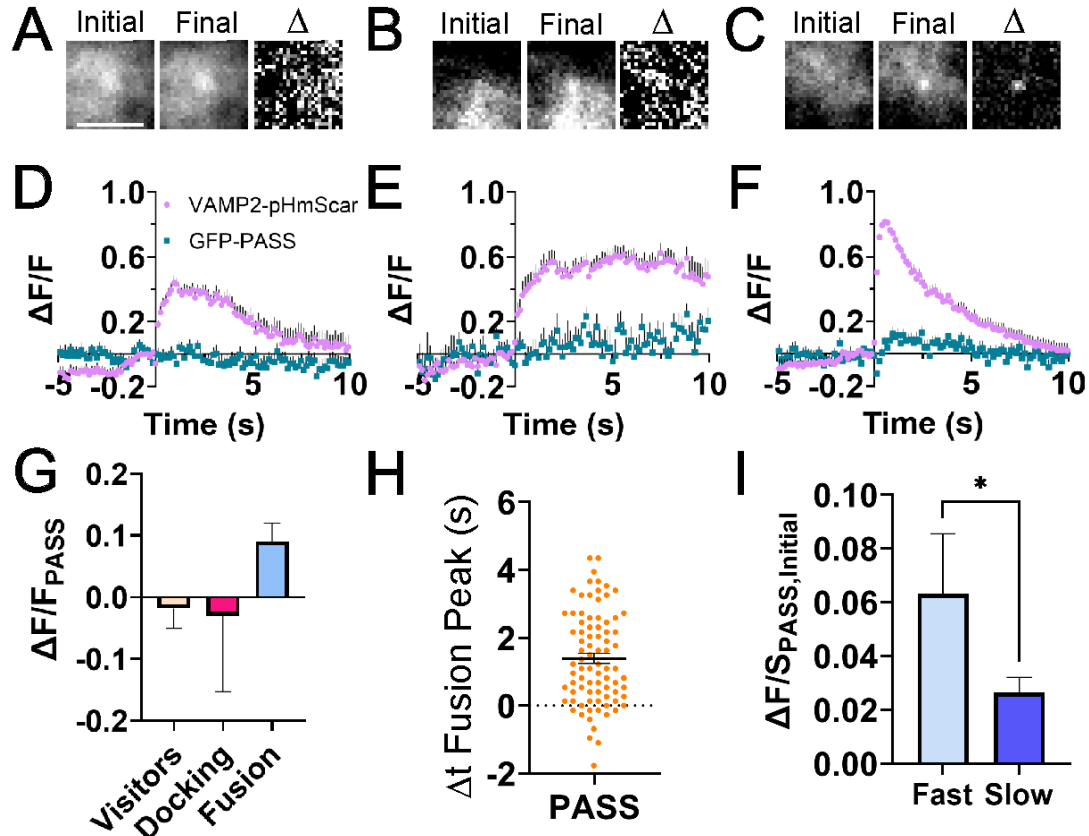
Figure 2.7: PA Is Present During Fusion. PC12 cells were transfected with GFP-PASS, a PA binding protein, and VAMP2-pHmScarlet, then cells were imaged to visualize A) visiting, B) docking and C) fusing vesicles. A-C) Average images of GFP-PASS prior to onset (left), at the peak (middle) of the VAMP2 intensity, and a difference image between the two (right). Scale bar: 2 μm. Before and after images are contrasted identically and are averages of 5 frames (n=51, 12 and 46 for A-C, respectively). D-F) Average intensity ($\Delta F/F$) traces of VAMP2-pHmScarlet (purple circles) and GFP-PASS (teal squares). Error bars are SEM (n = 62, 21, 83 events for D-F, respectively). G) Normalized intensity of GFP-PASS at peak or plateau of VAMP2 intensity during visiting, docking or fusing events. H) Time from peak VAMP2 intensity to peak PASS intensity. Each point represents one event. Line is average, error is SEM. I) Initial VAMP2 decay slopes were binned into fast and slow events and the amount of PASS present was measured for each. Fast events have more PASS present.

initial $\Delta F/S$ of GFP-PASS was plotted against the initial decay of the VAMP2 intensity post-fusion (Figure 2.8) and a negative correlation was noted (Pearson's correlation coefficient = -0.1744), which indicates a higher PA presence during faster fusion events.
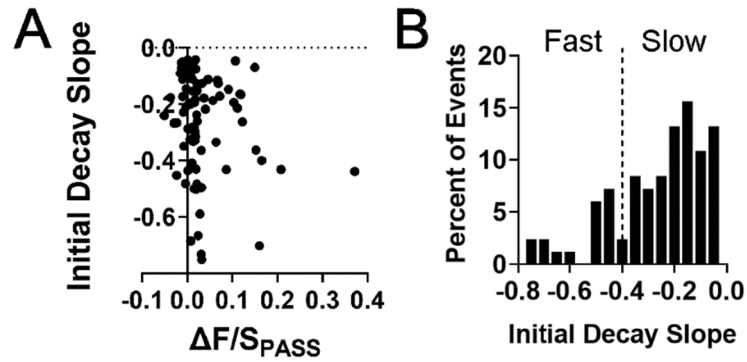
Figure 2.8: Correlation between the rate of decay and the amount of PA. A) Initial decay slopes of VAMP2 and ΔF/S of GFP-PASS during fusion, every 10 events were averaged. B) Fast and slow fusion decays were sorted by the slope of the VAMP2 fusion decay as measured from the VAMP2 fluorescence peak to 1s later.

Therefore, the rate of decay was binned into "fast" and "slow" events base on the histogram of slopes (Figure 2.8). There is significantly more GFP-PASS present on faster events (Figure 2.7I).

To probe whether PA is produced by PLD1 during fusion rather than recruited or produced by other means, PC12 cells expressing GFP-PASS and VAMP2-pHmScarlet were treated with inhibitors for PLD1 or PLD1/2 and compared to a vehicle control, as previously described (Figure 2.6). Cells were stimulated with K+ during imaging. Due to the fact that PLD inhibitors reduce fusion events (Figure 2.6A-B), the number of events observed in cells treated with inhibitors was low. GFP-PASS intensity from fusion locations were averaged before and during fusion, and the difference between the two was measured (Figure 2.9A-C). The average fusion traces were plotted (Figure 2.9D-F) and the GFP-PASS intensity at the peak of VAMP2 were calculated (Figure 2.9G). Inhibitory conditions show a decrease in PASS intensity, possibly due to new membrane lacking
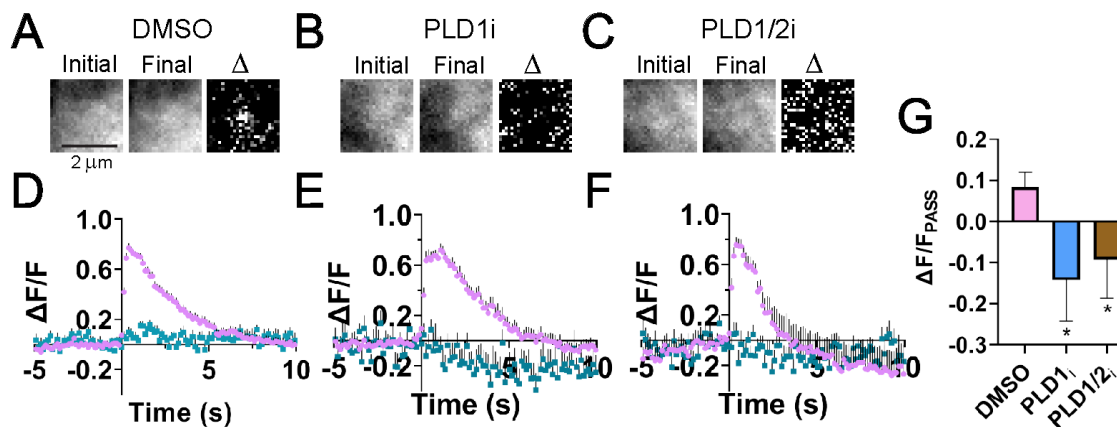
Figure 2.9: PLD1 Produces PA during Exocytosis. PC12 cells were transfected with GFP-PASS to mark PA and VAMP2-pHmScarlet, then cells were imaged at 37°C to visualize fusing vesicles in the presence of PLD inhibitors. A-C) Average PASS image (5 frames) at fusion onset (left), VAMP2 peak (middle) and the difference between the two (right) for A) DMSO (top, n = 40), B) PLD1 inhibition (middle, n = 12) and C) PLD1/2 inhibition (bottom, n = 13). D-F) Average normalized intensity traces of fusion events: VAMP2-pHmScarlet (purple) and GFP-PASS (cyan) for the D) control (52 events), E) PLD1 inhibition (16 events) and F) PLD1/2 inhibition (19 events). G) Average normalized PASS intensity during the peak of the VAMP2-pHmScarlet fusion event.

GFP-PASS being added to the fusion site. Both qualitatively and quantitatively, PASS increases in intensity in control conditions but not under either inhibitory condition.

PA accumulates at vesicle locations after docking and throughout exocytosis

PA is present near vesicle docking sites in EM data [13] and accumulates on the plasma membrane minutes after stimulation [28]. To determine the time course of PA arrival after vesicles dock, cells were stimulated with high K^+ and GFP-PASS was imaged and quantified during docking for 10s of seconds after the initial docking event (Figure 2.10A-B). Difference images show the increase of PASS at the docking cite (Figure 2.10A, bottom). After 10s, the GFP-PASS signal is significantly larger than the cytosolic-GFP
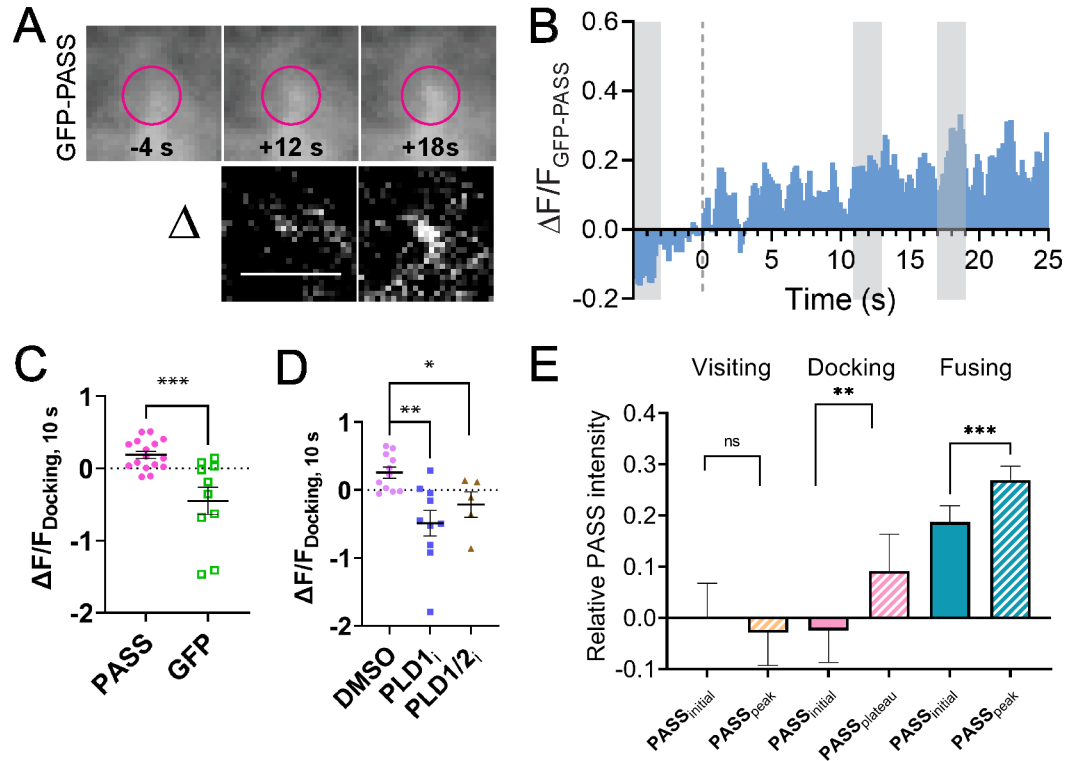
Figure 2.10: PLD1 Produces PA at Docked Vesicles over Time in Stimulated Cells.
A) Average images (n = 13 events) of PASS before onset of docking (-4s), after 8 s, and after 12 s post-docking (top). Pink circles mark the location of the docked vesicle. The difference between pre and post docking images (bottom). Initial and final images are contrasted identically. B) The average $\Delta F/F$ trace of GFP-PASS over extended periods of time after stimulation with 60 mM KCl. The grey boxes refer to the times shown in A. C) $\Delta F/F$ of PASS (pink circles) and GFP (green squares) 10 s after docking. One dot corresponds to one docking event. D) $\Delta F/F$ of PASS 10 seconds after docking in cells treated with DMSO (purple circles) with or without PLD1 inhibition (blue squares) or PLD1/2 inhibition (brown triangles). Lines are averages, error bars are SEM. E) PASS intensity over the different stages of membrane fusion. The initial intensity was measured at 0.5 to 0.1 s prior to the event. The PASS$_{initial}$ (visiting) was subtracted from all to obtain a relative intensity. Docking was measured after several seconds, when single events reached the plateau intensity in the VAMP2-pHmScarlet channel. * $p < 0.05$ ** $p < 0.005$ *** $p < 0.0005$. N = 25 docking events.

control (Figure 2.10C), and the GFP-PASS signal gradually increases as time goes on (Figure 2.10B). To identify if PA is formed or accumulated during vesicle docking, PLD inhibitors were used and both inhibitors block the formation of PA (Figure 2.10D),

therefore PA is formed by PLD1 during docking events and PLD2 cannot compensate for PLD1 inhibition. When PA formation is measured throughout the entire exocytosis process, from moving to docking to fusion, PA accumulates as exocytosis progresses (Figure 2.10E). When the intensity of GFP-PASS is measured relative to the amount present prior to docking (considered a non-specific, background fluorescence because GFP-PASS is present in the cytoplasm), the intensity of GFP-PASS increases after docking, then more prior to fusion, reaching a maximum post-fusion. This places PA in a position to regulate membrane fusion.

2.4: Discussion

In this work, we demonstrate that the production of PA via PLD1 activity is essential for exocytosis in PC12 cells. The inhibition of PLD1 or PLD1 and 2 reduces fusion events (Figure 2.6A-B). Specifically, PLD1 is required for fusion and the presence of PLD2 cannot compensate for the inhibition of PLD1 in PC12 cells (Figure 2.6). This agrees with the work of others, where the loss of PLD1 function by inhibitors, siRNA, or KO reduces stimulated secretion [29] and the frequency of fusion events in chromaffin cells [28]. A wide variety of cells, such as adipocytes [40], endothelial cells [41], mast cells [25] and neuroendocrine cells [13], [23], need PLD1 for proper secretion, albeit some cell types (mast cells) also use PLD2 during different stages of exocytosis [25].

By imaging single secretory vesicles concurrent with PLD1, PLD1 can be shown to localize with secretory vesicles, as well as Syx1 clusters under basal conditions, suggesting an association between PLD1 and secretory machinery (Figure 2.1). This places

PLD1 in a position to act when needed. As single vesicles were observed to visit the plasma membrane or dock, PLD1 intensity significantly increased (Figure 2.4A-B, D-E, G-H), indicating that PLD1 is trafficked on secretory vesicles. In regard to docking and visiting vesicles, the PLD1 intensity increase could be attributed to an increase in excitation as the vesicle moves into the TIRF field or an increase in the amount of PLD1, and these conclusions are challenging to disentangle. Therefore, we conclude that PLD1 is on vesicles as they dock and move near the plasma membrane and these results align with the established role of PLD1 in trafficking [29], [37], [38] and exocytosis [10]–[14].

One main function of PLD1 is to catalyze the production of PA from PC, where the formation of PA has been shown to interact with the polybasic region of Syx1a clusters [42] and hypothesized to stabilize negative curvature within the fusion pore [13], [43]. The role of PA and positioning of PLD1 is depicted in Figure 2.11 for docking, fusing, and visiting vesicles. Through high spatial and temporal imaging of single vesicles, the formation of PA was observed after vesicles stably dock (Figure 2.10A-C) and this formation requires PLD1 (Figure 2.10D). PA is not present on vesicles that merely visit the plasma membrane (Figure 2.7A-D) and the GFP-PASS intensity does not immediately increase as vesicles dock (Figure 2.7B-E), suggesting that PA is not carried on vesicles. Instead, vesicles dock and PA slowly accumulates (Figure 2.10A-C). It is not clear, in our work, whether PA formation occurs on the vesicle membrane or the plasma membrane, but ultrastructural studies show the accumulation of PA near or on the plasma membrane near docked vesicles [13]. PA accumulation at the plasma membrane post stimulation has also been observed in PC12 cells using cellular fractionation and mass spectrometry methods

[13], [28] and an increase in PA at the plasma membrane was also observed using fluorescence microscopy [13]. Together, this suggests that PA forms on the plasma membrane after docking. Similar to other fusion regulatory molecules, PA is not present in a cluster prior to docking; Syx1a clusters form after vesicles approach the membrane and Syx1a clusters are required for stable docking [39], [44]. PA also accumulates after vesicles dock, and we hypothesize that PA could be retained at the docking site via the established interaction with Syx1a [42].

We initially expected an increase in immobile/docked vesicles upon PLD inhibition because fusion was inhibited (Figure 2.6A-B), therefore vesicles should be waiting at the membrane, unable to secrete. However, the number of immobile vesicles was not significantly different with inhibition (Figure 2.6C). This supports the idea that PA production at the docking sites aids in stabilizing the protein machinery necessary for docking. This could occur through proteins that are known aid in docking and interact with PA, such as Syx1a. Syx1a clusters are stabilized by PA [42], essential for docking in neuroendocrine cells [44], and PLD1 accumulates at Syx1a clusters (Figure 2.1D). Others have noted that a longer treatment of high K^+ during PLD inhibition reduced docked vesicles in EM data [28], further supporting the model that PA forms due to PLD activity at vesicle docking sites. Overall, our findings suggest PA formation could be a hallmark of docked vesicles, possibly acting through Syx1a.

After secretory vesicles initially dock, the amount of PA at docked vesicle positions gradually increases (Figure 2.10B) and continues to increase throughout the stages of exocytosis where PA is present immediately prior to fusion (Figure 2.10E). PA then

30
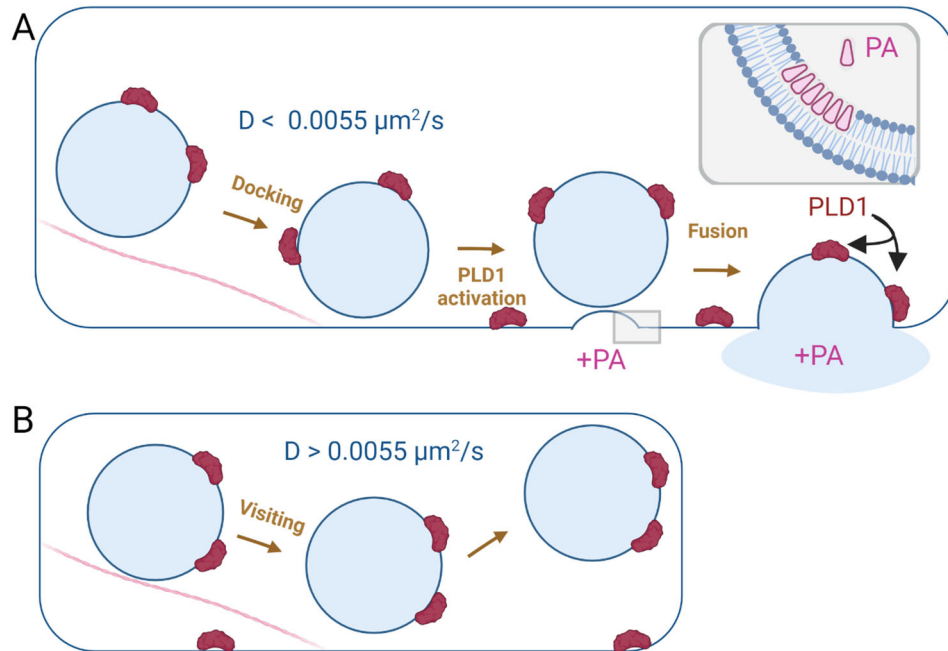
Figure 2.11: Model of PLD1 activity and localization. A) During docking and fusion, PA forms post-docking over the course of 10s of seconds and post-fusion, within seconds. *Inset:* A zoomed in look at the hypothesized role of PA pre-fusion at the grey box shown. PA has been shown to induce or sort at regions of negative membrane curvature and is hypothesized to assist with the membrane shape changes during fusion. B) Visiting secretory vesicles carry PLD1 but PA is not produced during movement. Moving vesicles move at a diffusion rate of $0.0055~\mu m^2/s$ or higher. Cartoon was created with BioRender.com.

increases post-fusion (Figure 2.7C, 2.7F, 2.7E) where GFP-PASS intensity hits a maximum at 1.4 s post fusion, on average (Figure 2.7H). To determine the source of PA, PLD1 and PLD1 and 2 were inhibited (Figure 2.9). Both inhibitors stop the accumulation of PASS at fusion sites, demonstrating that PLD1 is responsible for PA that accumulates post-fusion and the presence of PLD2 cannot compensate. PA could form *in situ* at the vesicle location or be recruited from PLD1 formed PA that is already present on the plasma membrane. Both potential sources of PA require PLD1 and cannot be compensated with PLD2 (Figure 2.9).

It is interesting to note that PLD1 is present in places where PA is not observed. For example, PLD1 is on both moving and docking vesicles (Figure 2.4), yet PA forms post-docking and post-fusion. This suggests that PLD1 is waiting for activation to begin PA production. PLD is activated by the V-ATP synthase subunit V0a1 and this interaction requires ARNO, a GEF protein for Arf6, which is an established PLD regulator [45]–[55]. This interaction happens after stimulation, suggesting that Ca^{2+} entry starts a cascade of events that leads to PA production, through these regulatory proteins. Therefore, PLD1 is present in positions where PA production could be needed, but only produces PA after activation.

Since PA is observed to be present post-fusion and PA is hypothesized as a lipid that stabilizes the fusion pore, we were curious if the amount of PA correlated to the rate of release as measured by the loss of VAMP2 from the fusion site. After binning fast fusion events from slow fusion events, more PA was observed at fast events (Figure 2.7I). The role of PA in membrane fusion is likely coupled to the proteins it interacts with. In the case of PI(4,5)P2, more PI(4,5)P2 slowed fusion by recruiting endocytic proteins that restrict fusion pore expansion [9]. Similarly, PA could also act by interacting with proteins that assist with fusion and future studies could assess the proteins involved.

Overall, PLD1 has been established as necessary for stimulated exocytosis [10]–[14]. The results shown in this work support the hypothesis that PLD1 is involved due to its production of PA. PLD1 is present on vesicles, PA is formed after vesicles dock and PA accumulates at the fusion site post-fusion. In both cases, the formation of PA depends on PLD1 activity, which cannot be compensated by PLD2.not be compensated by PLD2.

Chapter 2 References

[1]   T. Weber *et al.*, "SNAREpins: Minimal Machinery for Membrane Fusion," *Cell*, vol. 92, no. 6, pp. 759–772, Mar. 1998, doi: 10.1016/S0092-8674(00)81404-X.

[2]   R. Mohrmann, H. de Wit, M. Verhage, E. Neher, and J. B. Sørensen, "Fast Vesicle Fusion in Living Cells Requires at Least Three SNARE Complexes," *Science*, vol. 330, no. 6003, pp. 502–505, Oct. 2010, doi: 10.1126/science.1193134.

[3]   K. P. Stepien and J. Rizo, "Synaptotagmin-1–, Munc18-1–, and Munc13-1–dependent liposome fusion with a few neuronal SNAREs," *Proceedings of the National Academy of Sciences*, vol. 118, no. 4, Jan. 2021, doi: 10.1073/pnas.2019314118.

[4]   T. Lang *et al.*, "SNAREs are concentrated in cholesterol-dependent clusters that define docking and fusion sites for exocytosis.," *EMBO J*, vol. 20, no. 9, pp. 2202–13, May 2001, doi: 10.1093/emboj/20.9.2202.

[5]   A. Honigmann *et al.*, "Phosphatidylinositol 4,5-bisphosphate clusters act as molecular beacons for vesicle recruitment," *Nat Struct Mol Biol*, vol. 20, no. 6, pp. 679–686, Jun. 2013, doi: 10.1038/nsmb.2570.

[6]   J. Rohrbough and K. Broadie, "Lipid regulation of the synaptic vesicle cycle," *Nat Rev Neurosci*, vol. 6, no. 2, pp. 139–150, Feb. 2005, doi: 10.1038/nrn1608.

[7]   H. T. McMahon, M. M. Kozlov, and S. Martens, "Membrane Curvature in Synaptic Vesicle Fusion and Beyond," *Cell*, vol. 140, no. 5, pp. 601–605, Mar. 2010, doi: 10.1016/j.cell.2010.02.017.

[8]   L. V. Chernomordik and M. M. Kozlov, "Membrane Hemifusion: Crossing a Chasm in Two Leaps," *Cell*, vol. 123, no. 3, pp. 375–382, Nov. 2005, doi: 10.1016/j.cell.2005.10.015.

[9]   M. Omar-Hmeadi, A. Guček, and S. Barg, "Local PI(4,5)P2 signaling inhibits fusion pore expansion during exocytosis," *Cell Rep*, vol. 42, no. 2, p. 112036, Feb. 2023, doi: 10.1016/j.celrep.2023.112036.

[10]   Y. Humeau *et al.*, "A role for phospholipase D1 in neurotransmitter release," *Proceedings of the National Academy of Sciences*, vol. 98, no. 26, p. 15300, Dec. 2001, doi: 10.1073/pnas.261358698.

[11]   W. E. Hughes, Z. Elgundi, P. Huang, M. A. Frohman, and T. J. Biden, "Phospholipase D1 Regulates Secretagogue-stimulated Insulin Release in Pancreatic β-Cells," *Journal of Biological Chemistry*, vol. 279, no. 26, pp. 27534–27541, 2004, doi: 10.1074/jbc.M403012200.

[12]   G. M. Jenkins and M. A. Frohman, "Phospholipase D: a lipid centric review," *Cell Mol Life Sci*, vol. 62, no. 19–20, pp. 2305–2316, Oct. 2005, doi: 10.1007/s00018-005-5195-z.

[13]   M. Zeniou-Meyer *et al.*, "Phospholipase D1 Production of Phosphatidic Acid at the Plasma Membrane Promotes Exocytosis of Large Dense-core Granules at a Late Stage," *Journal of Biological Chemistry*, vol. 282, no. 30, pp. 21746–21757, 2007, doi: 10.1074/jbc.M702968200.

[14]   N. Vitale *et al.*, "Phospholipase D1: a key factor for the exocytotic machinery in neuroendocrine cells," *EMBO J*, vol. 20, no. 10, pp. 2424–2434, May 2001, doi: 10.1093/emboj/20.10.2424.

[15]   B. L. Bills and M. K. Knowles, "Phosphatidic Acid Accumulates at Areas of Curvature in Tubulated Lipid Bilayers and Liposomes," *Biomolecules*, vol. 12, no. 11, p. 1707, Nov. 2022, doi: 10.3390/biom12111707.

[16]   E. E. Kooijman, V. Chupin, B. de Kruijff, and K. N. J. Burger, "Modulation of Membrane Curvature by Phosphatidic Acid and Lysophosphatidic Acid," *Traffic*, vol. 4, no. 3, pp. 162–174, Mar. 2003, doi: 10.1034/j.1600-0854.2003.00086.x.

[17]   A. Callan-Jones, B. Sorre, and P. Bassereau, "Curvature-driven lipid sorting in biomembranes.," *Cold Spring Harb Perspect Biol*, vol. 3, no. 2, Feb. 2011, doi: 10.1101/cshperspect.a004648.

[18]   F. D. Brown *et al.*, "Phospholipase D1 localises to secretory granules and lysosomes and is plasma-membrane translocated on cellular stimulation," *Current Biology*, vol. 8, no. 14, pp. 835–838, Jul. 1998, doi: 10.1016/S0960-9822(98)70326-4.

[19]   S. Cockcroft, G. Way, N. O'Luanaigh, R. Pardo, E. Sarri, and A. Fensome, "Signalling role for ARF and phospholipase D in mast cell exocytosis stimulated by crosslinking of the high affinity FcεR1 receptor," *Mol Immunol*, vol. 38, no. 16–18, pp. 1277–1282, Sep. 2002, doi: 10.1016/S0161-5890(02)00075-5.

[20]   M. A. Frohman, "The phospholipase D superfamily as therapeutic targets," *Trends Pharmacol Sci*, vol. 36, no. 3, pp. 137–144, Mar. 2015, doi: 10.1016/J.TIPS.2015.01.001.

[21]   X. Peng and M. A. Frohman, "Mammalian phospholipase D physiological and pathological roles," *Acta Physiologica*, vol. 204, no. 2, pp. 219–226, Feb. 2012, doi: 10.1111/j.1748-1716.2011.02298.x.

[22]   J. Stutchfield and S. Cockcroft, "Correlation between secretion and phospholipase D activation in differentiated HL60 cells," *Biochemical Journal*, vol. 293, no. 3, pp. 649–655, Aug. 1993, doi: 10.1042/bj2930649.

[23] M. Zeniou-Meyer, A. Béglé, M.-F. Bader, and N. Vitale, "The Coffin-Lowry Syndrome-associated Protein RSK2 Controls Neuroendocrine Secretion through the Regulation of Phospholipase D1 at the Exocytotic Sites," *Ann N Y Acad Sci*, vol. 1152, no. 1, pp. 201–208, Jan. 2009, doi: 10.1111/j.1749-6632.2008.04001.x.

[24] R. Haslam and J. Coorssen, "Evidence that activation of phospholipase D can mediate secretion from permeabilized platelets ," *Advances in experimental medicine and biology* , vol. 344, pp. 149–164, 1993, doi: 10.1007/978-1-4615-2994-1_11.

[25] W. S. Choi, Y. M. Kim, C. Combs, M. A. Frohman, and M. A. Beaven, "Phospholipases D1 and D2 Regulate Different Phases of Exocytosis in Mast Cells," *The Journal of Immunology*, vol. 168, no. 11, pp. 5682–5689, Jun. 2002, doi: 10.4049/jimmunol.168.11.5682.

[26] Y. Hozumi, M. Yamazaki, and T. Nakano, "Immunocytochemistry of phospholipase D1 and D2 in cultured cells," *Biochem Biophys Res Commun*, vol. 625, pp. 161–166, Oct. 2022, doi: 10.1016/J.BBRC.2022.07.118.

[27] Z. Freyberg, D. Sweeney, A. Siddhanta, S. Bourgoin, M. Frohman, and D. Shields, "Intracellular Localization of Phospholipase D1 in Mammalian Cells," *Mol Biol Cell*, vol. 12, no. 4, pp. 943–955, Apr. 2001, doi: 10.1091/mbc.12.4.943.

[28] E. Tanguy *et al.*, "Mono- and Poly-unsaturated Phosphatidic Acid Regulate Distinct Steps of Regulated Exocytosis in Neuroendocrine Cells," *Cell Rep*, vol. 32, no. 7, p. 108026, Aug. 2020, doi: 10.1016/j.celrep.2020.108026.

[29] E. Tanguy *et al.*, "Phospholipase D1-generated phosphatidic acid modulates secretory granule trafficking from biogenesis to compensatory endocytosis in neuroendocrine cells," *Adv Biol Regul*, vol. 83, p. 100844, Jan. 2022, doi: 10.1016/J.JBIOR.2021.100844.

[30] T. W. Bumpus and J. M. Baskin, "Clickable Substrate Mimics Enable Imaging of Phospholipase D Activity," *ACS Cent Sci*, vol. 3, no. 10, pp. 1070–1077, Oct. 2017, doi: 10.1021/acscentsci.7b00222.

[31] E. E. Kooijman *et al.*, "Spontaneous Curvature of Phosphatidic Acid and Lysophosphatidic Acid," *Biochemistry*, vol. 44, no. 6, pp. 2097–2102, Feb. 2005, doi: 10.1021/bi0478502.

[32] F. Zhang *et al.*, "Temporal Production of the Signaling Lipid Phosphatidic Acid by Phospholipase D2 Determines the Output of Extracellular Signal-Regulated Kinase Signaling in Cancer Cells," *Mol Cell Biol*, vol. 34, no. 1, pp. 84–95, Jan. 2014, doi: 10.1128/MCB.00987-13.

[33] A. Mahmood *et al.*, "Exosome secretion kinetics are controlled by temperature," *Biophys J*, vol. 122, no. 7, pp. 1301–1314, Apr. 2023, doi: 10.1016/j.bpj.2023.02.025.

[34] A. Edelstein, N. Amodaj, K. Hoover, R. Vale, and N. Stuurman, "Computer Control of Microscopes Using µManager," *Curr Protoc Mol Biol*, vol. 92, no. 1, Oct. 2010, doi: 10.1002/0471142727.mb1420s92.

[35] J. C. Crocker and D. G. Grier, "Methods of Digital Video Microscopy for Colloidal Studies," *J Colloid Interface Sci*, vol. 179, no. 1, pp. 298–310, Apr. 1996, doi: 10.1006/jcis.1996.0217.

[36] A. Liu *et al.*, "pHmScarlet is a pH-sensitive red fluorescent protein to monitor exocytosis docking and fusion steps," *Nat Commun*, vol. 12, no. 1, p. 1413, Mar. 2021, doi: 10.1038/s41467-021-21666-7.

[37] L. Brito De Souza, L. Lamberti Pinto Da Silva, M. Cé Lia Jamur, and C. Oliver, "Phospholipase D Is Involved in the Formation of Golgi Associated Clathrin Coated Vesicles in Human Parotid Duct Cells," 2014, doi: 10.1371/journal.pone.0091868.

[38] L.-D. Luo, G. Li, and Y. Wang, "PLD1 promotes dendritic spine development by inhibiting ADAM10-mediated N-cadherin cleavage OPEN," 2017, doi: 10.1038/s41598-017-06121-2.

[39] S. Barg, M. K. Knowles, X. Chen, M. Midorikawa, and W. Almers, "Syntaxin clusters assemble reversibly at sites of secretory granules in live cells," *Proceedings of the National Academy of Sciences*, vol. 107, no. 48, pp. 20804–20809, Nov. 2010, doi: 10.1073/pnas.1014823107.

[40] P. Huang, Y. M. Altshuller, J. C. Hou, J. E. Pessin, and M. A. Frohman, "Insulin-stimulated plasma membrane fusion of Glut4 glucose transporter-containing vesicles is regulated by phospholipase D1," *Mol Biol Cell*, vol. 16, no. 6, pp. 2614–2623, Jun. 2005, doi: 10.1091/mbc.e04-12-1124.

[41] J. Disse, N. Vitale, M.-F. Bader, and V. Gerke, "Phospholipase D1 is specifically required for regulated secretion of von Willebrand factor from endothelial cells," *Blood*, vol. 113, no. 4, pp. 973–980, Jan. 2009, doi: 10.1182/blood-2008-06-165282.

[42] A. D. Lam, P. Tryoen-Toth, B. Tsai, N. Vitale, and E. L. Stuenkel, "SNARE-catalyzed fusion events are regulated by Syntaxin1A-lipid interactions," *Mol Biol Cell*, vol. 19, no. 2, pp. 485–497, Feb. 2008, doi: 10.1091/mbc.e07-02-0148.

[43] S. Gasman and N. Vitale, "Lipid remodelling in neuroendocrine secretion," *Biol Cell*, vol. 109, no. 11, pp. 381–390, Nov. 2017, doi: 10.1111/boc.201700030.

[44] M. K. Knowles, S. Barg, L. Wan, M. Midorikawa, X. Chen, and W. Almers, "Single secretory granules of live cells recruit syntaxin-1 and synaptosomal associated protein 25 (SNAP-25) in large copy numbers," *Proceedings of the National Academy of Sciences*, vol. 107, no. 48, pp. 20810–20815, Nov. 2010, doi: 10.1073/pnas.1014840107.

[45] Q. Wang *et al.*, "V-ATPase modulates exocytosis in neuroendocrine cells through the activation of the ARNO-Arf6-PLD pathway and the synthesis of phosphatidic acid," *Front Mol Biosci*, vol. 10, Apr. 2023, doi: 10.3389/fmolb.2023.1163545.

[46] M.-C. Galas, J. B. Helms, N. Vitale, D. Thiersé, D. Aunis, and M.-F. Bader, "Regulated Exocytosis in Chromaffin Cells," *Journal of Biological Chemistry*, vol. 272, no. 5, pp. 2788–2793, Jan. 1997, doi: 10.1074/jbc.272.5.2788.

[47] A.-S. Caumont, M.-C. Galas, N. Vitale, D. Aunis, and M.-F. Bader, "Regulated Exocytosis in Chromaffin Cells," *Journal of Biological Chemistry*, vol. 273, no. 3, pp. 1373–1379, Jan. 1998, doi: 10.1074/jbc.273.3.1373.

[48] A.-S. Caumont, N. Vitale, M. Gensse, M.-C. Galas, J. E. Casanova, and M.-F. Bader, "Identification of a Plasma Membrane-associated Guanine Nucleotide Exchange Factor for ARF6 in Chromaffin Cells," *Journal of Biological Chemistry*, vol. 275, no. 21, pp. 15637–15644, May 2000, doi: 10.1074/jbc.M908347199.

[49] C. Z. Yang and M. Mueckler, "ADP-ribosylation Factor 6 (ARF6) Defines Two Insulin-regulated Secretory Pathways in Adipocytes," *Journal of Biological Chemistry*, vol. 274, no. 36, pp. 25297–25300, Sep. 1999, doi: 10.1074/jbc.274.36.25297.

[50] N. Vitale, S. Chasserot-Golaz, and M.-F. Bader, "Regulated Secretion in Chromaffin Cells," *Ann N Y Acad Sci*, vol. 971, no. 1, pp. 193–200, Oct. 2002, doi: 10.1111/j.1749-6632.2002.tb04463.x.

[51] N. Vitale, S. Chasserot-Golaz, Y. Bailly, N. Morinaga, M. A. Frohman, and M.-F. Bader, "Calcium-regulated exocytosis of dense-core vesicles requires the activation of ADP-ribosylation factor (ARF)6 by ARF nucleotide binding site opener at the plasma membrane," *Journal of Cell Biology*, vol. 159, no. 1, pp. 79–89, Oct. 2002, doi: 10.1083/jcb.200203027.

[52] J. Matsukawa, K. Nakayama, T. Nagao, H. Ichijo, and T. Urushidani, "Role of ADP-ribosylation Factor 6 (ARF6) in Gastric Acid Secretion," *Journal of Biological Chemistry*, vol. 278, no. 38, pp. 36470–36475, Sep. 2003, doi: 10.1074/jbc.M305444200.

[53] L. Liu *et al.*, "SCAMP2 Interacts with Arf6 and Phospholipase D1 and Links Their Function to Exocytotic Fusion Pore Formation in PC12 Cells," *Mol Biol Cell*, vol. 16, no. 10, pp. 4463–4472, Oct. 2005, doi: 10.1091/mbc.e05-03-0231.

[54] A. Béglé, P. Tryoen-Tóth, J. de Barry, M.-F. Bader, and N. Vitale, "ARF6 Regulates the Synthesis of Fusogenic Lipids for Calcium-regulated Exocytosis in Neuroendocrine Cells," *Journal of Biological Chemistry*, vol. 284, no. 8, pp. 4836–4845, Feb. 2009, doi: 10.1074/jbc.M806894200.

[55] L. E. Pelletán *et al.*, "ADP Ribosylation Factor 6 (ARF6) Promotes Acrosomal Exocytosis by Modulating Lipid Turnover and Rab3A Activation," *Journal of Biological Chemistry*, vol. 290, no. 15, pp. 9823–9841, Apr. 2015, doi: 10.1074/jbc.M114.629006.

Chapter Three: Phospholipase D1 Affects Late Endosome Fate and Produces

Phosphatidic Acid at Sites of Docked Multivesicular Endosome

Phospholipase D1 (PLD1) is an enzyme essential for secretion of exosomes, which are released from multivesicular endosomes (MVEs). Others have shown that PLD1 localizes to the plasma membrane and MVEs, and inhibition or knockouts of PLD1 significantly diminishes secretion of small extracellular vesicles (EVs). However, when and where PLD1 and phosphatidic acid (PA) are required in the MVE cycle is unknown. In this chapter, fluorescently-tagged PLD1 and a PA binding protein are used in tandem with an MVE marker (CD63-pHmScarlet) under total internal reflection fluorescence microscopy to monitor the presence of PLD1 and formation of PA during the secretion of exosomes. Single MVEs were observed during three stages of exosome secretion; visiting, docking and fusion, and the corresponding PLD1 or PA channel were quantified to identify their presence and formation. PLD1 is present on MVEs at all stages. PLD1 or PLD1/2 inhibition significantly reduces the rate of both docking and fusing MVEs, but not PLD1 localization to MVEs. PA is produced slowly (~10 s) during docking, and this production is also eliminated under PLD1 inhibition. PLD1 production of PA is necessary for stable MVE docking, potentially regulating release of exosomes. When small EVs are collected, isolated and measured for amount by blotting methods or particle counting, PLD1 or PLD1/2 inhibition reduces the amount of EVs secreted. In events that do occur under PLD inhibition, PA production is reduced during docking but not fusion. PLD1 inhibition

additionally increases the density of lysosomes containing Magic Red, a dye specific to catalytically active lysosomes. Together, these results indicate a role for PLD1 in endosome fate and exosome secretion.

In order, co-authors for this section include an undergraduate student, Megan Hulser, and graduate student, Melodie Nguyen, who assisted with data collection and analysis in this chapter (~5% each). Michelle Knowles assisted with revising writing (~20%).

Non co-authors who contributed include Schuyler van Engelenburg and Claire Jiang, who cloned the CD63-pHmScarlet probe used. Christina Coughlan at the University of Colorado Anschutz helped us use her NanoSight for small EV statistics.

3.1: Introduction

There are multiple classes of late endosomes, with a continuum between secretory MVEs and catalytic lysosomes [1]–[3]. MVEs are a class of late endosomes in which intraluminal vesicles are formed [4]–[6]. MVEs can then fuse with the plasma membrane, releasing their ILVs as exosomes [6]–[9]. Exosomes function as a method of intercellular communication, as well as maintaining cellular functions such as motility [10], [11] and homeostasis [12]. Small molecule secretion is generally limited to nearby cells, but exosomes can communicate with cells further away [13]–[15]. While this pathway is necessary for healthy cells, it is also involved in cancer metastasis [13]–[16] and neurodegenerative disorders [17]–[19], where disease states are thought to spread to the transfer of unhealthy biomolecules to healthy cells [6], [20]–[23]. Proteins involved in

MVEs could also affect the fate of late endosomes, favoring either CD63+ MVEs or catalytically active lysosomes. For instance, inhibition of endolysosome fusion increases secreted exosomes [1]–[3].

There are various endosomal proteins that are present on MVEs/exosomes, particularly the tetraspanin protein, CD63 [24]–[27], which can be used as markers for observing MVE trafficking and fusion. Multiple labs have produced pH-sensitive fluorescently tagged CD63 (particularly, pHluorin and pHuji) to image exosome secretion [24]–[26]. Because both the N- and C-termini of CD63 are exposed to the more neutral cytosolic pH, pH probes are located midway in the protein on one of the luminal turns. As the probe is exposed to a more neutral pH during membrane fusion, it brightens significantly, allowing for fusion to be visualized as in Chapter 2. In this chapter, a pHmScarlet probe was developed with help of our collaborators, the van Engelenburg lab.

PLD1 and PLD2 have been implicated in MVE formation and secretion [28]. These proteins cleave choline from phosphatidylcholine, creating PA. In mammals, there are six isoforms, with PLD1 and PLD2 being catalytically active and specific to phosphatidylcholine [29]. PLD1, particularly, is required for exocytosis in many cell types [30]–[37]. In addition to its role in stimulated exocytosis, PLD1 has been shown to localize to the plasma membrane and multiple classes of endosomes [38]–[43]. PLD1 appears to be involved throughout the endocytic pathway. It is required for certain types of endocytosis, particularly receptor-induced and compensatory endocytosis [44]–[47]. PLD1 has also been shown to be involved in various late endosome processes, such as regulating autophagy [48]–[50] and exosome secretion [51].

PLDs and exosomes both play roles in cancers [13]–[16], [28], [52]–[68], and evidence supports a role for PLD1 in MVEs [28], [51], [69]. PLD1 is overexpressed in various cancers, including melanoma and certain breast cancers. PLD1 has been implicated in many cancer functions including apoptosis suppression [52]–[54], cancer proliferation [55]–[57], angiogenesis [58], [59], metastasis [58], [60] and exosome release [28], [51], [69]. Exosomes are also associated with cancer proliferation, and exosomes can serve as markers for metastasis [13]–[16], [61]–[68]. Previous work has already shown that PLD1 produces PA in some MVEs [51]. However, imaging of PLD1 and PA during the various stages of MVE development and secretion is lacking. This makes PLD1 an interesting target to study using imaging methods.

Analogous to the methods described in Chapter 2, GFP-PLD1 and GFP-PA biosensor with superior sensitivity (GFP-PASS) were measured concurrent with imaging MVEs during visiting, docking and fusing events. CD63 was used as an MVE marker, with a pH-sensitive probe, pHmScarlet, on the first extracellular loop. Red fluorescent protein-tagged lysosome associated membrane protein-1 (LAMP1-RFP) was used to identify whether PLD1/PASS localized to late endosomes in general, particularly lysosomes. Single fusion events were imaged to measure PLD1 and PASS presence as MVEs docked and fused. PLD1 colocalizes to CD63+ MVEs to a higher extent than LAMP1+ late endosomes, and is present on mobile and fusing MVEs. Additionally, PA localizes to MVEs slowly during docking and quickly during fusion. The former is PLD1-dependent, but PA production/recruitment during fusion appears to be PLD1-independent. PLD1 inhibition also increases concentration of lysosomes at the cell surface.

3.2: Materials and Methods

Cell Culture:

A549 cells were cultured in Dulbecco's modified eagle medium (DMEM, ThermoFisher, Waltham, MA, USA) with 10% fetal bovine serum (ThermoFisher, Waltham, MA, USA), incubated at 37°C and 5% CO_2. For imaging, cells were plated in 8 well plates (Cellvis, Mountain View, CA, USA) treated with poly-L-lysine (Sigma Aldrich, St. Louis, MO, USA). Cells were transfected with DNA encoding fluorescently tagged proteins with Lipofectamine 2000 (ThermoFisher, Waltham, MA, USA) and plasmids (25-100 ng/well). The EGFP-PLD1 plasmid was a gift from Jeremy Baskin [70]. GFP-PASS was a gift from Guangwei Du (Addgene plasmid # 193970) [71]. Cells were tested for mycoplasma using MycoFluor (ThermoFisher, Waltham, MA, USA) according to manufacturer protocols.

For immunostaining, A549 cells expressing CD63-GFP were fixed in 3.2% paraformaldehyde (Electron Microscopy Sciences, Hatfield, PA, USA) for 30 minutes and immediately permeabilized with 0.1% Triton-X 100 (Sigma Aldrich, St. Louis, MO, USA) for 10 minutes. Cells were then blocked in 0.5 mg/mL BSA (ThermoFisher, Waltham, MA, USA) for 4 hours at 4°C and treated with mouse anti-PLD1 (Santa Cruz Biotechnology, Santa Cruz, CA, USA) overnight. Cells were then treated with Alexa-594 conjugated rabbit anti-mouse (ThermoFisher, Waltham, MA, USA) for 4 hours. Transfection efficiency was 50-60% based on the number of cells observed to be transfected.

Total Internal Reflection Fluorescence Microscopy:

A549 cells were imaged in Fluobrite DMEM (ThermoFisher, Waltham, MA, USA) using a TIRF microscope (Nikon Ti-U) and 491 nm and 561 nm lasers, described previously [72]. A 60x 1.49 NA objective and 2.5x magnifying lens were used with an EMCCD (Andor iXon897, Abingdon, UK). A DualView was used to split red and green fluorescence channels with a 565LP dichroic filter and 525/50 and 605/75 emission filters (Chroma Technologies, Bellows Falls, VT, USA). Both colors were imaged simultaneously via MicroManager at 0.109 µm/pixel and 136 ms/frame [73]. In inhibition studies, a stage heater maintaining cells at 37°C. Otherwise, cells were imaged at room temperature.

In PLD inhibition experiments, cells were incubated with 0.013% DMSO alone or with 100 nM pan-PLD inhibitor 5-fluoro-2-indolyl des-chlorohalopemide (PLD1/2$_i$, Sigma Aldrich, St. Louis, MO, USA) or 500 nM PLD1-specific inhibitor VU0155069 (PLD1$_i$, Sigma Aldrich, St. Louis, MO, USA). Cells were treated for 30 minutes at 37°C and imaged immediately. For Brefeldin A (BfA) studies, cells were transfected with CD63-pHmScarlet and incubated with 0.1% DMSO with or without 5 µg/mL BfA for 60 minutes at 37°C and imaged immediately.

Image Analysis:

As in Chapter 2, PLD1 localization was measured using $\Delta F/S$, as defined in Equation 3.1, where C is the average intensity of a 7 pixel diameter circle, A is the average

intensity of a 1 pixel wide annulus 1 pixel removed, and background is the average intensity surrounding the cell.

$$\frac{\Delta F}{S} = \frac{C-A}{A-bg} \tag{3.1}$$

Using fusion code described in Chapter 2, we identify sites of visiting, docking and fusing MVEs. However, for this project the fusion code was modified to calculate a modified, normalized $\Delta F/S$, $\Delta F/F_{max}$ (Equation 3.2), where A_i is the initial annulus intensity 0.1 s to 0.5 s before onset:

$$\frac{\Delta F}{\Delta F_{max}} = \frac{C-A_i}{C_{max}-A_i} \tag{3.2}$$

The strength of this measurement is that values are not forced to 0 prior to fusion. Additionally, the annulus, which increases in intensity as fluorescent probes spread after fusion, does not alter the intensity over time, because only the pre-fusion annulus intensity is used. This alteration allowed quantification of events where MVEs were docked prior to fusion, without losing that information by forcing the initial intensity to zero. One strength of pHmScarlet as a probe is that it allows visualization of proteins prior to fusion.

GFP-PLD1, GFP-PASS and cytosolic GFP were normalized using $\Delta F/F$ to measure the *change* of intensity (Equation 3.3), where C_t, C_0 and C_{max} are the average circle intensity at frame t, the average from 0.5 to 0.1 s prior to event onset, and the maximum circle intensity throughout the event, respectively:

$$\frac{\Delta F}{F} = \frac{C_t-C_0}{C_{max}-C_0} \tag{3.3}$$

Exosome Collection and Slot Blots:

Exosomes were collected using ExoQuick-TC (Systems Biosciences, Palo Alto, CA, USA) from A549 cells cultured in T75 flasks (CELLTREAT, Life Science Products, Frederick, CO, USA) for 48 hours after reaching 70-80% confluency following manufacturer's protocol. Cells were treated with identical concentrations of drugs as fluorescence experiments, for the duration of exosome collection.

Cells were grown in either T25 or T75 flasks (CELLTREAT, Life Science Products, Frederick, CO, USA) until reaching 70-80% confluency. In overexpression studies, cells were transfected with identical concentrations of plasmids (0.125 ng GFP-PLD1 plasmid/µL media) and Lipofectamine 2000 for 24 hours. Inhibition experiments followed the same duration as mentioned for exosome collection. Cells were trypsinized for 10-15 minutes until no longer attached to the flask, centrifuged, and rinsed with DMEM. Cells were centrifuged again and resuspended with a lysis buffer (50 mM Tris-HCl, 150 mM NaCl, 0.1% Triton X-100, 0.5% sodium deoxycholate, 0.1% sodium dodecyl sulfate, 1 mM sodium orthovanadate, 1 mM NaF, pH 8.0) on ice for 30 minutes and passed through a syringe until homogenous. 2x Laemmli buffer with 5% β-mercaptoethanol were added at equal proportions.

Once small EVs or cell lysate were collected, a slot blot (Bio-Rad, Hercules, CA, USA) was used with a nitrocellulose membrane (Genesee Scientific, El Cajon, CA, USA). Primary antibodies were incubated overnight at 4°C with constant agitation. Blots were then incubated in a fluorescent, secondary antibody for 4 hours and imaged using a ChemiDoc (Bio-Rad, Hercules, CA, USA). Small EVs were also collected and imaged

using a NanoSight NS300 (Malvern Panalytical, Malvern, UK), which was used to measure the concentration and size of collected extracellular vesicles.

3.3: Results

Phospholipase D1 Localizes to Late Endosomes

To determine if PLD1 was involved in exosome secretion, A549 cells transiently transfected with GFP-PLD1 and either CD63-pHmScarlet or LAMP1-RFP were imaged under TIRF microscopy (Figure 3.1A,B). CD63 predominantly labels MVEs, but it can be present on lysosomes as well [74]. Conversely, LAMP1 predominantly labels lysosomes but can be present on fusing MVEs [74]. PLD1 visually localizes with both of these proteins. To quantify colocalization, an object-based colocalization methods was used where the location of punctate spots in the LAMP1 or CD63 channel were selected and the
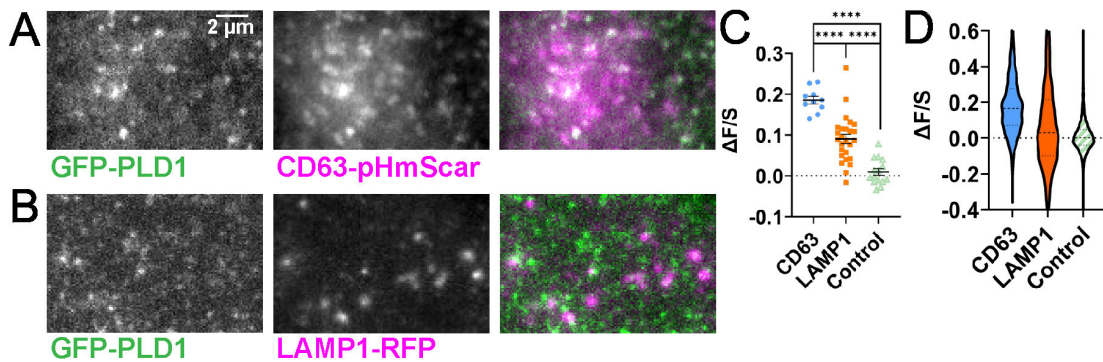
Figure 3.1: Phospholipase D1 Localizes to Late Endosomes. A,B) A549 cells were transfected with GFP-PLD1 (left) and A) CD63-pHmScarlet or B) LAMP1-RFP (middle) and imaged at room temperature using TIRF microscopy. Scale bar: 2 μm. C) ΔF/S of GFP-PLD1 at sites of CD63 (blue circles) or LAMP1 (orange squares), compared to cytosolic GFP at sites of CD63 as a negative control (green triangles). Each point represents the average of one cell. Lines are overall averages, error bars are SEM (n ≥ 17 cells), **** p < 0.0001. D) A violin plot of ΔF/S values for individual CD63 or LAMP1 spots showing distribution of GFP-PLD1 intensity. (n ≥ 3630 spots)

intensity, $\Delta F/S$, of PLD1 in the other channel was measured at those locations. The $\Delta F/S$ of GFP-PLD1 was measured as described in Equation 3.1 in Methods. The $\Delta F/S$ of GFP-PLD1 is significantly higher for both CD63 and LAMP1 than cytosolic GFP is (Figure 3.1C), indicating colocalization. Additionally, GFP-PLD1 is more present on CD63+ late endosomes than LAMP1+ late endosomes, and the distribution of individual endosomes further suggests this (Figure 3.1D). These results indicate that PLD1 localized to multiple populations of late endosomes, but especially MVEs.

One limitation of overexpressing PLD1 is that it may affect localization, as another study suggests [39]. By eye, GFP-PLD1 is not highly expressed, as cells are very dim compared to cells that express other proteins, like cytosolic GFP (Figure 3.2A). This suggests that GFP-PLD1 is not significantly overexpressed compared to endogenous PLD1. To further verify this, overexpression of PLD1 was quantified by slot blot (Figure 3.2B). PLD1 is overexpressed by approximately 40%. Given that about 50-60% of cells are transfected (Figure 3.2C), PLD1 is on average overexpressed by 80%. This value is higher than that identified in PC12 cells (17%). To determine if colocalization is affected, A549 cells expressing CD63-pHluorin were fixed and stained with anti-PLD1, which is present at sites of CD63-pHluorin (Figure 3.2D). Endogenous PLD1 colocalizes to CD63.
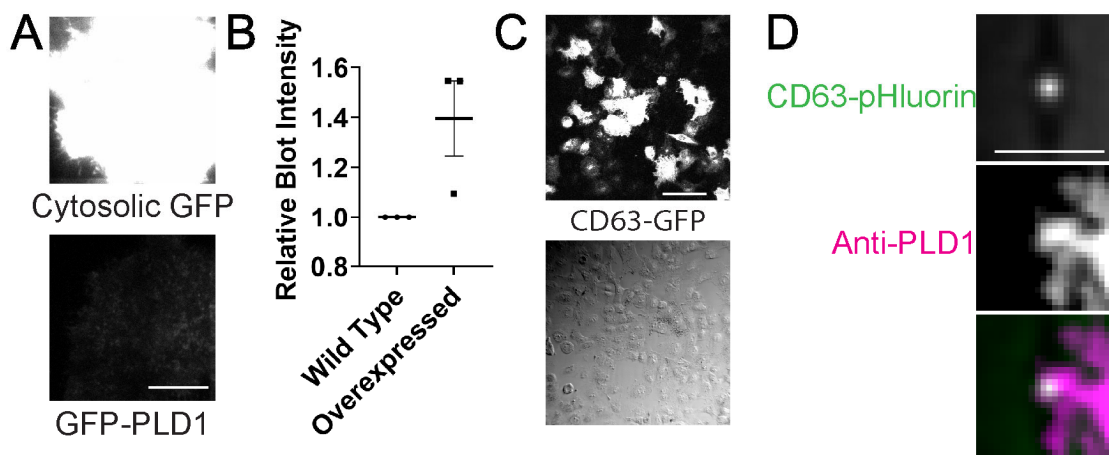
Figure 3.2: Overexpression and Immunostaining of PLD1. A) A549 cells expressing cytosolic GFP (top) or GFP-PLD1 (bottom) contrasted identically to show difference in expression levels. Scale bar: 5 μm. B) Normalized and corrected intensity of bands for PLD1. Values were corrected by normalizing to actin from the same cell lysate, then divided by the value of wild type cells from the same day. Lines are average, error bars are SEM (n = 3 days). C) Image of cells expressing CD63-GFP (top) and transmitted DIC image (bottom) of the same field of cells. Scale bar: 100 μm. D) Cells expressing CD63-pHluorin (top) were fixed, permeabilized and stained with anti-PLD1 and Alexa594-labeled anti-mouse (middle). Spots of CD63 were identified and cropped and averaged. An overlay of the two is shown (bottom). Scale bar: 2 μm.

CD63-pHmScarlet Allows Imaging of MVEs Before and After Fusion in One Channel

The CD63-pHmScarlet probe used in this chapter is newly developed with the help of other labs, including the van Engelenburg lab, as well as the lab that developed the VAMP2-pHmScarlet probe [75]. To test its function as a probe, A549 cells co-transfected with an established CD63-pHluorin probe and CD63-pHmScarlet were imaged (Figure 3.3A). Fusion events were then identified, and both channels were cropped (Figure 3.3B). Then, $\Delta F/\Delta F_{max}$ values for these events were plotted over time in both channels (Figure 3.3C).
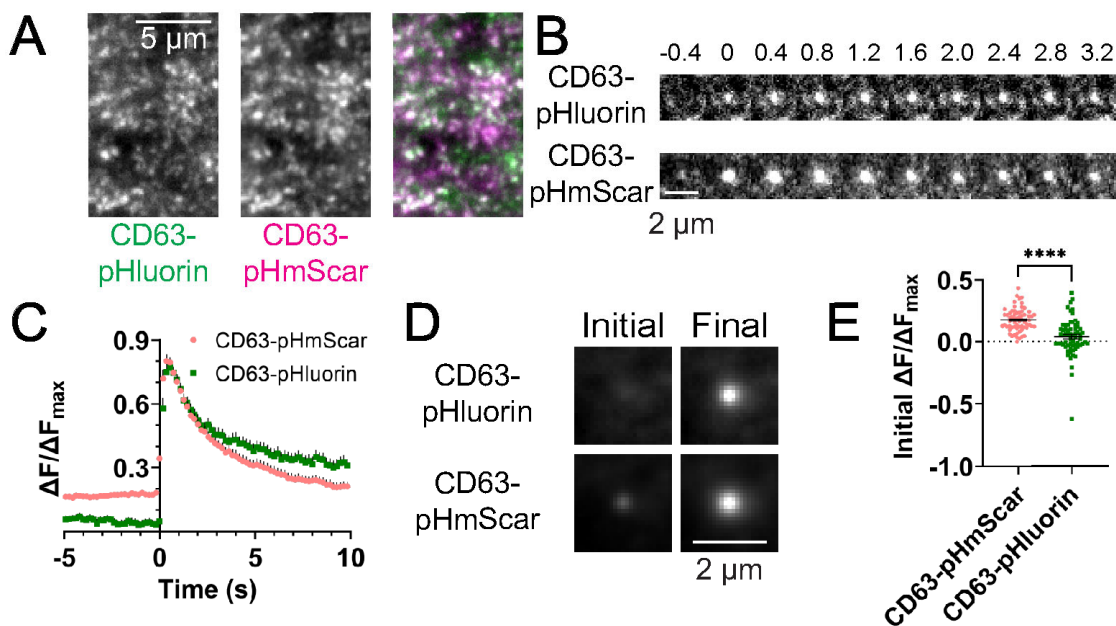
Figure 3.3: CD63-pHmScarlet Colocalizes with CD63-pHluorin and Can Be Measured Prior to Fusion. A) A549 cells expressing CD63-pHluorin (left) and CD63-pHmScarlet (middle) were imaged by TIRF microscopy. Scale bar: 5 μm. B) A montage of a fusion event. Every 4 frames were cropped from 0.4 s prior to fusion to 3.2 s after. Scale bar: 2 μm. C) Average trace of CD63-pHmScarlet (pink circles) and CD63-pHluorin (green squares). Error bars are SEM (n = 65 events). D) Average images of 52 fusion events of CD63-pHluorin (top) and CD63-pHmScarlet (bottom) for 5 frames prior to event onset (left) and at event peak (right). Scale bar: 2 μm. E) Average $\Delta F/\Delta F_{max}$ of CD63-pHmScarlet (pink circles) and CD63-pHluorin (green squares) for 3 frames prior to fusion. Each point is one event. Lines are averages, error bars are SEM. **** $p < 0.0001$.

Because pHmScarlet is not completely quenched under acidic conditions [75], its fusion traces begin significantly above zero (approximately 0.18), while pHluorin remains lower on average (~ 0.04). To visualize this, 52 events were averaged, and CD63 was observed before and during fusion (Figure 3.3D); events within 100 frames of the end of the movie were excluded from averaging. To confirm that pHmScarlet is significantly visible prior to fusion, initial values were quantified to show that pHmScarlet allows docked MVEs to be observed prior to fusion (Figure 3.3E). Overall, both probes are seen

during all fusion events, and the decays are similar. CD63-pHmScarlet decays slightly faster, possibly due to photobleaching. One strength of pHmScarlet as a probe is the visualization of MVEs during all stages. This probe is used throughout the chapter.

Phospholipase D1 Is Present at Sites of Visiting and Fusing MVEs

A549 cells expressing GFP-PLD1 and CD63-pHmScarlet were imaged in time using TIRF microscopy. Events that displayed a change in intensity in the CD63 channel were then located using a previously established method [72]. MVEs were divided into visiting, docking and fusing events based on whether the MVE moved through a movie (Figure 3.4A), appeared and remained static for several seconds (Figure 3.4B), or quickly brightened and spread from the center of the event (Figure 3.4C). To visualize the change
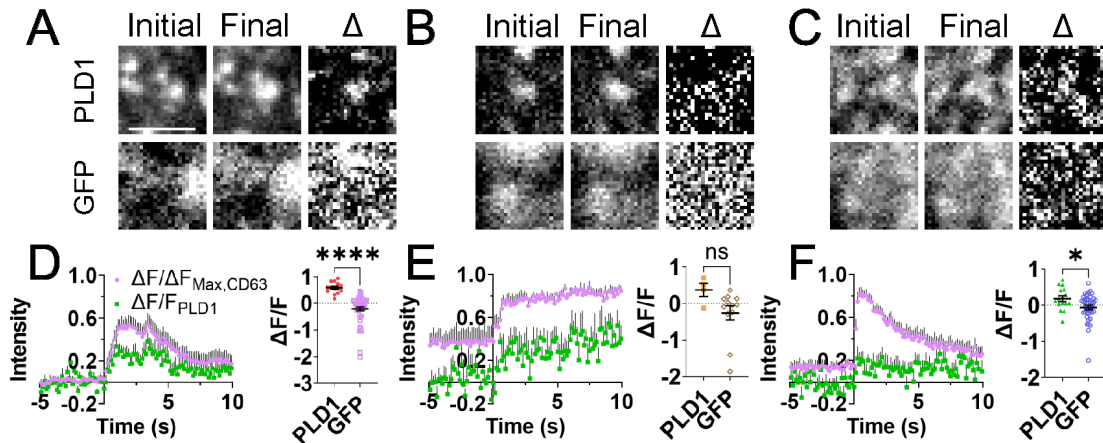
Figure 3.4: PLD1 Is Present on Visiting and Fusing MVEs. A-C) Average images of many visiting (A, 14 PLD1 and 44 GFP events), docking (B, 4 and 11 events) or fusing (C, 13 and 21 events) events at the onset (left) and peak/plateau (middle) for GFP-PLD1 (top) and cytosolic GFP (bottom). A difference image of each was produced (right). Initial and final images are contrasted identically. Scale bar: 2 μm. D-F) Left: Average intensity traces of CD63 (pink circles) and PLD1 (green squares) for visiting (D, n = 14), docking (E, n = 4) and fusing (F, n = 11) MVEs. Right: $\Delta F/F$ values of PLD1 (solid) and GFP (empty). Error bars are SEM, * $p < 0.05$, **** $p < 0.0001$.

in intensity, an average image of all events 0.5 to 0.1 s prior to onset and at the peak of CD63 intensity were made. Qualitatively, PLD1 is present on all three classes of MVEs, increasing in intensity during visiting and fusion (Figure 3.4D-F). Quantitative analysis of the amount of fluorescence present at MVE visiting, docking and fusion sites confirms this, with the average $\Delta F/F$ values at CD63 peak intensity during both of these classes of events being positive. Cytosolic GFP was used as a control. It should be noted that during docking there is a slight increase in PLD1 intensity but not cytosolic GFP. However, this value does not test statistically significant, and while there is a visible increase in intensity and the difference image, it is dim. This is likely due to the rarity of identified docking events. Overall, these results indicate that PLD1 is present on MVEs and trafficked with them.

CD63 Fusion Events Are Not Trafficked from the Golgi Apparatus

To confirm that CD63+ fusion events were MVE events and not CD63 being trafficked to the plasma membrane from the Golgi apparatus, fusion events were quantified in cells treated with Brefeldin A (BfA), which blocks Golgi activity by redistributing Golgi material to the ER [76]. A549 cells expressing CD63-pHmScarlet were treated with 0.1% DMSO with or without 5 µg/mL BfA and fusion events were averaged. Because VAMP2+ exocytosis is reduced with BfA [77]–[79], we expected that BfA would significantly reduce the rate of VAMP2 fusion. PC12 cells were used for this experiment due to their ability to be stimulated with KCl. These values were plotted alongside average VAMP2 events in stimulated PC12 cells with no drug treatment, normalized using $\Delta F/\Delta F_{max}$ (Figure 3.5A). Frequency of events were also quantified. There was no significant effect of BfA on CD63

event frequency (Figure 3.5B). To ensure that BfA was working as expected, PC12 cells

expressing VAMP2-pHmScarlet were treated with 0.1% DMSO with or without 5 µg/mL
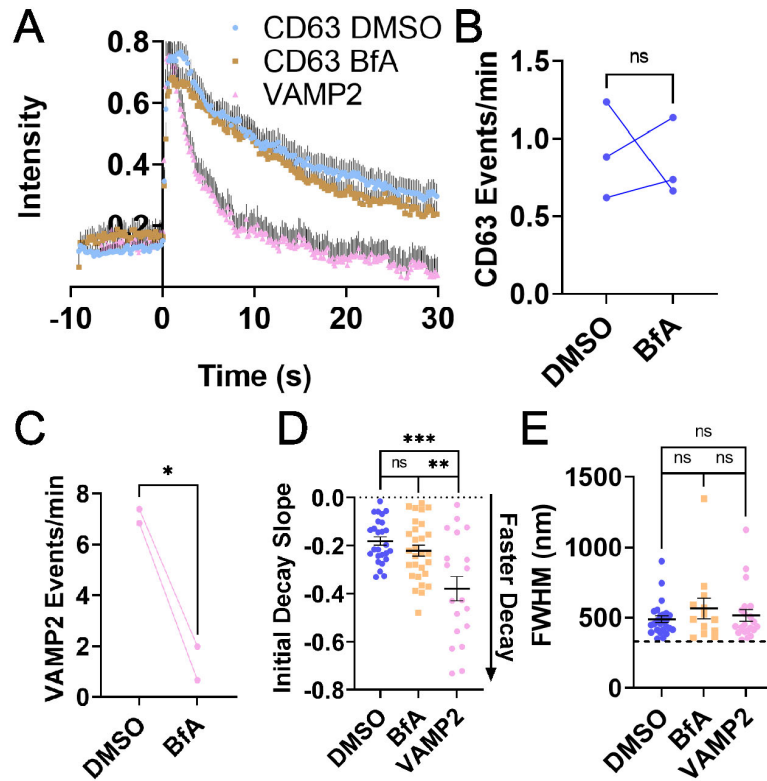
Figure 3.5: Brefeldin A Does Not Affect CD63 Event Frequency or Kinetics. A) Intensity plots of CD63-pHmScarlet in A549 cells treated with 0.1% DMSO with (brown squares) or without (blue circles) 5 µg/mL Brefeldin A (BfA). For comparison, the average VAMP2 trace in untreated PC12 cells was also plotted (pink triangles). B,C) Frequency of CD63 events in A549 cells (B, n = 3 days) and VAMP2 events in PC12 cells stimulated with 60 mM KCl (C, n = 2 days) in cells treated with carrier or BfA. Each pair of points is the average of cells in one day. D) Initial decay slopes of CD63 events in carrier (blue circles) or BfA (orange squares) or VAMP2 (pink triangles). Slopes were calculated from the first second after maximum CD63 or VAMP2 intensity. E) Average full width half max (FWHM) values of CD63 or VAMP2 events 0.5 to 0.1 s prior to event onset. Dashed line: diffraction limit identified with green 40 nm nanoparticles. Lines in D and E are averages, error bars are SEM. * $p < 0.05$, ** $p < 0.005$, *** $p < 0.0005$.

BfA, which were then stimulated with 60 mM KCl (Figure. 3.5C, [72]). There was a significant reduction in fusion event frequency in these cells.

While there was no change in event frequency in CD63 fusion events, initial decay slopes (Figure 3.5D) and full width half max (FWHM) values (Figure 3.5E) were plotted to observe if there was a change in kinetics or size. As we have previously reported, $t_{1/2}$ to the plateau was similarly unaffected [72]. The rate at which content is released from MVE fusion is drastically slower than stimulated VAMP2 vesicles (initial decay slopes of -0.18 vs -0.38, respectively), supporting the likelihood that these events are MVEs and not trafficking events. CD63 event kinetics were not significantly different from each other under either treatment. Similarly, the size of MVEs were not significantly different between any of these events. As our lab has previously published, we do not observe fusing lysosomes, either [72]. Therefore, most, if not all, fusion events we identified in this chapter were MVE fusion events and not trafficking of membrane proteins to the plasma membrane from the Golgi apparatus.

Phospholipase D1 Is Necessary for Multivesicular Endosome Docking, Fusion

To determine if PLD1, PLD2 or both affect MVE secretion, two PLD inhibitors were used. A549 cells expressing GFP-PLD1 and CD63-pHmScarlet were treated with 0.013% DMSO with or without 500 nM VU0155069, a PLD1-specific inhibitor (PLD1$_i$), or 100 nM FIPI, a pan-PLD inhibitor (PLD1/2$_i$). Because PLD1 is thought to affect MVE secretion and PLD2 is thought to affect MVE formation [28], we hypothesized that both of these inhibitors would affect exosome secretion. Under these three conditions, GFP-PLD1
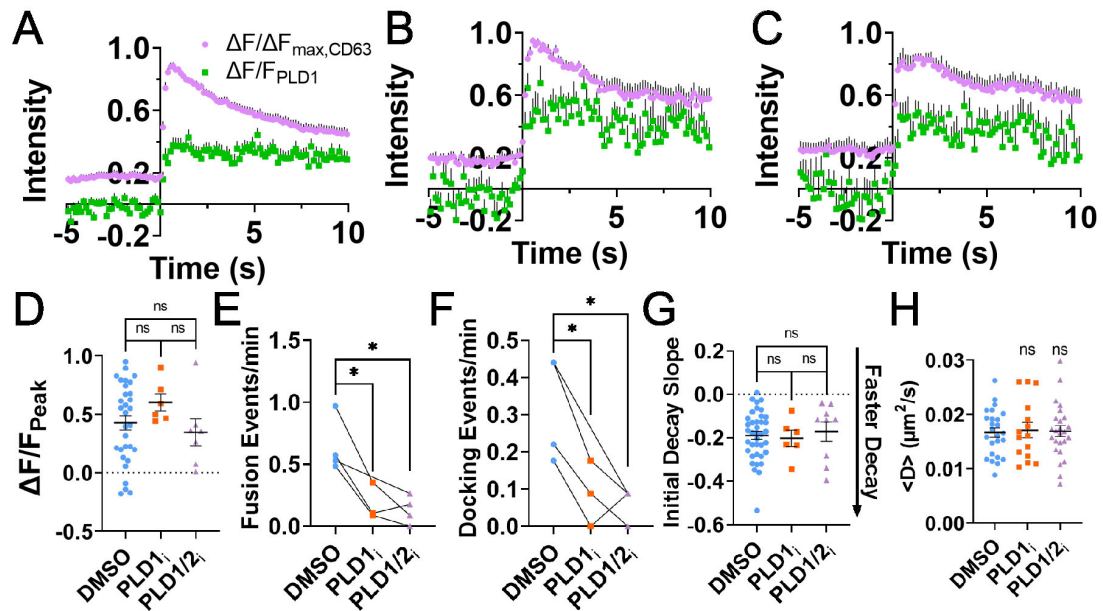
Figure 3.6: PLD1 Inhibition Reduces MVE Fusion, But Not Localization or Kinetics. A-C) Intensity traces of CD63-pHmScarlet (purple circles) fusion and corresponding GFP-PLD1 (green squares) in cells treated with 0.013% DMSO (A) and 500 nM VU0155069 (PLD1$_i$, B) or 100 nM FIPI (PLD1/2$_i$, C). D) $\Delta F/F$ values of GFP-PLD1 at peak CD63 intensity in treated cells. Each point represents one event. E,F) Frequency of fusion (E) and docking (F) in DMSO (blue circles), PLD1$_i$ (orange squares) or PLD1/2$_i$ (purple triangles). Each triplet or pair of points is the average of one day. * $p < 0.05$. G) Initial decay slopes for 1 s after peak CD63 intensity in treated cells. Each point represents one event H) Diffusion coefficients (D) of tracked MVEs. Each point is the average of all tracks in one cell. Lines are averages, error bars are SEM.

and CD63-pHmScarlet intensity traces were plotted (Figure 3.6A-C). GFP-PLD1 is present at sites of fusion under control, PLD1$_i$ and PLD1/2$_i$, suggesting that inhibition does not alter localization. No quantitative difference for GFP-PLD1 localization was noted (Figure 3.6D). However, PLD1 and PLD1/2 inhibition significantly reduced the rates of both docking and fusion (Figure 3.6E,F). While the rate of CD63 fluorescence appears to decay slower on average in PLD1/2$_i$, no difference was noted in the initial decay slope over the first second after fusion (Figure 3.6G). Others have reported that PLD inhibition reduces

55

mobility of secretory vesicles [44], so MVE diffusion was also measured under PLD inhibition, but no difference was noted (Figure 3.6H).

Phosphatidic Acid Localizes to Sites of Multivesicular Endosome Fusion

GFP-PASS, a PA marker, was used to observe PA production during all three types of events. Many events of each class were identified, cropped and averaged prior to visiting (Figure 3.7A), docking (Figure 3.7B) or fusing (Figure 3.7C) and at the peak or plateau of CD63 intensity. Difference images were also created by subtracting the initial image from the peak/plateau image (Figure 3.7A-C). PASS intensity increases in intensity during fusion, like with VAMP2 events described in Chapter 2. Traces were then averaged for each (Figure 3.7D-F). The only notable spot or increase in quantified intensity is during
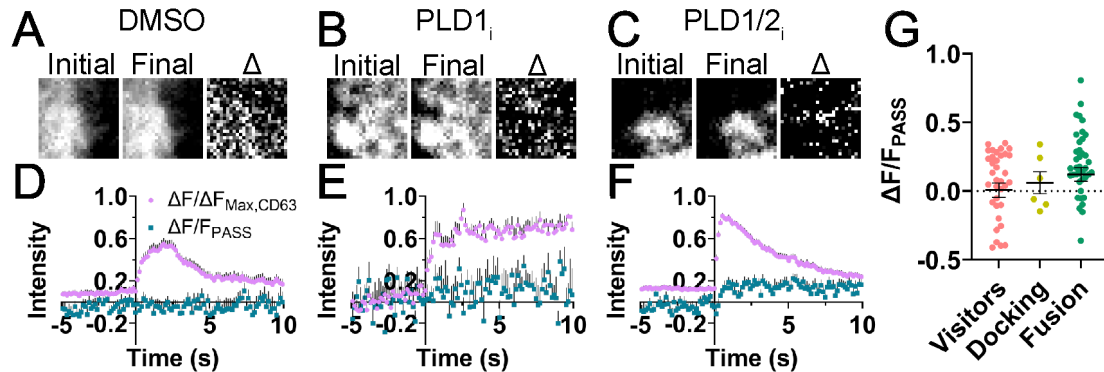
Figure 3.7: PASS Localizes to MVE Fusion Events. A-C) Left: Average images of GFP-PASS prior to visiting (A), docking (B) or fusing (C) MVE events. Middle: Average images of GFP-PASS at peak or plateau CD63 intensity. Right: Difference image between final and initial PASS images. Initial and final images are contrasted identically. D-F) Average traces of CD63-pHmScarlet (purple circles) and GFP-PASS (teal squares) during visiting (D), docking (E) and fusing (F) MVE events. G) Intensity of GFP-PASS at peak/plateau CD63 intensity during visiting (orange), docking (yellow) or fusing (green) events. Each point is an average of 3 frames beginning at peak/plateau CD63 intensity during one event.

fusion (Figure 3.7G). These results indicate that PA is likely produced on or recruited to MVEs during fusion. Interestingly, despite PLD2 having been implicated in formation of MVEs, there is no significant presence of PASS on mobile MVEs (Figure 3.7A,D). This could be due to PASS not being internalized by MVEs, as GFP does not appear to localize to MVEs, either (Figure 3.4).

To determine if cytosolic GFP or GFP-PASS are internalized within MVEs and present on exosomes, slot blots of small EVs from cells expressing GFP-PASS, cytosolic GFP or neither were stained with anti-GFP (Figure 3.8A). Bands were normalized based on cell lysate actin as described in Figure 3.2. Both GFP and GFP-PASS are brighter than wild type, indicating that both GFP and GFP-PASS are internalized by small EVs, but there is no difference between the intensity of these bands (Figure 3.8B). This result indicates
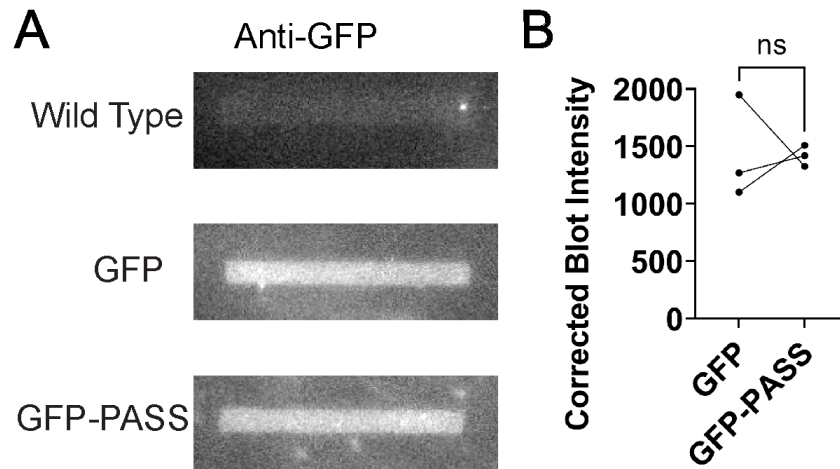
Figure 3.8: GFP Internalization in Small EVs. A) Example slot blot bands of small EVs in wild type A549 cells (top) and A549 cells expressing cytosolic GFP (middle) or GFP-PASS (bottom). Bands are contrasted identically. B) Corrected band intensities of blots. Bands were normalized to actin bands for the same day based on wild type actin bands, then the intensity of wild type bands from the same day were subtracted. Each pair of points is for one day. ns $p > 0.05$.

that GFP is internalized by small EVs, but no conclusions can be drawn about internalization of PASS or formation of PA within them.

Phospholipase D1 Produces Phosphatidic Acid at Sites of Docked Multivesicular Endosomes, but not during Fusion

A549 cells expressing GFP-PASS and CD63-pHmScarlet were treated with DMSO with or without PLD inhibitors. As noted previously (Figure 3.6E), events are significantly reduced under inhibitory conditions. Events that did occur were averaged as discussed previously (Figure 3.9A-C), with the initial, final and difference images shown (Figure 3.9A-C). Traces of PASS during fusion were then plotted for DMSO, PLD1$_i$ and PLD1/2$_i$ (Figure 3.9D-F). PASS presence was observed during fusion in cells treated with DMSO.
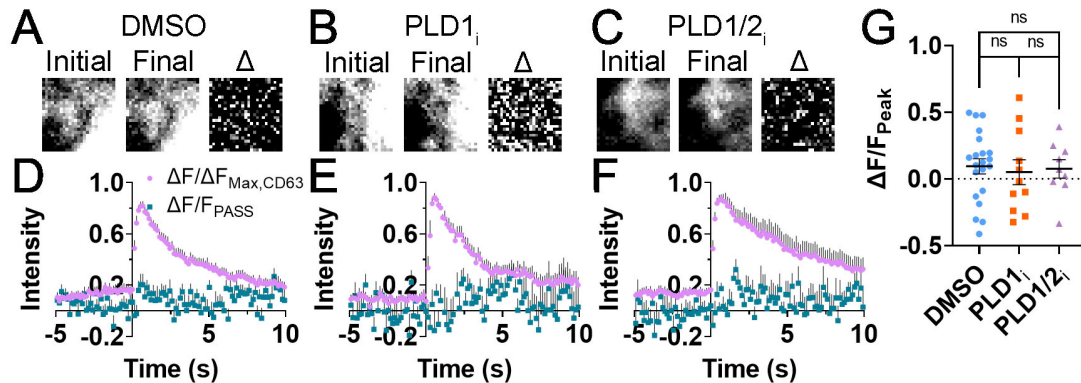
Figure 3.9: PLD Is Not Solely Responsible for PA Production in Fusing MVEs. A-C) Left: Average images of GFP-PASS prior to fusion in cells treated with DMSO (A), PLD1 inhibition (B) or PLD1/2 inhibition (C). Middle: Average images of GFP-PASS at peak CD63 intensity. Right: Difference image between final and initial PASS images. Initial and final images are contrasted identically. D-F) Average traces of CD63-pHmScarlet (purple circles) and GFP-PASS (teal squares) during MVE fusion in DMSO (D), PLD1$_i$ (E) and PLD1/2$_i$ (F). G) Intensity of GFP-PASS at peak/plateau CD63 intensity during fusion events in DMSO (blue circles), PLD1$_i$ (orange squares) or PLD1/2$_i$ (purple triangles). Each point is an average of 3 frames beginning at peak/plateau CD63 intensity during one event. Lines are averages, error bars are SEM.

Interestingly, however, cells treated with PLD1$_i$ or PLD1/2$_i$ still displayed an increase in PASS presence, indicating that there may be PA production or recruitment from other sources than PLD in at least some population of CD63 events, as this value is positive, while cytosolic GFP decreases in intensity (Figure 3.4F). While the results for PLD inhibition do not test significant to DMSO, the average $\Delta F/F$ of PASS during fusion is slightly lower under PLD1$_i$ and lower still in PLD1/2$_i$ than in DMSO (Figure 3.9G).

PLD inhibition also reduced docking events (Figure 3.6F), so PASS localization to sites of MVE docking were also observed. Events were cropped and averaged prior to docking and after 12 and 18 seconds (Figure 3.10A). Traces of PASS intensity during docking were plotted over a longer time course (Figure 3.10B). Under control conditions (DMSO), PASS was consistently positive post docking, but in either inhibitor intensity remained approximately zero, indicating PA production by PLD1 during docking over a longer period. By 10 seconds after docking, as indicated by the CD63 plateau, this difference starts to become clearer (Figure 3.10C), and by 15 seconds DMSO is significantly positive compared to either inhibitor (Figure 3.10D).

Fewer Small Extracellular Vesicles Are Collected When Phospholipase D1 Is Inhibited

As another test for PLD's effect on exosome secretion, Exoquick was used to collect small EVs from A549 cells treated with DMSO with or without PLD inhibitors as described in Methods, and then blotted for CD63 on a slot blot (Figure 3.11A). As a control for the concentration of cells, cell lysates for the same samples were also collected and
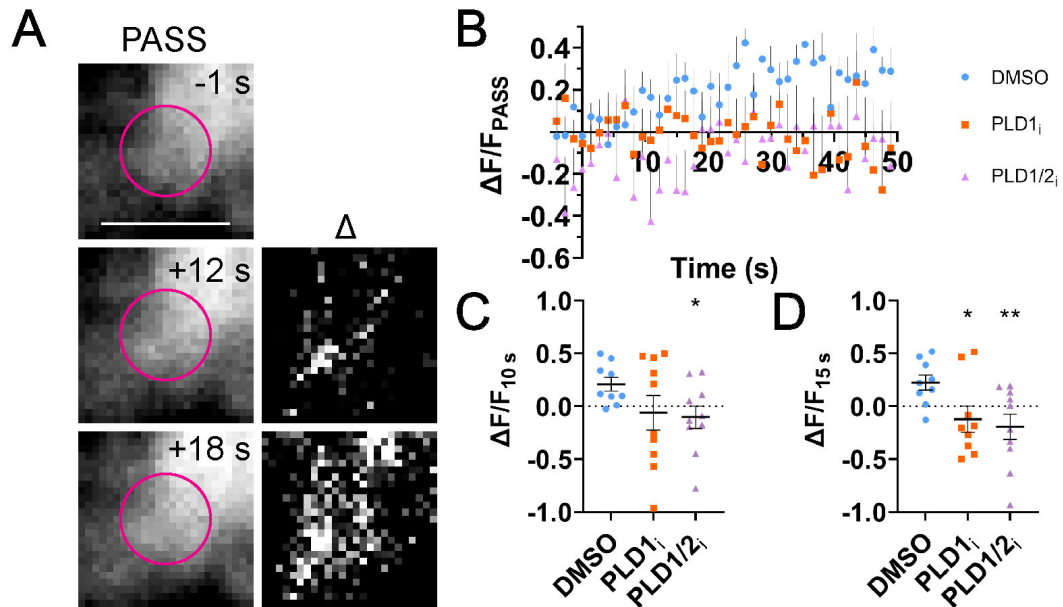
Figure 3.10: PLD1 Produces PA at Docked MVEs over Time. A) Average images (n = 9 events) of PASS 1 s before onset of docking, after 12 s and after 18 s (left). Pink circles mark the location of the docked MVE. The difference between pre and post docking images (right). Initial and final images are contrasted identically. B) Average trace of PASS intensity during docking in DMSO (blue circles, n = 11 events), $PLD1_i$ (orange squares, n = 10 events) or $PLD1/2_i$ (purple triangles, n = 11 events). Only every tenth point is plotted for clarity. Error bars are SEM. C,D) $\Delta F/F$ of PASS 10 s (C) or 15 s (D) after plateau of docking in DMSO (blue circles), $PLD1_i$ (orange squares) or PLD1/2

blotted for actin. Blots show a consistent reduction of exosomes secreted under either inhibitory condition. Additionally, small EVs were imaged via a NanoSight, and a built-in tracking algorithm identified the size of small EVs in all three treatments based on Brownian motion (Figure 3.11C-H). No consistent or significant difference in the average diameter of small EVs was noted between the treatments (Figure 3.11C). This software also counted small EVs, but due to the low concentration of small EVs in these samples, no conclusions regarding concentration could be drawn from this technique alone (Figure

3.11D). Distribution of sEV sizes were also plotted for all three conditions (Figure 3.11E-

G). Then, these distributions were overlayed within normal exosome size range (40-160

nm, Figure 3.11H) [80]. Under either inhibitory condition, the peaks of these size

distributions were probably shifted, indicating some effect of PLD1 on the size of small

EVs, which likely includes exosomes. In future studies, it would be interesting to explore

this change further.
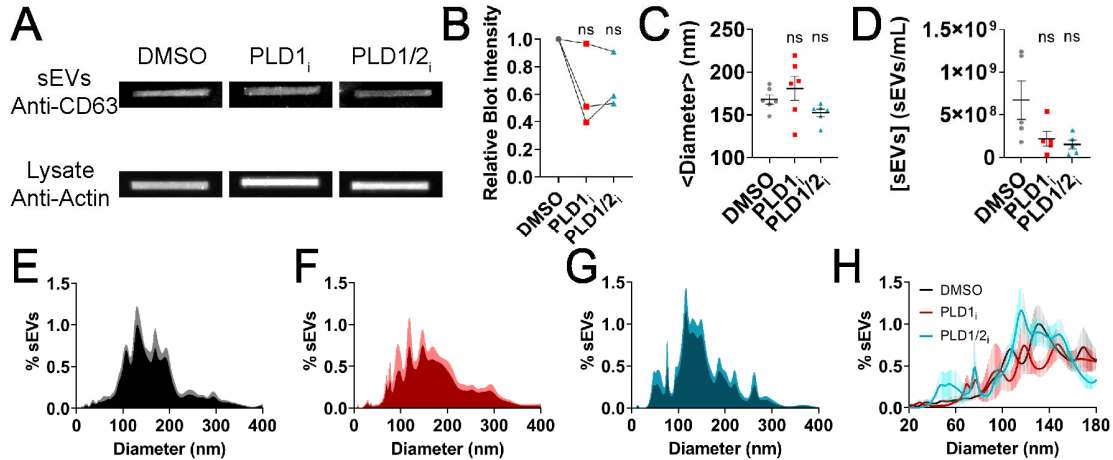
Figure 3.11: PLD Inhibition Reduces Number of Small EVs Collected and Alters Small EV Size Distribution. A) Example slot blots of collected small EVs and corresponding cell lysates stained for CD63 and actin, respectively. B) Quantification of small EVs corrected for actin in cell cultures treated with DMSO (grey circles), PLD1$_i$ (red squares) or PLD1/2$_i$ (teal triangles) under identical concentrations as those used in fluorescence experiments. Values are corrected based on actin and normalized to the DMSO intensity for the same day. Each triplet of points is from the same day. C-H) Collected small EVs were imaged using an NTS instrument to identify size and concentration under PLD inhibition. C) Average size of small EVs. D) Concentrations of small EVs under PLD inhibition. Lines are averages, error bars are SEM. E-G) Size distribution of small EVs collected in DMSO (E), PLD1$_i$ (F) and PLD1/2$_i$ (G). H) Close up of distributions at common exosomes sizes for DMSO (black), PLD1$_i$ (red) and PLD1/2$_i$ (teal). Error bars are SEM (n = 6).

PLD Inhibition Increases Number of Lysosomes

PLD inhibition significantly reduces rate of MVE docking and secretion (Figure 3.6E,F), and PA production after docking (Figure 3.10), but it has no effect on kinetics of fusion (Figure 3.6G) or presence of PA (Figure 3.9). One hypothesis is that PLD1 and/or PLD2 may be involved in trafficking. However, diffusion coefficients were not affected by PLD inhibition treatments (Figure 3.6H). Another potential role for PLD is late endosome fate, because MVEs may fuse with the plasma membrane, or they can fuse with lysosomes and lead to degradation [1]–[3]. Others have noted that PLDs may be involved in late endosome fate [81]. Therefore, A549 cells expressing CD63-GFP and either co-expressing
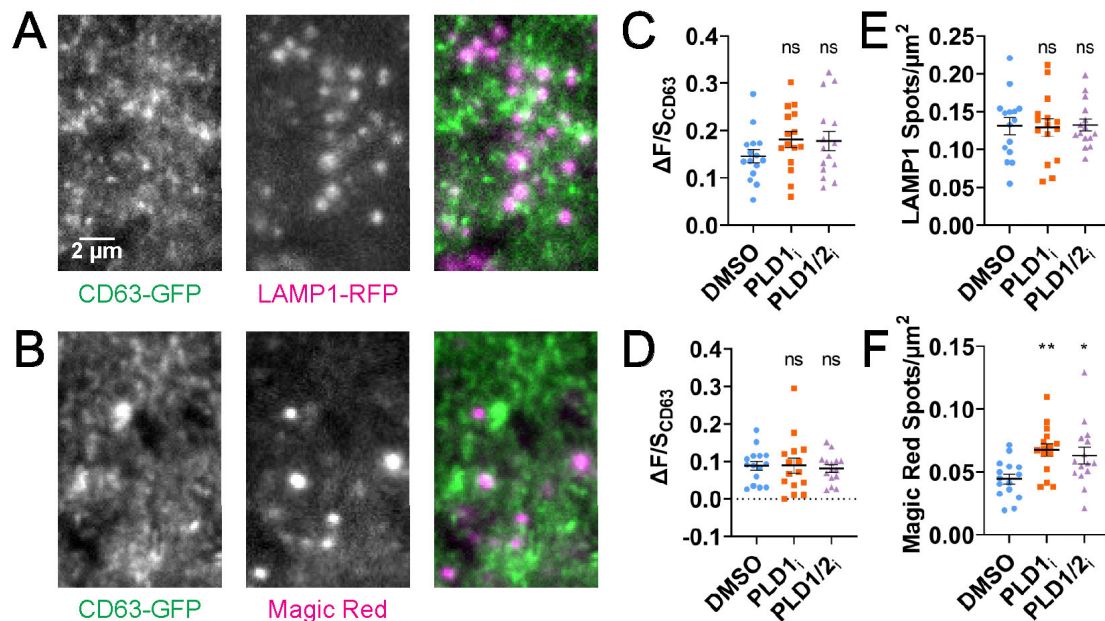
Figure 3.12: PLD1 Inhibition Increases Number of Lysosomes. A,B) A549 cells were transfected with CD63-GFP (left) and LAMP1-RFP (middle, A) or treated with Magic Red (middle, B). Scale bar: 2 μm. C,D) Average ΔF/S values for CD63 at LAMP1 spots (C) or Magic Red spots (D). E,F) Number of spots identified containing LAMP1 (E) or Magic Red (F) per surface area under TIRF microscopy. Each point in C-F is one cell. Lines are averages, error bars are SEM. ns $p > 0.05$, * $p < 0.05$, ** $p < 0.005$.

LAMP1-RFP (Figure 3.12A) or treated with lysosome-specific marker Magic Red (Figure 3.12B) were observed under these conditions to identify the effects of PLD inhibition on late endosome populations. MVEs containing LAMP1 are less likely to fuse, although LAMP1 is present during MVE fusion to an extent [74]. No change was observed in CD63 colocalization with LAMP1+ endosomes or Magic Red+ lysosomes was noted (Figures 3.12C,D). The number of LAMP1+ endosomes identified in the TIRF field was likewise unaffected (Figure 3.12E). However, 42-52% more Magic Red+ lysosomes were noted under PLD inhibition, indicating a likely role in late endosome fate (Figure 3.12F). These results support the hypothesis that PLD is involved in MVE fate, favoring eventual exosome secretion, while its inhibition favors the lysosomal pathway.

3.4: Discussion

In this work, we demonstrate that PLD1 activity is essential for exosome secretion in A549 cells, as well as the fate of late endosomes. Others have noted that PLD1 localizes to late endosomes [38]–[43], which this work supports. PLD1 localizes to late endosomes, particularly CD63+ late endosomes (Figure 3.1C,D and 3.2D), which are predominantly MVEs [74]. PLD1 also displays some localization to LAMP1+ late endosomes (Figure 3.1C,D). However, in individual endosomes there are more LAMP1 endosomes without PLD1 than there are CD63 endosomes without PLD1, indicated by the former having a median ~0.03 and CD63 having a median ~0.16 (Figure 3.1D). PLD1 localization to MVEs sets the stage for a potential role in PLD1 in the exosome secretion pathway, as others have

noted [28], [51], similar to its role in stimulated exocytic processes [33], [37], [44], [82]–[85].

By observing single visiting and fusing MVEs using a pH sensitive marker, CD63-pHmScarlet, alongside GFP-PLD1, it was confirmed that PLD1 is present on MVEs during all stages (Figure 3.4), as its intensity significantly increased during visiting and fusing MVEs. Thus, there is likely a strong association between PLD1 and late endosomes. Additionally, while it was not significantly brighter during docking, this could be attributed to the rarity of docking MVE events noted in this work, which is supported by PASS accumulating at sites of docking only when PLD1 is not inhibited (Figure 3.10). We hypothesized that cytosolic GFP may be internalized in ILVs. However, GFP intensity *decreased* during all three classes of events, indicating this was likely not the case, as GFP is slightly pH sensitive and would increase upon fusion, puff and spread radially; it would also be visible during visiting and docking (Figure 3.4C). Therefore, PLD1 is present on MVEs and is likely involved in this pathway, in line with previous colocalization studies [38]–[43] and exosome secretion [28], [51], [69] of PLD1. PLD1 and PLD2 are present on exosomes [86], and inhibition or knockout experiments of either PLD1 or PLD2 significantly reduced secreted exosomes in 4T1 and ovarian cancer cells [51], [69].

The main enzymatic activity of PLD1 is the conversion of the lipid PC to PA, which is hypothesized to stabilize negative curvature. Therefore, we hypothesized that it may stabilize the fusion pore, as it likely does for VAMP2 events, or that it may support the formation of ILVs. To explore this possibility, a GFP-labeled PA marker, GFP-PASS, was

used. PASS was noted during MVE fusion (Figure 3.7), and over a long time during MVE docking (Figure 3.10). Thus, production of PA is important for docking and fusing MVEs.

It is interesting to note that PLD1 is present on mobile MVEs, but PASS is not. One possibility is that PLD1 is involved in fate or mobility. PLD inhibition had no effect on mobility of endosomes (Figure 3.6H), or CD63 localization to other late endosome or lysosome markers (Figure 3.12C,D), but it did increase the density of lysosomes present. This result suggests that PLD1 has a role in late endosome fate, favoring formation of exocytosis bound MVEs rather than lysosomes.

Given this result and that PA is more enriched on exosomes from PC-3 cells than the cells themselves [86], [87], and reduction of PLD1/2 activity reduce secreted exosomes [51], [69], it is likely that PLD1 produces PA at some point in the MVE formation process. It is possible that PASS is not observed in MVEs prior to fusion due to GFP quenching at low pH, but this is unlikely as GFP is not nearly as quenched as pHmScarlet. It is more likely that it is excluded from intraluminal vesicles. The fact that cytosolic GFP intensity drops during fusion could support the latter, and blotting small EVs in cells expressing cytosolic GFP or GFP-PASS suggests that both are internalized to the same extent (Figure 3.8B). However, small EVs other than exosomes are also collected, and PLD1 production of PA is noted in production of microvesicles, another class of EVs [88], which may explain this discrepancy.

One other possibility is that PLD1 among other PLDs are internalized in exosomes, as others have noted [89]–[91], and PA is not always easily detectable in intraluminal vesicles [81], [86], [92], [93]. This could mean that PA production is too low to measure

with PASS, or that PA is only temporarily produced as an intermediate lipid or when needed [90], [94], and that it is only detectable in larger quantities of exosomes. Overall, the presence of PASS during fusion is consistent with those observed in VAMP2 secretion, and with previous hypotheses that PLD1 involvement in the exocytic processes is due to its production of PA.

Like in VAMP2 events, PA also does appear to slowly increase in intensity after MVEs dock. It is possible that PA is produced during both the formation of intraluminal vesicles and the docking/fusion processes. These results support the latter, with previous lipid studies supporting the former [87]. Bands on slot blots of cells expressing GFP and GFP-PASS in small EVs are brighter than wild type cells for anti-GFP (Figure 3.8A), indicating that both are internalized by small EVs, either to an extent in exosomes that is too low to view with these fluorescent techniques, or a greater extent in other EVs. However, GFP and GFP-PASS are not significantly different from one another, suggesting that PASS is not significantly internalized. This does not mean that PA is not produced within ILVs. Given the fact that both are present to similar extents, it indicates that the increase in intensity during fusion is not due to exosomal PA, as this intensity increase is not noted with GFP during fusion (Figure 3.4F). This means the difference in intensity between PASS and GFP must be due to production of PA on and/or recruitment to the plasma membrane and/or outer MVE membrane.

In order to specifically identify whether the role of PLD1 in this pathway is due to its production of PA, PLD1-specific and pan-PLD inhibitors were used. Consistent with our hypothesis that PLD1 is required for exocytosis, there was a significant reduction in

the rate of MVE fusion (Figure 3.6E). PLD1 was hypothesized to be involved in this process due to its production of PA. However, under PLD inhibition, there was no change in the localization of PASS to sites of fusion (Figure 3.8). This result indicates that there is another role for PLD1 in the MVE pathway than simply producing PA during secretion. The fact that PA increases during fusion regardless of inhibitor used indicates that there is likely a source in addition to PLD1 for exocytosis.

Interestingly, there was also a significant reduction in the rate of MVE docking (Figure 3.6F). PA is produced slowly during docking by PLD1, however, as PASS intensity increases in DMSO but not under either inhibitory condition. Another interesting note about PA formation in MVE docking events is that, while PA is formed near the center of docked secretory vesicles (Figure 2.10A), it is formed offset around the center of docked MVEs (Figure 3.10A), while during fusion it appears near the center (Figure 3.7C).

If PLD1 production of PA is not specifically required for exocytosis, why does PA intensity increase during fusion? Syx2, Syx3 and Syx4 have been shown to be involved in exosome secretion [26]. Syntaxins in both yeast [95] and humans [96] have been shown to have PA-binding domains. It is possible that Syntaxin-4 recruits PA, but as there is no compensatory recruitment in VAMP2 secretion (Figure 2.5), this is unlikely. Other methods for PA production include diacylglycerol kinases (DGKs), with DGKα having been implicated in exosome secretion [97]–[101]. DGKα may provide a compensatory method for PA production during MVE fusion but not during docking.

To begin identifying possible other roles for PLD beyond the formation of PA at the fusion site, A549 cells expressing CD63-GFP either with LAMP1-RFP or while treated

with Magic Red were imaged under treatment with PLD inhibitors. There is some overlap between CD63 and LAMP1 endosomes (Figure 3.12C), as others have noticed [26], [27], [102], and some amount of CD63 present on lysosomes (Figure 3.12D). Endosomes that are LAMP1+ have been shown to be less likely to fuse [74], which may indicate a different population of late endosomes that are LAMP1+ and CD63+. As we and others have previously reported, CD63 fusion events do not contain Magic Red [72], [74]. Additionally, reduction of endolysosome fusion causes more exosomes to be secreted [1]–[3], while induction of autophagy reduces exosome secretion [3], [103]. Magic Red specifically marks catalytic lysosomes. While no change in colocalization was noted between CD63 and LAMP1 or Magic Red, more Magic Red+ lysosomes were identified under PLD1 inhibition (Figure 3.12F), likely indicating that PLD1 is involved in determining whether late endosomes become MVEs or lysosomes. Since PLD1 and exosome secretion are both elevated in cancer [13]–[16], and PLD1 inhibition increases lysosome density, it appears involved in late endosome fate in addition to docking.

Overall, PLD1 is necessary for exosome secretion, as others have shown and the clear reduction of MVE fusion under PLD1 inhibition supports. However, the reason for PLD1 involvement is less clear, as PA localization to fusion sites is not dependent on PLD1. Its production of PA during docking, however, could still support fusion. PLD1 is present on MVEs during all stages, but it is only required to produce PA during docking. The presence of catalytic lysosomes near the cell surface is increased under PLD1 inhibition, suggesting that PLD1 is involved in determining fate of MVEs, therefore indirectly influencing fusion, unlike its more direct involvement with secretory vesicles.

Chapter 3 References

[1]   G. V. Shelke, C. D. Williamson, M. Jarnik, and J. S. Bonifacino, "Inhibition of endolysosome fusion increases exosome secretion," *Journal of Cell Biology*, vol. 222, no. 6, Jun. 2023, doi: 10.1083/jcb.202209084.

[2]   N. P. Hessvik *et al.*, "PIKfyve inhibition increases exosome release and induces secretory autophagy," *Cellular and Molecular Life Sciences*, vol. 73, no. 24, pp. 4717–4737, Dec. 2016, doi: 10.1007/s00018-016-2309-8.

[3]   C. Villarroya-Beltri *et al.*, "ISGylation controls exosome secretion by promoting lysosomal degradation of MVB proteins," *Nat Commun*, vol. 7, no. 1, p. 13588, Nov. 2016, doi: 10.1038/ncomms13588.

[4]   J. Kowal, M. Tkach, and C. Théry, "Biogenesis and secretion of exosomes," *Curr Opin Cell Biol*, vol. 29, pp. 116–125, Aug. 2014, doi: 10.1016/j.ceb.2014.05.004.

[5]   M. Colombo, G. Raposo, and C. Théry, "Biogenesis, Secretion, and Intercellular Interactions of Exosomes and Other Extracellular Vesicles," *Annu Rev Cell Dev Biol*, vol. 30, no. 1, pp. 255–289, Oct. 2014, doi: 10.1146/annurev-cellbio-101512-122326.

[6]   M. P. Bebelman, M. J. Smit, D. M. Pegtel, and S. R. Baglio, "Biogenesis and function of extracellular vesicles in cancer," *Pharmacol Ther*, vol. 188, pp. 1–11, Aug. 2018, doi: 10.1016/j.pharmthera.2018.02.013.

[7]   N. P. Hessvik and A. Llorente, "Current knowledge on exosome biogenesis and release," *Cellular and Molecular Life Sciences*, vol. 75, no. 2, pp. 193–208, Jan. 2018, doi: 10.1007/s00018-017-2595-9.

[8]   C. Théry, L. Zitvogel, and S. Amigorena, "Exosomes: composition, biogenesis and function," *Nat Rev Immunol*, vol. 2, no. 8, pp. 569–579, Aug. 2002, doi: 10.1038/nri855.

[9]   G. van Niel, G. D'Angelo, and G. Raposo, "Shedding light on the cell biology of extracellular vesicles," *Nat Rev Mol Cell Biol*, vol. 19, no. 4, pp. 213–228, Apr. 2018, doi: 10.1038/nrm.2017.125.

[10]   R. A. Colvin *et al.*, "Synaptotagmin-mediated vesicle fusion regulates cell migration," *Nat Immunol*, vol. 11, no. 6, pp. 495–502, Jun. 2010, doi: 10.1038/ni.1878.

[11]   V. Proux-Gillardeaux, G. Raposo, T. Irinopoulou, and T. Galli, "Expression of the Longin domain of TI-VAMP impairs lysosomal secretion and epithelial cell

migration," *Biol Cell*, vol. 99, no. 5, pp. 261–271, May 2007, doi: 10.1042/BC20060097.

[12] A. Takahashi *et al.*, "Exosomes maintain cellular homeostasis by excreting harmful DNA from cells," *Nat Commun*, vol. 8, no. 1, p. 15287, May 2017, doi: 10.1038/ncomms15287.

[13] C. Kahlert and R. Kalluri, "Exosomes in tumor microenvironment influence cancer progression and metastasis," *J Mol Med*, vol. 91, no. 4, pp. 431–437, Apr. 2013, doi: 10.1007/s00109-013-1020-6.

[14] T. B. Steinbichler, J. Dudás, H. Riechelmann, and I.-I. Skvortsova, "The role of exosomes in cancer metastasis," *Semin Cancer Biol*, vol. 44, pp. 170–181, Jun. 2017, doi: 10.1016/j.semcancer.2017.02.006.

[15] V. Hyenne *et al.*, "Studying the Fate of Tumor Extracellular Vesicles at High Spatiotemporal Resolution Using the Zebrafish Embryo," *Dev Cell*, vol. 48, no. 4, pp. 554-572.e7, Feb. 2019, doi: 10.1016/j.devcel.2019.01.014.

[16] W. Feng, D. C. Dean, F. J. Hornicek, H. Shi, and Z. Duan, "Exosomes promote pre-metastatic niche formation in ovarian cancer," *Mol Cancer*, vol. 18, no. 1, p. 124, Dec. 2019, doi: 10.1186/s12943-019-1049-4.

[17] A. Stuendl *et al.*, "Induction of α-synuclein aggregate formation by CSF exosomes from patients with Parkinson's disease and dementia with Lewy bodies," *Brain*, vol. 139, no. 2, pp. 481–494, Feb. 2016, doi: 10.1093/brain/awv346.

[18] I. Russo, L. Bubacco, and E. Greggio, "Exosomes-associated neurodegeneration and progression of Parkinson's disease," *Am J Neurodegener Dis*, vol. 1, no. 3, pp. 217–225, 2012.

[19] L. Rajendran *et al.*, "Alzheimer's disease β-amyloid peptides are released in association with exosomes," *Proceedings of the National Academy of Sciences*, vol. 103, no. 30, pp. 11172–11177, Jul. 2006, doi: 10.1073/pnas.0603838103.

[20] J. Shen, X. Zhu, J. Fei, P. Shi, S. Yu, and J. Zhou, "Advances of exosome in the development of ovarian cancer and its diagnostic and therapeutic prospect," *Onco Targets Ther*, vol. Volume 11, pp. 2831–2841, May 2018, doi: 10.2147/OTT.S159829.

[21] S. W. Messenger, S. S. Woo, Z. Sun, and T. F. J. Martin, "A Ca2+-stimulated exosome release pathway in cancer cells is regulated by Munc13-4," *Journal of Cell Biology*, vol. 217, no. 8, pp. 2877–2890, Aug. 2018, doi: 10.1083/jcb.201710132.

[22] R. Chowdhury, J. P. Webber, M. Gurney, M. D. Mason, Z. Tabi, and A. Clayton, "Cancer exosomes trigger mesenchymal stem cell differentiation into pro-angiogenic and pro-invasive myofibroblasts," *Oncotarget*, vol. 6, no. 2, pp. 715–731, Jan. 2015, doi: 10.18632/oncotarget.2711.

[23] J. Clancy and C. D'Souza-Schorey, "Extracellular Vesicles in Cancer," *The Cancer Journal*, vol. 24, no. 2, pp. 65–69, Mar. 2018, doi: 10.1097/PPO.0000000000000306.

[24] B. H. Sung, T. Ketova, D. Hoshino, A. Zijlstra, and A. M. Weaver, "Directional cell movement through tissues is controlled by exosome secretion," *Nat Commun*, vol. 6, no. 1, p. 7164, May 2015, doi: 10.1038/ncomms8164.

[25] B. H. Sung *et al.*, "A live cell reporter of exosome secretion and uptake reveals pathfinding behavior of migrating cells," *Nat Commun*, vol. 11, no. 1, p. 2092, Apr. 2020, doi: 10.1038/s41467-020-15747-2.

[26] F. J. Verweij *et al.*, "Quantifying exosome secretion from single cells reveals a modulatory role for GPCR signaling," *Journal of Cell Biology*, vol. 217, no. 3, pp. 1129–1142, Mar. 2018, doi: 10.1083/jcb.201703206.

[27] M. Mathieu *et al.*, "Specificities of exosome versus small ectosome secretion revealed by live intracellular tracking of CD63 and CD9," *Nat Commun*, vol. 12, no. 1, p. 4389, Jul. 2021, doi: 10.1038/s41467-021-24384-2.

[28] A. Wolf, E. Tanguy, Q. Wang, S. Gasman, and N. Vitale, "Phospholipase D and cancer metastasis: A focus on exosomes," *Adv Biol Regul*, vol. 87, p. 100924, Jan. 2023, doi: 10.1016/J.JBIOR.2022.100924.

[29] M. A. Frohman, "The phospholipase D superfamily as therapeutic targets," *Trends Pharmacol Sci*, vol. 36, no. 3, pp. 137–144, Mar. 2015, doi: 10.1016/J.TIPS.2015.01.001.

[30] Y. Humeau *et al.*, "A role for phospholipase D1 in neurotransmitter release," *Proceedings of the National Academy of Sciences*, vol. 98, no. 26, p. 15300, Dec. 2001, doi: 10.1073/pnas.261358698.

[31] W. E. Hughes, Z. Elgundi, P. Huang, M. A. Frohman, and T. J. Biden, "Phospholipase D1 Regulates Secretagogue-stimulated Insulin Release in Pancreatic β-Cells," *Journal of Biological Chemistry*, vol. 279, no. 26, pp. 27534–27541, 2004, doi: 10.1074/jbc.M403012200.

[32] G. M. Jenkins and M. A. Frohman, "Phospholipase D: a lipid centric review," *Cell Mol Life Sci*, vol. 62, no. 19–20, pp. 2305–2316, Oct. 2005, doi: 10.1007/s00018-005-5195-z.

[33] M. Zeniou-Meyer *et al.*, "Phospholipase D1 Production of Phosphatidic Acid at the Plasma Membrane Promotes Exocytosis of Large Dense-core Granules at a Late Stage," *Journal of Biological Chemistry*, vol. 282, no. 30, pp. 21746–21757, 2007, doi: 10.1074/jbc.M702968200.

[34] N. Vitale *et al.*, "Phospholipase D1: a key factor for the exocytotic machinery in neuroendocrine cells," *EMBO J*, vol. 20, no. 10, pp. 2424–2434, May 2001, doi: 10.1093/emboj/20.10.2424.

[35] R. Haslam and J. Coorssen, "Evidence that activation of phospholipase D can mediate secretion from permeabilized platelets ," *Advances in experimental medicine and biology* , vol. 344, pp. 149–164, 1993, doi: 10.1007/978-1-4615-2994-1_11.

[36] J. Stutchfield and S. Cockcroft, "Correlation between secretion and phospholipase D activation in differentiated HL60 cells," *Biochemical Journal*, vol. 293, no. 3, pp. 649–655, Aug. 1993, doi: 10.1042/bj2930649.

[37] M. Zeniou-Meyer, A. Béglé, M.-F. Bader, and N. Vitale, "The Coffin-Lowry Syndrome-associated Protein RSK2 Controls Neuroendocrine Secretion through the Regulation of Phospholipase D1 at the Exocytotic Sites," *Ann N Y Acad Sci*, vol. 1152, no. 1, pp. 201–208, Jan. 2009, doi: 10.1111/j.1749-6632.2008.04001.x.

[38] F. D. Brown *et al.*, "Phospholipase D1 localises to secretory granules and lysosomes and is plasma-membrane translocated on cellular stimulation," *Current Biology*, vol. 8, no. 14, pp. 835–838, Jul. 1998, doi: 10.1016/S0960-9822(98)70326-4.

[39] Z. Freyberg, D. Sweeney, A. Siddhanta, S. Bourgoin, M. Frohman, and D. Shields, "Intracellular Localization of Phospholipase D1 in Mammalian Cells," *Mol Biol Cell*, vol. 12, no. 4, pp. 943–955, Apr. 2001, doi: 10.1091/mbc.12.4.943.

[40] G. Du *et al.*, "Regulation of phospholipase D1 subcellular cycling through coordination of multiple membrane association motifs," *Journal of Cell Biology*, vol. 162, no. 2, pp. 305–315, Jul. 2003, doi: 10.1083/jcb.200302033.

[41] K. Toda, M. Nogami, K. Murakami, Y. Kanaho, and K. Nakayama, "Colocalization of phospholipase D1 and GTP-binding-defective mutant of ADP-ribosylation factor 6 to endosomes and lysosomes," *FEBS Lett*, vol. 442, no. 2–3, pp. 221–225, Jan. 1999, doi: 10.1016/S0014-5793(98)01646-9.

[42] Y. H. Jang and D. S. Min, "The hydrophobic amino acids involved in the interdomain association of phospholipase D1 regulate the shuttling of phospholipase D1 from vesicular organelles into the nucleus," *Exp Mol Med*, vol. 44, no. 10, p. 571, 2012, doi: 10.3858/emm.2012.44.10.065.

[43]   L. S. Arneson, J. Kunz, R. A. Anderson, and L. M. Traub, "Coupled Inositide Phosphorylation and Phospholipase D Activation Initiates Clathrin-coat Assembly on Lysosomes," *Journal of Biological Chemistry*, vol. 274, no. 25, pp. 17794–17805, Jun. 1999, doi: 10.1074/jbc.274.25.17794.

[44]   E. Tanguy *et al.*, "Phospholipase D1-generated phosphatidic acid modulates secretory granule trafficking from biogenesis to compensatory endocytosis in neuroendocrine cells," *Adv Biol Regul*, vol. 83, p. 100844, Jan. 2022, doi: 10.1016/J.JBIOR.2021.100844.

[45]   M. H. Park, K.-Y. Choi, and D. S. Min, "The pleckstrin homology domain of phospholipase D1 accelerates EGFR endocytosis by increasing the expression of the Rab5 effector, rabaptin-5," *Exp Mol Med*, vol. 47, no. 12, pp. e200–e200, Dec. 2015, doi: 10.1038/emm.2015.101.

[46]   Y. Shen, L. Xu, and D. A. Foster, "Role for Phospholipase D in Receptor-Mediated Endocytosis," *Mol Cell Biol*, vol. 21, no. 2, pp. 595–602, Jan. 2001, doi: 10.1128/MCB.21.2.595-602.2001.

[47]   J. G. Donaldson, "Phospholipase D in endocytosis and endosomal recycling pathways," *Biochimica et Biophysica Acta (BBA) - Molecular and Cell Biology of Lipids*, vol. 1791, no. 9, pp. 845–849, Sep. 2009, doi: 10.1016/j.bbalip.2009.05.011.

[48]   C. Dall'Armi *et al.*, "The phospholipase D1 pathway modulates macroautophagy," *Nat Commun*, vol. 1, no. 1, p. 142, Dec. 2010, doi: 10.1038/ncomms1144.

[49]   K. Søreng, H. Knævelsrud, P. Holland, and A. Simonsen, "HS1BP3 inhibits autophagy by regulation of PLD1," *Autophagy*, vol. 13, no. 5, pp. 985–986, May 2017, doi: 10.1080/15548627.2017.1291483.

[50]   M. Cai *et al.*, "Phospholipase D1-regulated autophagy supplies free fatty acids to counter nutrient stress in cancer cells," *Cell Death Dis*, vol. 7, no. 11, pp. e2448–e2448, Nov. 2016, doi: 10.1038/cddis.2016.355.

[51]   S. Ghoroghi *et al.*, "Ral GTPases promote breast cancer metastasis by controlling biogenesis and organ targeting of exosomes," *Elife*, vol. 10, Jan. 2021, doi: 10.7554/eLife.61539.

[52]   Y. Chen, Y. Zheng, and D. A. Foster, "Phospholipase D confers rapamycin resistance in human breast cancer cells," *Oncogene*, vol. 22, no. 25, pp. 3937–3942, Jun. 2003, doi: 10.1038/sj.onc.1206565.

[53]   J. H. Cho *et al.*, "Overexpression of phospholipase D suppresses taxotere-induced cell death in stomach cancer cells," *Biochimica et Biophysica Acta (BBA) -*

Molecular Cell Research, vol. 1783, no. 5, pp. 912–923, May 2008, doi: 10.1016/j.bbamcr.2007.11.019.

[54] Y. Wang *et al.*, "Blockade of PLD1 potentiates the antitumor effects of bortezomib in multiple myeloma cells by inhibiting the mTOR/NF-κB signal pathway," *Hematology*, vol. 25, no. 1, pp. 424–432, Jan. 2020, doi: 10.1080/16078454.2020.1845501.

[55] D. W. Kang *et al.*, "Triptolide-induced suppression of phospholipase D expression inhibits proliferation of MDA-MB-231 breast cancer cells," *Exp Mol Med*, vol. 41, no. 9, p. 678, 2009, doi: 10.3858/emm.2009.41.9.074.

[56] Y.-C. Chang *et al.*, "Aldolase A and Phospholipase D1 Synergistically Resist Alkylating Agents and Radiation in Lung Cancer," *Front Oncol*, vol. 11, Jan. 2022, doi: 10.3389/fonc.2021.811635.

[57] A. R. Noble, N. J. Maitland, D. M. Berney, and M. G. Rumsby, "Phospholipase D inhibitors reduce human prostate cancer cell proliferation and colony formation," *Br J Cancer*, vol. 118, no. 2, pp. 189–199, Jan. 2018, doi: 10.1038/bjc.2017.391.

[58] Q. Chen *et al.*, "Key Roles for the Lipid Signaling Enzyme Phospholipase D1 in the Tumor Microenvironment During Tumor Angiogenesis and Metastasis," *Sci Signal*, vol. 5, no. 249, Nov. 2012, doi: 10.1126/scisignal.2003257.

[59] Q. Zhang *et al.*, "PLD1-dependent PKCγ activation downstream to Src is essential for the development of pathologic retinal neovascularization," *Blood*, vol. 116, no. 8, pp. 1377–1385, Aug. 2010, doi: 10.1182/blood-2010-02-271478.

[60] Y. Zhang and M. A. Frohman, "Cellular and Physiological Roles for Phospholipase D1 in Cancer," *Journal of Biological Chemistry*, vol. 289, no. 33, pp. 22567–22574, Aug. 2014, doi: 10.1074/jbc.R114.576876.

[61] L. Wang *et al.*, "CD103-positive CSC exosome promotes EMT of clear cell renal cell carcinoma: role of remote MiR-19b-3p," *Mol Cancer*, vol. 18, no. 1, p. 86, Dec. 2019, doi: 10.1186/s12943-019-0997-z.

[62] J. Liao, R. Liu, Y.-J. Shi, L.-H. Yin, and Y.-P. Pu, "Exosome-shuttling microRNA-21 promotes cell migration and invasion-targeting PDCD4 in esophageal cancer," *Int J Oncol*, vol. 48, no. 6, pp. 2567–2579, Jun. 2016, doi: 10.3892/ijo.2016.3453.

[63] R. Munagala, F. Aqil, and R. C. Gupta, "Exosomal miRNAs as biomarkers of recurrent lung cancer," *Tumor Biology*, vol. 37, no. 8, pp. 10703–10714, Aug. 2016, doi: 10.1007/s13277-016-4939-8.

[64] S. Pfeffer *et al.*, "Detection of Exosomal miRNAs in the Plasma of Melanoma Patients," *J Clin Med*, vol. 4, no. 12, pp. 2012–2027, Dec. 2015, doi: 10.3390/jcm4121957.

[65] J. L. Hood, R. S. San, and S. A. Wickline, "Exosomes Released by Melanoma Cells Prepare Sentinel Lymph Nodes for Tumor Metastasis," *Cancer Res*, vol. 71, no. 11, pp. 3792–3801, Jun. 2011, doi: 10.1158/0008-5472.CAN-10-4455.

[66] N. Ludwig, S. S. Yerneni, B. M. Razzo, and T. L. Whiteside, "Exosomes from HNSCC Promote Angiogenesis through Reprogramming of Endothelial Cells," *Molecular Cancer Research*, vol. 16, no. 11, pp. 1798–1808, Nov. 2018, doi: 10.1158/1541-7786.MCR-18-0358.

[67] M. Gong *et al.*, "Mesenchymal stem cells release exosomes that transfer miRNAs to endothelial cells and promote angiogenesis," *Oncotarget*, vol. 8, no. 28, pp. 45200–45212, Jul. 2017, doi: 10.18632/oncotarget.16778.

[68] K. Pakravan *et al.*, "MicroRNA-100 shuttled by mesenchymal stem cell-derived exosomes suppresses in vitro angiogenesis through modulating the mTOR/HIF-1α/VEGF signaling axis in breast cancer cells," *Cellular Oncology*, vol. 40, no. 5, pp. 457–470, Oct. 2017, doi: 10.1007/s13402-017-0335-7.

[69] H. Onallah, S. T. Mannully, B. Davidson, and R. Reich, "Exosome Secretion and Epithelial-Mesenchymal Transition in Ovarian Cancer Are Regulated by Phospholipase D," *Int J Mol Sci*, vol. 23, no. 21, p. 13286, Oct. 2022, doi: 10.3390/ijms232113286.

[70] T. W. Bumpus and J. M. Baskin, "Clickable Substrate Mimics Enable Imaging of Phospholipase D Activity," *ACS Cent Sci*, vol. 3, no. 10, pp. 1070–1077, Oct. 2017, doi: 10.1021/acscentsci.7b00222.

[71] F. Zhang *et al.*, "Temporal Production of the Signaling Lipid Phosphatidic Acid by Phospholipase D2 Determines the Output of Extracellular Signal-Regulated Kinase Signaling in Cancer Cells," *Mol Cell Biol*, vol. 34, no. 1, pp. 84–95, Jan. 2014, doi: 10.1128/MCB.00987-13.

[72] A. Mahmood *et al.*, "Exosome secretion kinetics are controlled by temperature," *Biophys J*, vol. 122, no. 7, pp. 1301–1314, Apr. 2023, doi: 10.1016/j.bpj.2023.02.025.

[73] A. Edelstein, N. Amodaj, K. Hoover, R. Vale, and N. Stuurman, "Computer Control of Microscopes Using µManager," *Curr Protoc Mol Biol*, vol. 92, no. 1, Oct. 2010, doi: 10.1002/0471142727.mb1420s92.

[74] F. J. Verweij *et al.*, "ER membrane contact sites support endosomal small GTPase conversion for exosome secretion," *Journal of Cell Biology*, vol. 221, no. 12, Dec. 2022, doi: 10.1083/jcb.202112032.

[75] A. Liu *et al.*, "pHmScarlet is a pH-sensitive red fluorescent protein to monitor exocytosis docking and fusion steps," *Nat Commun*, vol. 12, no. 1, p. 1413, Mar. 2021, doi: 10.1038/s41467-021-21666-7.

[76] P. Chardin and F. McCormick, "Brefeldin A," *Cell*, vol. 97, no. 2, pp. 153–155, Apr. 1999, doi: 10.1016/S0092-8674(00)80724-2.

[77] N. Vashi, S. B. A. Andrabi, S. Ghanwat, M. Suar, and D. Kumar, "Ca2+-dependent Focal Exocytosis of Golgi-derived Vesicles Helps Phagocytic Uptake in Macrophages," *Journal of Biological Chemistry*, vol. 292, no. 13, pp. 5144–5165, Mar. 2017, doi: 10.1074/jbc.M116.743047.

[78] J. M. Alderton, S. A. Ahmed, L. A. Smith, and R. A. Steinhardt, "Evidence for a vesicle-mediated maintenance of store-operated calcium channels in a human embryonic kidney cell line," *Cell Calcium*, vol. 28, no. 3, pp. 161–169, Sep. 2000, doi: 10.1054/ceca.2000.0144.

[79] S. Xu *et al.*, "Autocrine insulin increases plasma membrane KATP channel via PI3K-VAMP2 pathway in MIN6 cells," *Biochem Biophys Res Commun*, vol. 468, no. 4, pp. 752–757, Dec. 2015, doi: 10.1016/j.bbrc.2015.11.028.

[80] R. Kalluri and V. S. LeBleu, "The biology, function, and biomedical applications of exosomes," *Science*, vol. 367, no. 6478, Feb. 2020, doi: 10.1126/science.aau6977.

[81] R. Ghossoub *et al.*, "Syntenin-ALIX exosome biogenesis and budding into multivesicular bodies are controlled by ARF6 and PLD2," *Nat Commun*, vol. 5, no. 1, p. 3477, Mar. 2014, doi: 10.1038/ncomms4477.

[82] E. Tanguy *et al.*, "Mono- and Poly-unsaturated Phosphatidic Acid Regulate Distinct Steps of Regulated Exocytosis in Neuroendocrine Cells," *Cell Rep*, vol. 32, no. 7, p. 108026, Aug. 2020, doi: 10.1016/j.celrep.2020.108026.

[83] P. Huang, Y. M. Altshuller, J. C. Hou, J. E. Pessin, and M. A. Frohman, "Insulin-stimulated plasma membrane fusion of Glut4 glucose transporter-containing vesicles is regulated by phospholipase D1," *Mol Biol Cell*, vol. 16, no. 6, pp. 2614–2623, Jun. 2005, doi: 10.1091/mbc.e04-12-1124.

[84] J. Disse, N. Vitale, M.-F. Bader, and V. Gerke, "Phospholipase D1 is specifically required for regulated secretion of von Willebrand factor from endothelial cells," *Blood*, vol. 113, no. 4, pp. 973–980, Jan. 2009, doi: 10.1182/blood-2008-06-165282.

[85] W. S. Choi, Y. M. Kim, C. Combs, M. A. Frohman, and M. A. Beaven, "Phospholipases D1 and D2 Regulate Different Phases of Exocytosis in Mast Cells," *The Journal of Immunology*, vol. 168, no. 11, pp. 5682–5689, Jun. 2002, doi: 10.4049/jimmunol.168.11.5682.

[86] A. Llorente *et al.*, "Molecular lipidomics of exosomes released by PC-3 prostate cancer cells," *Biochimica et Biophysica Acta (BBA) - Molecular and Cell Biology of Lipids*, vol. 1831, no. 7, pp. 1302–1309, Jul. 2013, doi: 10.1016/j.bbalip.2013.04.011.

[87] T. Skotland, N. P. Hessvik, K. Sandvig, and A. Llorente, "Exosomal lipid composition and the role of ether lipids and phosphoinositides in exosome biology," *J Lipid Res*, vol. 60, no. 1, pp. 9–18, Jan. 2019, doi: 10.1194/jlr.R084343.

[88] V. Muralidharan-Chari *et al.*, "ARF6-Regulated Shedding of Tumor Cell-Derived Plasma Membrane Microvesicles," *Current Biology*, vol. 19, no. 22, pp. 1875–1885, Dec. 2009, doi: 10.1016/j.cub.2009.09.059.

[89] K. Laulagnier *et al.*, "PLD2 is enriched on exosomes and its activity is correlated to the release of exosomes," *FEBS Lett*, vol. 572, no. 1–3, pp. 11–14, Aug. 2004, doi: 10.1016/j.febslet.2004.06.082.

[90] C. Subra *et al.*, "Exosomes account for vesicle-mediated transcellular transport of activatable phospholipases and prostaglandins," *J Lipid Res*, vol. 51, no. 8, pp. 2105–2120, Aug. 2010, doi: 10.1194/jlr.M003657.

[91] B. Liang *et al.*, "Characterization and proteomic analysis of ovarian cancer-derived exosomes," *J Proteomics*, vol. 80, pp. 171–182, Mar. 2013, doi: 10.1016/j.jprot.2012.12.029.

[92] K. Laulagnier *et al.*, "Mast cell- and dendritic cell-derived exosomes display a specific lipid composition and an unusual membrane organization," *Biochemical Journal*, vol. 380, no. 1, pp. 161–171, May 2004, doi: 10.1042/bj20031594.

[93] J. F. Brouwers *et al.*, "Distinct lipid compositions of two types of human prostasomes," *Proteomics*, vol. 13, no. 10–11, pp. 1660–1666, May 2013, doi: 10.1002/pmic.201200348.

[94] A. L. Egea-Jimenez and P. Zimmermann, "Lipids in Exosome Biology," in *Lipid Signaling in Human Diseases*, J. Gomez-Cambronero and M. Frohman, Eds., 2019, pp. 309–336. doi: 10.1007/164_2019_220.

[95] R. Mendonsa and J. Engebrecht, "Phosphatidylinositol-4,5-Bisphosphate and Phospholipase D-Generated Phosphatidic Acid Specify SNARE-Mediated Vesicle

Fusion for Prospore Membrane Formation," *Eukaryot Cell*, vol. 8, no. 8, pp. 1094–1105, Aug. 2009, doi: 10.1128/EC.00076-09.

[96] A. D. Lam, P. Tryoen-Toth, B. Tsai, N. Vitale, and E. L. Stuenkel, "SNARE-catalyzed fusion events are regulated by Syntaxin1A-lipid interactions," *Mol Biol Cell*, vol. 19, no. 2, pp. 485–497, Feb. 2008, doi: 10.1091/mbc.e07-02-0148.

[97] R. Alonso *et al.*, "Diacylglycerol kinase α regulates the formation and polarisation of mature multivesicular bodies involved in the secretion of Fas ligand-containing exosomes in T lymphocytes," *Cell Death Differ*, vol. 18, no. 7, pp. 1161–1173, Jul. 2011, doi: 10.1038/cdd.2010.184.

[98] R. Alonso, C. Mazzeo, I. Mérida, and M. Izquierdo, "A new role of diacylglycerol kinase α on the secretion of lethal exosomes bearing Fas ligand during activation-induced cell death of T lymphocytes," *Biochimie*, vol. 89, no. 2, pp. 213–221, Feb. 2007, doi: 10.1016/j.biochi.2006.07.018.

[99] G. Bossi and G. M. Griffiths, "Degranulation plays an essential part in regulating cell surface expression of Fas ligand in T cells and natural killer cells," *Nat Med*, vol. 5, no. 1, pp. 90–96, Jan. 1999, doi: 10.1038/4779.

[100] M. Izquierdo, M. C. Ruiz-Ruiz, and A. López-Rivas, "Stimulation of phosphatidylinositol turnover is a key event for Fas-dependent, activation-induced apoptosis in human T lymphocytes.," *Journal of Immunology*, vol. 157, no. 1, pp. 21–28, Jul. 1996, doi: 10.4049/jimmunol.157.1.21.

[101] E. J. Quann, E. Merino, T. Furuta, and M. Huse, "Localized diacylglycerol drives the polarization of the microtubule-organizing center in T cells," *Nat Immunol*, vol. 10, no. 6, pp. 627–635, Jun. 2009, doi: 10.1038/ni.1734.

[102] Y. Zou *et al.*, "Determination of protein regions responsible for interactions of amelogenin with CD63 and LAMP1," *Biochemical Journal*, vol. 408, no. 3, pp. 347–354, Dec. 2007, doi: 10.1042/BJ20070881.

[103] C. M. Fader, D. Sánchez, M. Furlán, and M. I. Colombo, "Induction of Autophagy Promotes Fusion of Multivesicular Bodies with Autophagic Vacuoles in K562 Cells," *Traffic*, vol. 9, no. 2, pp. 230–250, Nov. 2007, doi: 10.1111/j.1600-0854.2007.00677.x.

Chapter Four: Phosphatidic Acid Accumulates at Areas of Curvature in Tubulated

Lipid Bilayers

Phosphatidic acid (PA) is a signaling lipid that is produced enzymatically from phosphatidylcholine (PC), lysophosphatidic acid, or diacylglycerol. Compared to PC, PA lacks a choline moiety on the headgroup, making the headgroup smaller than that of PC and PA, and PA has a net negative charge. Unlike the cylindrical geometry of PC, PA, with its small headgroup relative to the two fatty acid tails, is proposed to support negatively curved membranes. Thus, PA is thought to play a role in a variety of biological processes that involve bending membranes, such as the formation of intraluminal vesicles in multivesicular bodies and membrane fusion. Using supported tubulated lipid bilayers (STuBs), the extent to which PA localizes to curved membranes was determined. STuBs were created via liposome deposition with varying concentrations of NaCl (500 mM to 1 M) on glass to form supported bilayers with connected tubules. The location of fluorescently labeled lipids relative to tubules was determined by imaging with total internal reflection or confocal fluorescence microscopy. The accumulation of various forms of PA (with acyl chains of 16:0-6:0, 16:0-12:0, 18:1-12:0) were compared to PC and headgroup labeled phosphatidylethanolamine (PE), a lipid that has been shown to accumulate at regions of curvature. PA and PE accumulated more at tubules and led to the formation of more tubules than PC. Using large unilamellar liposomes in a dye quenching assay, the location of headgroup labeled PE was determined to be mostly on the outer,

positively curved leaflet, whereas tail-labeled PA was located more on the inner, negatively curved leaflet. This study demonstrates that PA localizes to regions of negative curvature in liposomes and supports the formation of curved, tubulated membranes. This is one way that PA could be involved with curvature formation during a variety of cell processes. This work has been published in *Biomolecules* and is available via:

https://doi.org/10.3390/biom12111707

4.1: Introduction

Phosphatidic acid (PA) is a lipid that can be produced from phosphatidylcholine (PC), diacylglycerol, lysophosphatidic acid (LPA) or *de novo* from glycerol 3-phosphate or dihydroxyacetone phosphate [1], [2]. The roles of PA are currently best described in plants, particularly *Arabidopsis thaliana*, where PA is involved in a wide variety of processes, from stress response and growth, acting primarily as a signaling molecule [3]. In yeast, PA is involved in sporulation and secretion [3]. In mammals, PA is involved in exocytosis, intraluminal formation, cell proliferation, signaling, tumor progression and cell differentiation [3].

Many of the roles that PA has in biology are hypothesized to be related to the geometry of PA itself. PA has been shown to regulate cellular functions by altering membrane shape locally on the plasma membrane or organelle membranes [4]. PA has an inverse conical shape when compared to PC [5]. Inverse conical shaped lipids are predicted to ease membrane bending by fitting well into negatively curved membranes, whereas

conical shaped lipids, such as LPA [5] and PE with a large fluorescent dye label on the headgroup, are predicted to sort into positively curved membrane areas [6]. The presences of lipids with intrinsic membrane shape makes membrane bending easier and could also be a mechanism by which lipids are sorted [7], [8].

Several studies have focused on the interplay between membrane shape and the intrinsic lipid shape. Positively curved membranes accumulated single tailed lipids, such as fluorescein-labeled hexadecanoic acid [6] and LPA [9], which are conical in shape. Interestingly, lipids with two tails also accumulate (fluorescein 1,2-dihexadecanoyl-sn-glycero-3-phosphoethanolamine, Fl-DHPE) to a higher extent [6], [10]. An alternative model for lipid sorting depends on the defect sites in the bilayer that are present when a membrane bends [11]. The positively curved side has packing defect sites that, when present, allow for the insertion of hydrophobic protein motifs or lipids [10], [12]. Therefore, defect sites are places in the membrane that can be stabilized by filling with lipids. Lipids with more carbons in the tails (either longer tails or two tails) have been shown to accumulate more at these sites [6], [10]. This is in contrast to the concept of sorting based on the intrinsic lipid shape, and the work presented here focuses on both the role of lipid tails and the small headgroup in PA curvature membrane sorting.

To measure how lipids and proteins are recruited by or induce curved membranes, several model curved membrane assays exist, such as curved supported lipid bilayers [13], tubules [14], membrane coated nanopatterned surfaces [15]–[17], and small liposome-based assays [10], [18]. Recently, an assay using NaCl to induce tubule formation in supported lipid bilayers (SLBs) was developed by Schenk *et al* [19]. These supported

tubulated bilayers (STuBs) were used to study Sar1B, a vesicle budding protein [19], but in this study, we demonstrate that this assay is useful for measuring lipid accumulation at curvature as well. This assay was chosen partly due to the simplicity of creating the tubules but also because the tubes are connected to the flat supported bilayer, allowing the measurement of recruitment to curved regions to be directly compared to flat areas in the same measurement.

In this work, STuBs were used to measure the recruitment of PA to curvature and to determine if PA supports membrane curvature formation and if PA accumulates at regions of curvature. STuBs were created from POPC, DOPE-PEG and a fluorescent lipid (either PA, PC or PE) and imaged using confocal and TIRF microscopies. From image data, the number of tubes per area and the intensity of dye labeled lipid per tube were quantified relative to the flat areas of the same samples. As an alternative, extruded large unilamellar liposomes were measured in bulk and the accessibility of the dye to quenching agents was assessed to determine which leaflet accumulated PA. Our results demonstrate that PA stabilizes curvature and prefers negatively curved areas relative to PC controls.

4.2: Materials and Methods

Liposome and STuBs Assembly:

Lipids were mixed in chloroform to specified concentrations using glass syringes for a total of 250 nmol. Chloroform was evaporated using nitrogen and vacuum. Lipids were resuspended in 2 mL of buffer containing 140 mM KCl, 20 mM HEPES and varying concentrations of NaCl at pH 7.4. The solution was probe sonicated for 5 min on ice. For

SLBs, 8 well dishes were cleaned by submerging in 0.1% SDS for 1 hour, followed by 1% bleach overnight, then 100 µL of 2% Hellmanex was added to each well for one hour. Afterwards, wells were rinsed three times in buffer containing 140 mM KCl, 20 mM HEPES and varying concentrations of NaCl at pH 7.4. 100 µL of liposome stocks were deposited per well in 8 well dishes and incubated at 37°C for 1 hour. SLBs were then imaged immediately. Lipids used in this study include 1-palmitoyl-2-oleoyl-glycero-3-phosphocholine (POPC, Avanti Polar Lipids, 850457), 1,2-dioleoyl-sn-glycero-3-phosphoethanolamine-N-[methoxy(polyethylene glycol)-2000] (DOPE-PEG, Avanti Polar Lipids, 880234), Marina Blue- 1,2-dihexadecanoyl-sn-glycero-3-phosphoethanolamine (MB-DPPE, ThermoFisher, M12652), 1,1′-dioctadecyl-3,3,3′,3′-tetramethylindodicarbocyanine, 4-chlorobenzenesulfonate salt (DiD, ThermoFisher, D7757), 1,1′-dioctadecyl-3,3,3′,3′-tetramethylindocarbocyanine perchlorate (DiI, ThermoFisher, D282), 1-palmitoyl-2-{6-[(7-nitro-2-1,3-benzoxadiazol-4-yl)amino]hexanoyl}-sn-glycero-3-phosphate (16:0 6:0-NBD PA, Avanti Polar Lipids, 810173), 1-palmitoyl-2-{12-[(7-nitro-2-1,3-benzoxadiazol-4-yl)amino]dodecanoyl}-sn-glycero-3-phosphate (16:0 12:0-NBD PA Avanti Polar Lipids, 810174), 1-oleoyl-2-{12-[(7-nitro-2-1,3-benzoxadiazol-4-yl)amino]dodecanoyl}-sn-glycero-3-phosphate (18:1 12:0-NBD PA, Avanti Polar Lipids, 810176), 1-oleoyl-2-[12-[(7-nitro-2-1,3-benzoxadiazol-4-yl)amino]dodecanoyl]-sn-glycero-3-phosphocholine (18:1 12:0-NBD PC, Avanti Polar Lipids, 810133), and 1,2-dipalmitoyl-sn-glycero-3-phosphoethanolamine-N-(7-nitro-2-1,3-benzoxadiazol-4-yl) (NBD-DPPE, Avanti Polar Lipids, 810144). Liposomes contained 98% POPC, 1% DOPE-PEG and 1% NBD-labeled

83

lipid. SLBs used for FRAP contained 96.9% POPC 1% DOPE-PEG, 2% MB-DPPE and 0.1% DiD. SLBs used for TIRF contained 98% POPC, 1% DOPE-PEG, and 1% NBD-labeled lipid. MB-DPPE concentration was 2%, the same as past work [16], and NBD labeled PA lipids were used at a concentration relevant to what is observed in cells [20], [21]. POPC concentration was adjusted to accommodate the difference. All lipids were purchased from Avanti Polar Lipids (Alabaster, Alabama, USA), except for MB-DPPE, DiI and DiD, which were purchased from ThermoFisher. DiI was used in TIRF measurements andDiD was used for confocal measurements of the membrane tubule size due to the excitation wavelengths available on different microscopes. MB-DPPE was used for measuring fluidity.

Fluorescence Recovery After Photobleaching (FRAP):

FRAP was performed on a point-scanning confocal microscope (Olympus Fluoview 3000) to test fluidity of bilayers and connectivity of tubules. The FRAP region was a 60-pixel diameter (6.01 μm) circle. A 640 nm laser was used for DiD and a 405 nm laser for MB-DPPE. The imaging rate was 2.17 seconds per frame during 2-color imaging. 3 frames were taken prior to bleaching, then FRAP region was bleached for 1s, followed by 45 frames for recovery. FRAP occurred at room temperature 20-22°C. FRAP data was corrected for photobleaching and normalized to the average of the pre-bleach frames as described in previous work [6], [16]. Graphpad Prism was used for plotting, fitting and t-testing.

Total Internal Reflection Fluorescence Microscopy:

STuBs samples were imaged immediately after assembly. Two color imaging data were taken with a 60x (1.49 NA) objective followed by a 2.5x magnifying lens to obtain a magnification that is 0.109 µm/pixel on the detector (EMCCD, Andor iXon897). A DualView (Optical Insights) was used to split the red and green fluorescence (565LP dichroic with 525/50 and 605/75 emission filters, Chroma Technologies) into separate channels onto the camera. Movies were taken at 1 frame/second using Micromanager [22].

For image analysis, the red and green images were aligned using 200 nm carboxylate modified, yellow-green fluospheres (ThermoFisher, F8811) and home-built alignment code in MATLAB, as used previously [23], [24]. These nanoparticles (diameter = 200 nm) were also used to identify the diffraction limit of the TIRF in full width half max (FWHM) calculations [21,22]. Tubule positions were located by bandpass filtering with 9 pixels followed by spot finding with a pixel size of 5 and a variable threshold. All spot-finding code was initially written in IDL [25], then made available in MATLAB [26]. Radial plots were calculated as described previously [27], and the intensity from each peak was normalized to the intensity ~500nm away. These plots were used to calculate the FWHM of tubules based on the max intensity and the flat intensity, also ~500nm away. Intensity ($\Delta F/S$) measurements were calculated using Equation 4.1:

$$\frac{\Delta F}{S} = \frac{C - A}{A - bg} \tag{4.1}$$

where C is the average intensity of a circle with a 5-pixel diameter and A is the intensity of an annulus 1 pixel wide, 7 pixels from the peak, were used (Figure 4.1). This is
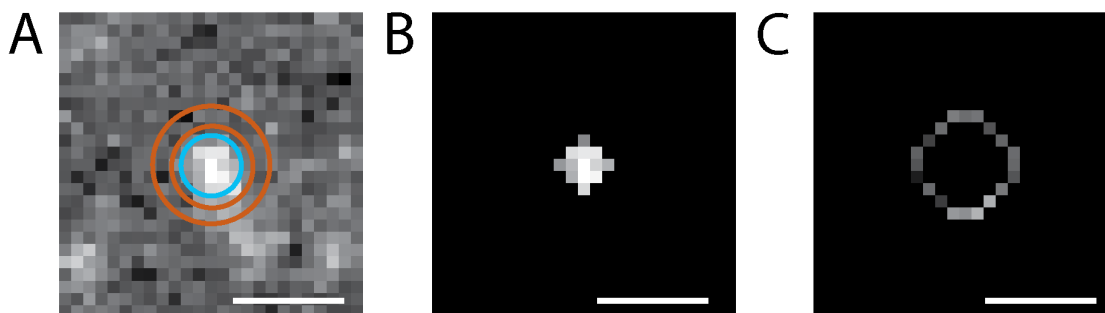
Figure 4.1: Description of ΔF/S Measurements. A) Depiction of the circle (blue) and annulus (orange) regions overlaid on the image of a tubule in the DiD (red) channel. There is a 1-pixel thick ring that separates the circle and annulus regions. B) Example of the same tubule with the circle intensity shown. The average of this region constitutes the circle intensity. C) Example of the same tubule with the annulus region intensity shown. The average of this ring constitutes the annulus intensity. The intensities of the circle and annulus are obtained and used to calculate ΔF/S, where ΔF = circle – annulus and S = annulus – background, where background is the average intensity of a POPC membrane with no fluorophores present. Scale bars = 1 μm.

normalized using the background was defined as the intensity of a membrane with no fluorophores present. This has been described in detail previously [23]. Longer length tubules were occasionally noted as others observed previously [19]. These tubules are typically disconnected from the bilayer and rare. Therefore, these were not used in measurements for this paper. All analysis was performed in MATLAB and code will be made available upon request. All statistical testing was performed in GraphPad Prism.

Fluorimetry:

NBD labeled liposomes in 2.5 mL buffer (140 mM KCl, 20 mM HEPES and 15mM NaCl at pH 7.4) were extruded through 100 nm filters and put in a 1 cm quartz cuvette with a stir bar. 250 μL of 0.1 mM dithionite was added after 30 s. Readings were taken on a Cary Eclipse once per second, with 0.1 second exposure, an excitation wavelength of 463

nm and emission of 533 nm. Excitation and emission slit widths were variable depending on intensity of samples, between 5 and 20 nm.

4.3: Results

The Formation of STuBs Depends on NaCl Concentration

To determine what concentration of NaCl reliably formed tubules, SLBs were formed using 96.9% POPC, 1% DOPE-PEG, 2% Marina Blue-DPPE and 0.1% DiD at varying concentrations of NaCl (Figure 4.2A). The lowest and highest concentration were chosen to replicate the original STuBs study [19]. This combination of lipids was intended to be a simple mixture that mimics the plasma membrane and includes PEGylated lipids to cushion the bilayer from the glass surface [28] and mimic the crowded cellular environment [29]. Increasing the concentration of NaCl reproducibly induced formation of more tubules (Figure 4.2A,B). On rare occasion, long tubules formed as seen in other labs [19], but were not included in our analyses due to their rarity and their shapes complicating analysis. Instead, smaller tubules were measured and are fluid with the rest of the bilayer (Figure 4.3), which suggests they are connected structures, rather than liposomes. These tubule structures recovered to the same extent as the flat regions of the membrane (Figure 4.3). The tubules were diffraction limited (Figure 4.2A,E), but the intensity of the tubules varied with NaCl concentration (Figure 4.2D) based on measurements of ΔF/S, described in Figure 4.1. Specifically, tubules assembled in 1000 mM NaCl were significantly more intense than those at 500 or 750 mM (Figure 4.2D), while differences in FWHM values of tubules at any [NaCl] were not significant (Figure
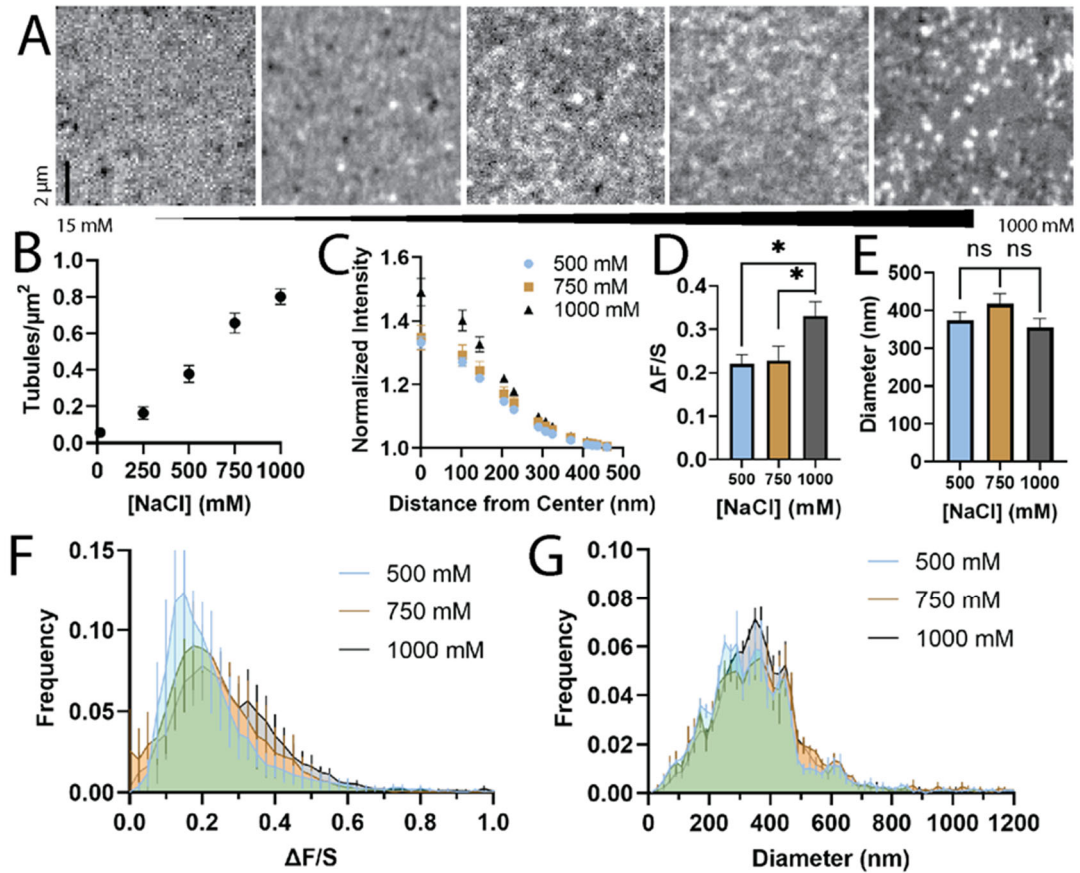
Figure 4.2 Tubules Form in the Presence of 500–1000 mM NaCl. Lipid tubules were characterized using 0.1% DiD as a lipid marker. Increasing concentration of NaCl increases number of tubules per area. A) Tubules were imaged using confocal microscopy. [NaCl] from top to bottom (mM): 15, 250, 500, 750, 1000. All images are autoscaled. B) DiD-labeled tubule density as a function of NaCl concentration. C) Radial plots of intensity of DiD at 500 mM (blue circles), 750 mM (brown squares), and 1000 mM (black triangles), normalized to intensity at 951 nm from center. D) Average intensity of lipids at sites of tubules for different [NaCl], displayed as ΔF/S, a function of tubule intensity and surrounding intensity. Significant differences noted by *, where a t-test p value < 0.05. E) Average size in nm at [NaCl] of 500, 750, and 1000 mM. All error bars are SEM (n = 9). No significant (ns) differences measured. F) The distribution of intensities of single tubules. G) The distribution of the diameter, as measured from the FWHM of the imaged tubule. Error bars in histograms are SEM from three days.

4.2E). This suggests that tubules may be larger with higher concentration of NaCl. Since

single tubules can be observed in this assay, the distribution of intensity and sizes can also

88
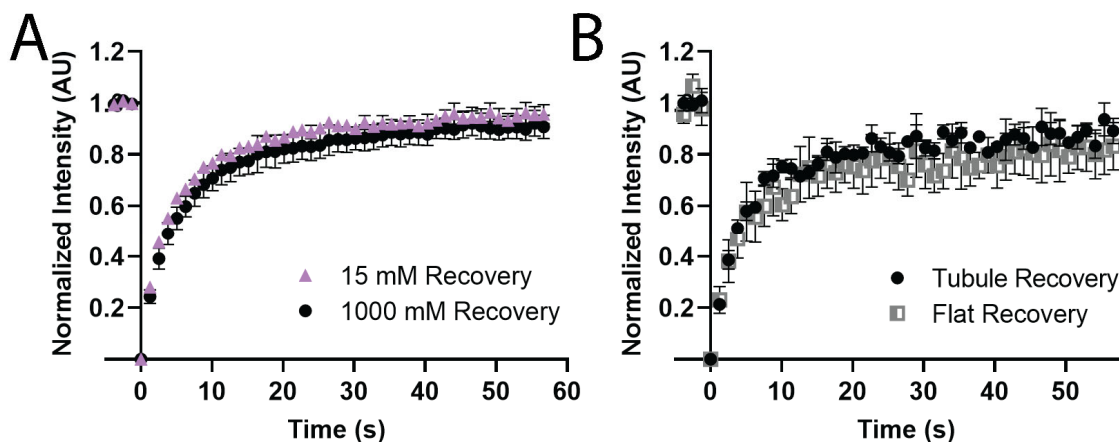
Figure 4.3: STuBs Do Not Affect Fluidity of MB-DHPE. A) FRAP recovery of SLBs deposited in 15 mM NaCl buffer (purple triangles) or 1000 mM NaCl buffer (black circles). B) FRAP recovery of tubules (black circles) or flat regions (grey squares) specifically. For both graphs, intensity was normalized for photobleaching such that 1 is the average of three pre-FRAP frames and 0 is the frame immediately after FRAP. Error bars are SEM (n = 3).

be quantified (Figure 4.2G). The distributions of intensity ($\Delta F/S$) and the tubule size (FWHM) is similar for tubules prepared with 500, 750 or 1000mM NaCl.

PA and DPPE Form More Tubules Than PC

To determine if lipids with intrinsic curvature affected STuBs formation or accumulate in certain regions, tail labeled PA (NBD-PA) and headgroup labeled DPPE (DPPE-NBD) were incorporated separately into the STuBs. In this experiment, all lipids were identical except the ones labeled on the axis in Figure 4.4. Membranes were formed in 1000 mM NaCl buffer, using 98% POPC, 1% DOPE-PEG, and 1% either DPPE-NBD, (18:1 12:0)-NBD-PC, or (18:1 12:0)-NBD-PA and imaged using TIRF microscopy (Figure 4.4A). In this experiment, PC acted as a negative control, while DPPE-NBD was a positive control because it sorts into positively curved membranes [6], [30]. The NBD-PA produced
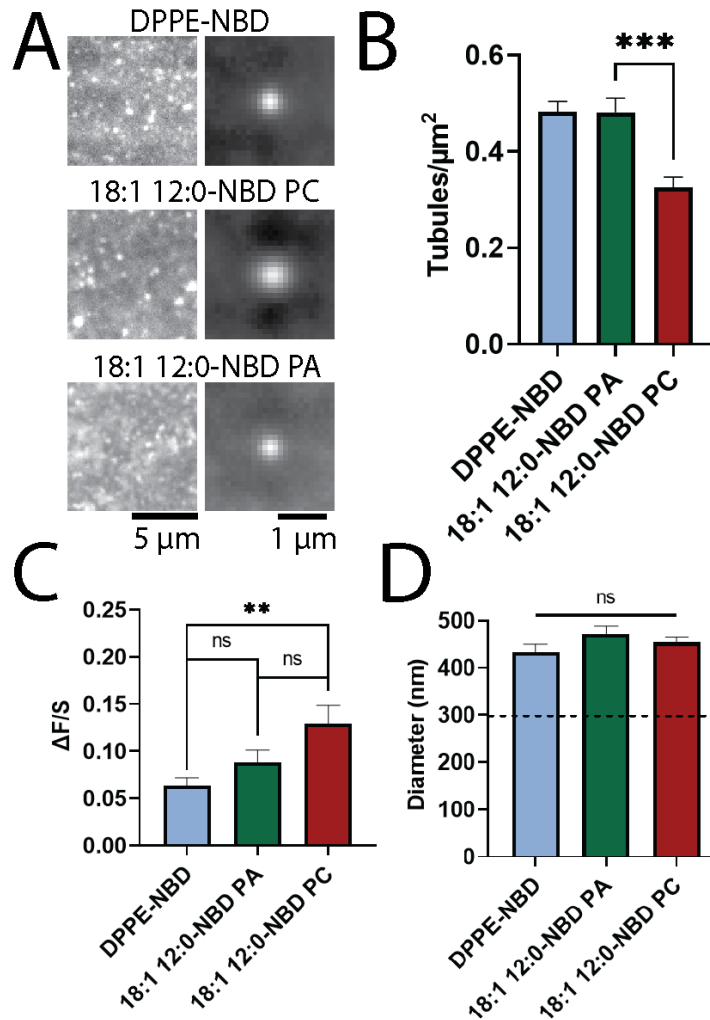
Figure 4.4: Tubulated Lipid Bilayers with PA and DPPE Induce More Tubule Formation Than PC. A) Examples of bilayers with 18:1 12:0-NBD PA (top), 18:1 12:0-NBD PC (middle), and DPPE-NBD (bottom), with examples of STuBs (left) and averaged tubules (right). B) Average tubule density of bilayers with respective lipids. C) Average ΔF/S of lipids. D) Average diameter (FWHM) of lipids. On our microscope, the average FWHM of diffraction-limited 200 nm green polystyrene nanoparticles is 296 nm (dashed line). Error bars are SEM. n = 12 membranes between 3 days. ** $p < 0.005$, *** $p < 0.0005$ and ns = not significant on a t-test.

more tubules than NBD-PC and as many as DPPE-NBD (Figure 4.4B). This supports the

hypothesis that PA affects membrane curvature formation. Next, the intensity of the

tubules was evaluated to determine if tubules contained higher amounts of the NBD-

labeled lipids. The intensity (ΔF/S) varied as a function of the lipid headgroups with NBD-PA tubules being dimmer than NBD-PC tubules (Figure 4.4C). The higher intensity (Figure 4.4C) suggests that either more PC is present in tubules, relative to PA and DPPE, or tubules are larger when NBD-PC is present. However, no significant difference in the tubule diameter (FWHM) was observed between PA, PC or PE (Figure 4.4D). Therefore, more PC is likely present on the tubules.

Longer Fatty Acid Chains Support Tubule Formation

Although the headgroup of a lipid likely plays a key role in determining localization to curved membranes [5]–[9], the acyl chains have also been shown to affect the overall geometry and sorting on different membranes shapes [6], [10]. To determine the role that the acyl chains play in lipid sorting, several PAs with modified tails were compared for their ability to sort into curved membranes and support the formation of tubules. Specifically, two fully saturated NBD-PAs (16:0 12:0-NBD PA and 16:0 6:0-NBD PA) were used in addition to the monounsaturated 18:1 12:0-NBD PA (Figure 4.4). The presence of 18:1 12:0 NBD PA led to more tubule formation than 16:0 12:0 NBD PA and 16:0 12:0 NBD PA led to more tubule formation than 16:0 6:0 PA, showing a trend with the size of the lipid tails (Figure 4.5A,B). PA supports the formation of more tubules when more carbons are present in the fatty acid chains, as shown by the higher density of tubules with PA as compared to PC with identical acyl chains (Figure 4.5B). Unlike the density of tubules, the intensity of tubules (Figure 4.4C) did not trend with the number of carbons in the fatty acyl chains. Instead, tubules with 16:0 12:0-NBD PA appear brighter than either

91
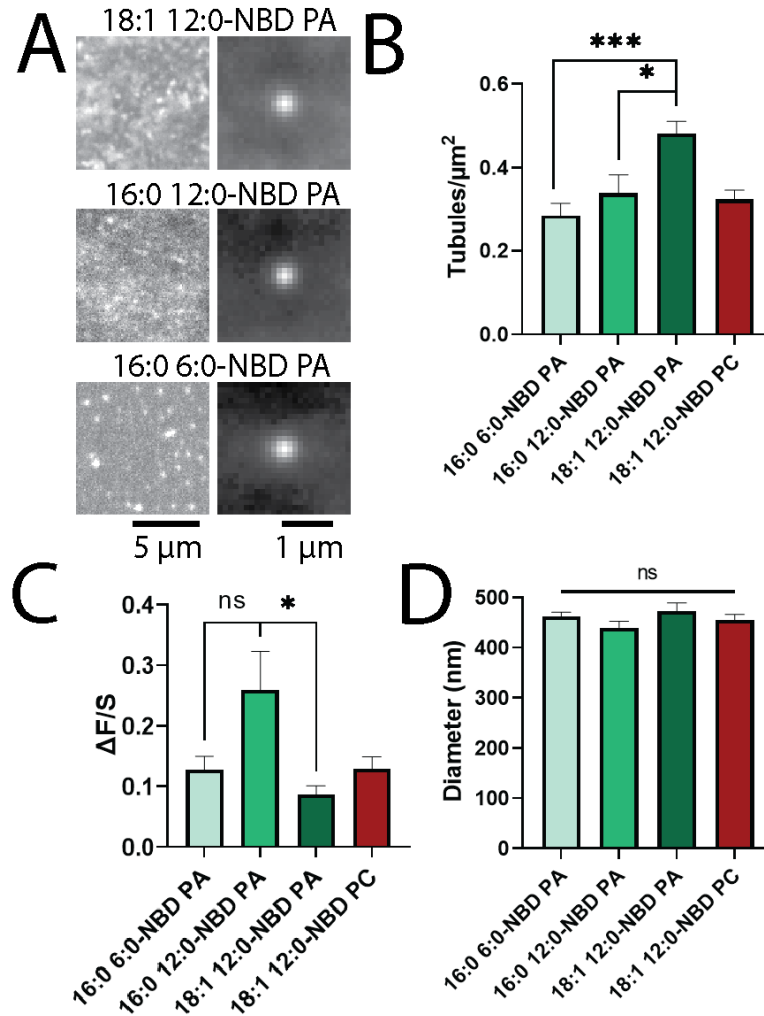
Figure 4.5: Lipids with Longer Fatty Acid Chains Form More Tubules. A) Examples of tubules containing 1% fatty-acid-labeled PA. 18:1 12:0-NBD PA (top), 16:0 12:0-NBD PA (middle), 16:0 6:0-NBD PA (bottom). B) Tubule density of bilayers with respective lipids. C) Average ΔF/S values of lipids. D) Average FWHM of lipids. All differences are not significant in D. Error bars are SEM. n = 12 membranes between 3 days. * $p < 0.05$, *** $p < 0.0005$ and ns = not significant on a t-test.

16:0 6:0-NBD-PA or 18:1 12:0-NBD PA (Figure 4.5C); however, the variation observed in tubule intensities was large for all tubules. The size of the tubules formed did not vary as a function of the fatty acid tail, with no significant difference in FWHM of tubules noted between PAs (Figure 4.5D). Overall, this suggests that longer acyl chains and the

incorporation of a bent, unsaturated tail on PA lipids can enhance the formation of membrane curvature, but the acyl tails do not affect the overall size distribution of the tubules that form.

Dithionite Quenching of NBD Reveals PA Localization to Negative Curvature

The presence of PA enhances tubule formation, but it is not clear from imaging of STuBs which leaflet PA sorts into. To determine if PA prefers the inner leaflet (negative curvature) or the outer leaflet (positive curvature), a dithionite quenching assay was performed with liposomes extruded through a 100 nm filter. Typically, the extrusion process yields a distribution of liposomes sizes ranging from approximately 50-150 nm [10]. Dithionite quenches NBD fluorescence [31]–[33]; however, dithionite does not usually penetrate through a synthetic lipid barrier. Therefore, the outer leaflet is quenched preferentially. Figure 4.6 shows that dithionite quenched DPPE-NBD, a positive curvature sorting lipid, to a greater extent that NBD-PC. This suggests a greater localization to the outer, positively curved leaflet. Conversely, all NBD-PAs tested quenched to a lesser extent, supporting a localization to the negatively curved leaflet (Figure 4.6A-D). Melittin was used to form pores in the vesicles to quench the remaining inner leaflet NBD molecules (Figure 4.7) [6], [34]. The fatty acid tails made no difference in the quenching assay (Figure 4.6D), suggesting that all PAs tested were similarly sorted to the interior of the liposomes.
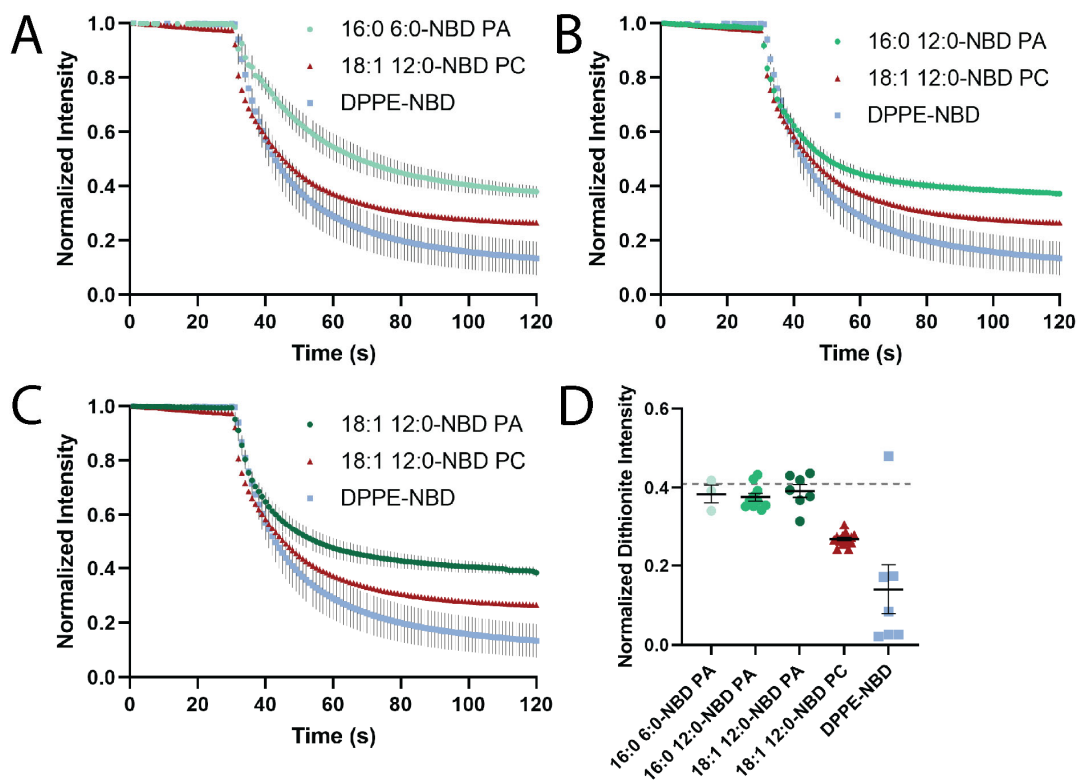
Figure 4.6: PA Localizes to Negative Curvature in a Liposome-Based Dithionite Assay. Liposomes containing 98% POPC, 1% DOPE-PEG, and 1% NBD-labeled lipids were extruded through 100 nm filters and fluorescence was measured in a fluorimeter. After 30 s, dithionite was added. A–C): the fluorescence traces over time. D): Normalized intensity after addition of dithionite. Dashed line: theoretical intensity if only the outer leaflets were quenched and liposomes were symmetric, accounting for surface area and dilution. Error bars are SEM; error on PC was smaller than the data points.

4.4: Discussion

In this work, a new membrane curvature assay that leads to the formation of tubules protruding from a supported lipid bilayer [19] has been used to determine if PA prefers and/or stabilizes curved membranes. Although STuBs are simple to form and allow for the visualization of lipids at regions with and without curvature simultaneously, there are challenges. To form STuBs, much higher concentrations of NaCl than is physiologically

94
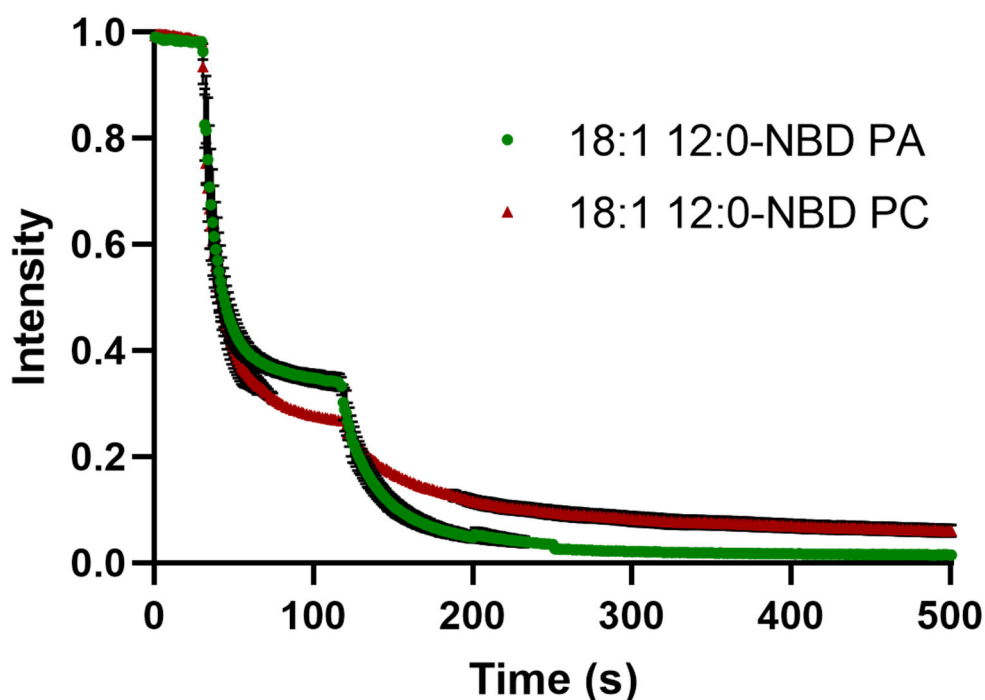
Figure 4.7 Dithionite and Melittin Fluorimetry Traces of 18:1 12:0-NBD PA and PC. Normalized intensity trace of NBD-PC (red triangles) and NBD-PA (green squares), where dithionite was added at 30 seconds and melittin was added at 120 seconds to a final concentration of 1.76 μM. Error bars are SEM for three independent replicates and often are smaller than the data points.

relevant are needed. Additionally, the read-out of the assay is fluorescence, necessitating fluorophores on lipids. Studies using NMR experiments [35] and MD simulations [36] suggest that acyl NBD labels can bend towards the water interface. This likely complicates NBD quenching assays (Figure 4.6) and could affect localization. To account for dye labeling effects, the use of an identically labeled PC as a control was essential for comparison. Despite these challenges, the use of fluorescent lipids also provides advantages. Fluorescence assays have high signal to noise, allowing lower concentrations of lipids to be assessed, down to single molecules level concentrations [16]. In this work,

the sensitivity of the assay allows PA curvature localization to be probed at a concentration that is similar to the amount of PA in mammalian and plant cells [20], [21].

The formation of STuBs is straightforward and the addition of 500-1000 mM NaCl reliably formed tubular structures (Figure 4.2A,B), similar to what others have observed [19]. These structures have varying diameters and intensity (Figure 4.2C-E), which provides a method to observe localization of dye labeled lipids to varying curvatures. The wide distribution of tubule sizes (Figure 4.2G) provides an advantage over previous work using a nanoparticle templated supported lipid bilayer [16], which contains only one size per sample as determined by the template choice. In the STuBs assay flat regions are also present and in continuum with curved membranes (Figure 4.3), which allows for a direct comparison to regions with curvature, overcoming a limitation of liposome-based curvature sensing methods [10]. By having flat regions present, slight variations in the fluorescent lipid content when preparing STuBs or in microscopy, such as laser power, are internally corrected.

The STuBs assay was used to determine the sorting of phospholipids at curvature relative to flat regions and whether certain lipids could aid in curvature formation. From TIRF microscopy images, several features of the samples were quantified to determine if tail labeled PA and PC, and headgroup labeled PE affected tubule formation or were recruited to tubules. First, the density of tubules was determined to depend upon the lipid composition; lipids that support curvature (NBD-PAs and PE-NBD) led to the formation of more tubules when compared to the control, NBD-PC (Figure 4.4B). Second, the accumulation of fluorescently labeled lipids at tubule sites relative to the surrounding flat

regions (ΔF/S) was measured. In this measurement, NBD-PA and PE-NBD (Figure 4.4C) accumulated slightly less than or similar to PC and this depended on the tails on PA (Figure 4.5C). Direct comparison of the role of the head group was determined by comparing PC to PA, both with 18:1 12:0 NBD labeled tails (Figure 4.4). PA stabilized curvature as observed in the increase in the number of tubules present (Figure 4.4B). However, the intensity of PA at tubule positions was slightly, but not significantly, less than PC (Figure 4.4C). Meanwhile, PE-NBD both stabilized tubule formation (Figure 4.4B) and was significantly less intense at tubule positions (Figure 4.4C).

We hypothesized that a reduction in intensity of PE and PA relative to PC (Figure 4.4C), could be due to preferential localization to one leaflet, thus excluding the curvature sensing lipids from a portion of the tubule bilayer and reducing fluorescence (Figure 4.8). To test this, a fluorescence quenching assay was performed in liposomes extruded through 100 nm filters and shown in Figure 4.6. NBD-PAs quenched the least, followed by NBD-PC then PE-NBD. This suggests that PA is protected from dithionite, which cannot penetrate the membrane to reach the inner leaflet, PC is quenched more, whereas PE-NBD is quenched the most (about 85%) and likely preferentially sorted to the outer leaflet (Figure 4.6D). Overall, we conclude that both NBD-PA and PE-NBD assist with the formation or stabilization of membrane curvature with NBD-PA sorting to the inner, negatively curved leaflet and PE-NBD sorted to the outer, positively curved leaflet (Figure 4.8). The sorting of head group labeled PE to the inner, positively curved leaflet agrees with past work [5], [6], [9], [30], [37]–[39], although the preference for curvature of PE-NBD may depend on the acyl chains of other lipids present [40].
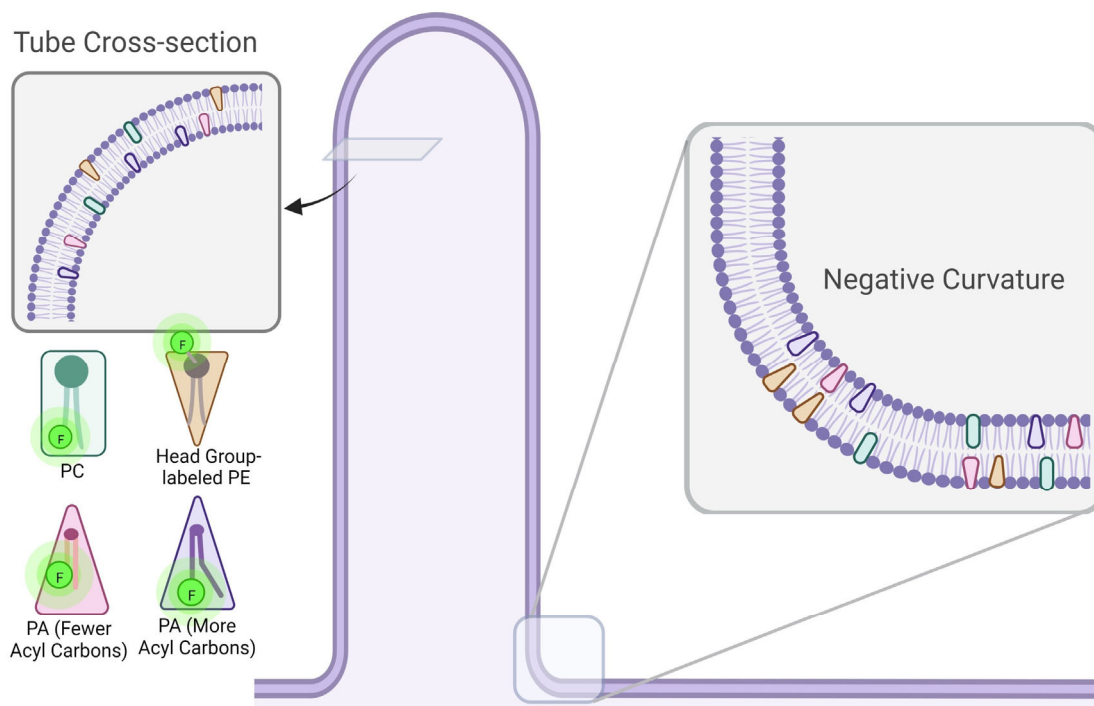
Figure 4.8: Model Depicting Curvature Sorting of Lipids in STuBs. Bottom left: Lipids used and their intrinsic geometry. Right: Side view of a tubule in a STuB. Insets: Depictions of curvature within tubules and the localization of lipids described, with enrichment of lipids in their respective curvature preferences.

Curvature-based lipid sorting is often discussed in reference to the lipid headgroup, with smaller headgroups preferring negatively curved lipid membranes and larger headgroups preferring positively curved membranes. However, the fatty acyl chains present on a lipid are essential for sorting within cells [41] and on curved synthetic membranes [10], with lysolipids showing a strong preference for positive curvature lipids showing a strong preference for positive curvature. Conversely, previous studies have also demonstrated that lipids with more carbons in the acyl chains have a greater preference for curvature, where two-tailed lipids and longer lipid tails accumulate more at positively curved membranes [6,10]. In our past work, a lipid with two acyl chains (Fluorescein-

DPPE) accumulated more at curvature than a single-tailed, fluorescein-labeled fatty acid (hexadecanoic acid) [6]. This suggests a mechanism that is different from the geometry of the lipid, and a "defect" site mechanism has been proposed [10]–[12]. In this model, the bent area in the positively curved membrane leads to the formation of packing defect sites, portrayed as a larger gap in the headgroups. This space can be filled with lipids or acylated proteins, where more carbon in the tails leads to more accumulation [10]. To test whether the tail composition affected PA accumulation, acyl-labeled PAs with varying tails were used, namely 16:0 12:0-NBD PA, 16:0 6:0-NBD PA, and 18:1 12:0-NBD PA (Figure 4.5A). PAs with shorter acyl chains formed significantly fewer tubules, with 16:0 6:0-NBD PA forming the fewest and 18:1 12:0-NBD PA forming the most (Figure 4.5B). The average size of the tubules did not depend on the tails, as all lipids yielded tubules that were approximately the same diameter (Figure 4.5D). However, the amount of NBD-labeled lipids that accumulated at tubule positions did not trend with the acyl chain length (Figure 4.5C). The saturated 16:0 12:0-NBD PA accumulated more than the unsaturated 18:1 12:0-NBD PA. This could be due to a more limited access to the positively curved leaflet, which is not supported by our data pertaining to NBD quenching within liposomes (Figure 4.6D). Instead, it is useful to note that the longest lipid is also unsaturated and, thus, bent, whereas 16:0 12:0-NBD PA and 16:0 6:0-NBD PA are both saturated lipids. Therefore, the interpretation of the accumulation (Figure 4.5C) could also be due to differences in tail saturation, with unsaturated lipids accumulating less at tubule sites. However, more lipids should be examined in future work to develop a model based on lipid

unsaturation. Overall, the longer-tailed PA lipids and curvature-sensing lipids (PA and PE) both support the formation of more tubules.

In a complementary but independent assay, dithionite was used to quench NBD-labeled lipids to determine which leaflet of a membrane lipids prefer [31]–[33]. Using LUVs extruded through 100 nm pores, dithionite quenched more than 50% of all lipids tested. As a control that should not prefer curvature, NBD-PC fluorescence was measured (Figure 4.6D). NBD-PC was quenched more than expected by dithionite. This could be due to accessibility of the dye [32], [33], and this is in line with previous studies that show the slow transport of dithionite across some membranes [31], [32], [40], but disagrees with others [40]. A second reason PC is quenched by more than 50% could be due to the liposome size; on small liposomes, the surface area on the outer leaflet is greater than the inner leaflet. However, we calculated this difference (Figure 4.6D, dashed line) and it does not account for the observed loss in fluorescence from dithionite treatment. Therefore, NBD-PC was used as a negative control to compare other lipids to because it is a lipid expected to have limited curvature preference [42]. PE-NBD was a positive control because several studies demonstrated that dye-labeled PE lipids have shown a preference for positive curvature in SLB studies and tubules extending from giant unilamellar vesicles [6], [30]. However, another study in highly curved, small unilamellar vesicles ($d < 100$nm), only weak sorting was observed for PE-NBD, suggesting that the intrinsic shape of a lipid is not the only driving force for membrane curvature sorting [18]. The positive curvature preference we measure could be likely due to the dye on the headgroup altering its geometry or another mechanism, such as the defect site model [10]. When compared in the

quenching assay, PE-NBD was quenched significantly more than NBD-PC (Figure 4.6D). This suggests that PE-NBD accumulated more on the outer leaflet of liposomes and was more accessible to dithionite treatment. Additionally, when compared to the NBD-PC control, PE-NBD formed more tubules (Figure 4.4B), suggesting a preference for curvature and possibly stabilization thereof. Unexpectedly, the PE-NBD tubules were significantly dimmer than the NBD-PC tubules (Figure 4.4C). One possible explanation is that PE-NBD localizes to the positive curvature specifically, while PC may be on both leaflets, and the liposome-quenching assay supports this hypothesis. Meanwhile, dithionite quenched fluorescent PAs to a lesser extent in the liposome assay (Figure 4.6), and 18:1 12:0-NBD PA tubules were dimmer than 18:1 12:0 NBD-PC tubules, although not significantly (Figure 4.4C). Following the same reasoning as above for PE, we conclude that PA is likely sorted to the inner leaflet of liposomes. In fact, all three PAs with varying tails quenched to the same value in the presence of dithionite, suggesting a similar preference for negative curvature (Figure 4.6). Together, these data suggest PE-NBD predominantly localizes to the outer, positively curved leaflet of STuBs and liposomes, whereas PA-labeled lipids prefer the inner, negatively curved leaflet, in agreement with others [6], [30], [31], [39]. Overall, STuBs are a new method for measuring the curvature sorting of lipids and curvature stabilization, and PA and headgroups labeled PE are curvature-stabilizing lipids.

Chapter 4 References

[1]   M. N. Hodgkin, T. R. Pettitt, A. Martin, R. H. Michell, A. J. Pemberton, and M. J. O. Wakelam, "Diacylglycerols and phosphatidates: which molecular species are intracellular messengers?," *Trends Biochem Sci*, vol. 23, no. 6, pp. 200–204, 1998, doi: 10.1016/S0968-0004(98)01200-6.

[2]   R. Thakur, A. Naik, A. Panda, and P. Raghu, "Regulation of Membrane Turnover by Phosphatidic Acid: Cellular Functions and Disease Implications," *Front Cell Dev Biol*, vol. 7, Jun. 2019, doi: 10.3389/fcell.2019.00083.

[3]   X. Wang, S. P. Devaiah, W. Zhang, and R. Welti, "Signaling functions of phosphatidic acid," *Prog Lipid Res*, vol. 45, no. 3, pp. 250–278, 2006, doi: 10.1016/j.plipres.2006.01.005.

[4]   J. Rohrbough and K. Broadie, "Lipid regulation of the synaptic vesicle cycle," *Nat Rev Neurosci*, vol. 6, no. 2, pp. 139–150, Feb. 2005, doi: 10.1038/nrn1608.

[5]   E. E. Kooijman *et al.*, "Spontaneous Curvature of Phosphatidic Acid and Lysophosphatidic Acid," *Biochemistry*, vol. 44, no. 6, pp. 2097–2102, Feb. 2005, doi: 10.1021/bi0478502.

[6]   P. P. Cheney, A. W. Weisgerber, A. M. Feuerbach, and M. K. Knowles, "Single Lipid Molecule Dynamics on Supported Lipid Bilayers with Membrane Curvature," *Membranes (Basel)*, vol. 7, no. 1, p. 15, 2017, doi: 10.3390/membranes7010015.

[7]   I. R. Cooke and M. Deserno, "Coupling between Lipid Shape and Membrane Curvature," *Biophys J*, vol. 91, no. 2, pp. 487–495, Jul. 2006, doi: 10.1529/biophysj.105.078683.

[8]   A. Callan-Jones, B. Sorre, and P. Bassereau, "Curvature-driven lipid sorting in biomembranes.," *Cold Spring Harb Perspect Biol*, vol. 3, no. 2, Feb. 2011, doi: 10.1101/cshperspect.a004648.

[9]   E. E. Kooijman, V. Chupin, B. de Kruijff, and K. N. J. Burger, "Modulation of Membrane Curvature by Phosphatidic Acid and Lysophosphatidic Acid," *Traffic*, vol. 4, no. 3, pp. 162–174, Mar. 2003, doi: 10.1034/j.1600-0854.2003.00086.x.

[10]   N. S. Hatzakis *et al.*, "How curved membranes recruit amphipathic helices and protein anchoring motifs," *Nat Chem Biol*, vol. 5, no. 11, pp. 835–841, 2009, doi: 10.1038/nchembio.213.

[11]   V. K. Bhatia, N. S. Hatzakis, and D. Stamou, "A unifying mechanism accounts for sensing of membrane curvature by BAR domains, amphipathic helices and

membrane-anchored proteins," *Semin Cell Dev Biol*, vol. 21, no. 4, pp. 381–390, Jun. 2010, doi: 10.1016/j.semcdb.2009.12.004.

[12] B. Nuscher *et al.*, "α-Synuclein Has a High Affinity for Packing Defects in a Bilayer Membrane," *Journal of Biological Chemistry*, vol. 279, no. 21, pp. 21966–21975, May 2004, doi: 10.1074/jbc.M401076200.

[13] R. Parthasarathy, C. Yu, and J. T. Groves, "Curvature-Modulated Phase Separation in Lipid Bilayer Membranes," *Langmuir*, vol. 22, no. 11, pp. 5095–5099, May 2006, doi: 10.1021/la060390o.

[14] T. J. Pucadyil and S. L. Schmid, "Real-Time Visualization of Dynamin-Catalyzed Membrane Fission and Vesicle Release," *Cell*, vol. 135, no. 7, pp. 1263–1275, 2008, doi: 10.1016/j.cell.2008.11.020.

[15] L. Hanson, Z. C. Lin, C. Xie, Y. Cui, and B. Cui, "Characterization of the Cell–Nanopillar Interface by Transmission Electron Microscopy," *Nano Lett*, vol. 12, no. 11, pp. 5815–5820, Nov. 2012, doi: 10.1021/nl303163y.

[16] J. C. Black, P. P. Cheney, T. Campbell, and M. K. Knowles, "Membrane curvature based lipid sorting using a nanoparticle patterned substrate," *Soft Matter*, vol. 10, no. 12, pp. 2016–2023, 2014, doi: 10.1039/C3SM52522H.

[17] A. M. Kabbani, X. Woodward, and C. v Kelly, "Revealing the Effects of Nanoscale Membrane Curvature on Lipid Mobility.," *Membranes (Basel)*, vol. 7, no. 4, Oct. 2017, doi: 10.3390/membranes7040060.

[18] M. M. Kamal, D. Mills, M. Grzybek, and J. Howard, "Measurement of the membrane curvature preference of phospholipids reveals only weak coupling between lipid shape and leaflet curvature," *Proceedings of the National Academy of Sciences*, vol. 106, no. 52, pp. 22245–22250, Dec. 2009, doi: 10.1073/pnas.0907354106.

[19] N. A. Schenk *et al.*, "A simple supported tubulated bilayer system for evaluating protein-mediated membrane remodeling," *Chem Phys Lipids*, vol. 215, pp. 18–28, 2018, doi: 10.1016/j.chemphyslip.2018.06.002.

[20] R. Welti *et al.*, "Profiling Membrane Lipids in Plant Stress Responses," *Journal of Biological Chemistry*, vol. 277, no. 35, pp. 31994–32002, Aug. 2002, doi: 10.1074/jbc.M205375200.

[21] T. Zech *et al.*, "Accumulation of raft lipids in T-cell plasma membrane domains engaged in TCR signalling," *EMBO J*, vol. 28, no. 5, pp. 466–476, Mar. 2009, doi: 10.1038/emboj.2009.6.

[22]   A. Edelstein, N. Amodaj, K. Hoover, R. Vale, and N. Stuurman, "Computer Control of Microscopes Using μManager," *Curr Protoc Mol Biol*, vol. 92, no. 1, Oct. 2010, doi: 10.1002/0471142727.mb1420s92.

[23]   S. Barg, M. K. Knowles, X. Chen, M. Midorikawa, and W. Almers, "Syntaxin clusters assemble reversibly at sites of secretory granules in live cells," *Proceedings of the National Academy of Sciences*, vol. 107, no. 48, pp. 20804–20809, Nov. 2010, doi: 10.1073/pnas.1014823107.

[24]   M. K. Knowles, S. Barg, L. Wan, M. Midorikawa, X. Chen, and W. Almers, "Single secretory granules of live cells recruit syntaxin-1 and synaptosomal associated protein 25 (SNAP-25) in large copy numbers," *Proceedings of the National Academy of Sciences*, vol. 107, no. 48, pp. 20810–20815, Nov. 2010, doi: 10.1073/pnas.1014840107.

[25]   J. C. Crocker and D. G. Grier, "Methods of Digital Video Microscopy for Colloidal Studies," *J Colloid Interface Sci*, vol. 179, no. 1, pp. 298–310, Apr. 1996, doi: 10.1006/jcis.1996.0217.

[26]   D. Blair and E. Dufresne, "The Matlab Particle Tracking Code Repository. [(accessed on 10 June 2014)]." Available online: https://site.physics.georgetown.edu/matlab/, 2005.

[27]   A. A. Alnaas, C. L. Moon, M. Alton, S. M. Reed, and M. K. Knowles, "Conformational Changes in C-Reactive Protein Affect Binding to Curved Membranes in a Lipid Bilayer Model of the Apoptotic Cell Surface," *J Phys Chem B*, vol. 121, no. 12, pp. 2631–2639, Mar. 2017, doi: 10.1021/acs.jpcb.6b11505.

[28]   A. J. Diaz, F. Albertorio, S. Daniel, and P. S. Cremer, "Double Cushions Preserve Transmembrane Protein Mobility in Supported Bilayer Systems," *Langmuir*, vol. 24, no. 13, pp. 6820–6826, Jul. 2008, doi: 10.1021/la800018d.

[29]   E. Karatekin *et al.*, "A fast, single-vesicle fusion assay mimics physiological SNARE requirements," *Proceedings of the National Academy of Sciences*, vol. 107, no. 8, pp. 3517–3521, Feb. 2010, doi: 10.1073/pnas.0914723107.

[30]   H. Zhao *et al.*, "Membrane-Sculpting BAR Domains Generate Stable Lipid Microdomains," *Cell Rep*, vol. 4, no. 6, pp. 1213–1223, Sep. 2013, doi: 10.1016/j.celrep.2013.08.024.

[31]   C. Angeletti and J. W. Nichols, "Dithionite Quenching Rate Measurement of the Inside−Outside Membrane Bilayer Distribution of 7-Nitrobenz-2-oxa-1,3-diazol-4-yl-Labeled Phospholipids," *Biochemistry*, vol. 37, no. 43, pp. 15114–15119, Oct. 1998, doi: 10.1021/bi9810104.

[32] J. C. McIntyre and R. G. Sleight, "Fluorescence assay for phospholipid membrane asymmetry," *Biochemistry*, vol. 30, no. 51, pp. 11819–11827, Dec. 1991, doi: 10.1021/bi00115a012.

[33] R. Volinsky, L. Cwiklik, P. Jurkiewicz, M. Hof, P. Jungwirth, and P. K. J. Kinnunen, "Oxidized phosphatidylcholines facilitate phospholipid flip-flop in liposomes," *Biophys J*, vol. 101, no. 6, pp. 1376–1384, Sep. 2011, doi: 10.1016/j.bpj.2011.07.051.

[34] A. S. Ladokhin, M. E. Selsted, and S. H. White, "Sizing membrane pores in lipid vesicles by leakage of co-encapsulated markers: pore formation by melittin," *Biophys J*, vol. 72, no. 4, pp. 1762–1766, Apr. 1997, doi: 10.1016/S0006-3495(97)78822-2.

[35] D. Huster, P. Müller, K. Arnold, and A. Herrmann, "Dynamics of Membrane Penetration of the Fluorescent 7-Nitrobenz-2-Oxa-1,3-Diazol-4-yl (NBD) Group Attached to an Acyl Chain of Phosphatidylcholine," *Biophys J*, vol. 80, no. 2, pp. 822–831, Feb. 2001, doi: 10.1016/S0006-3495(01)76061-4.

[36] L. M. S. Loura and J. P. P. Ramalho, "Location and dynamics of acyl chain NBD-labeled phosphatidylcholine (NBD-PC) in DPPC bilayers. A molecular dynamics and time-resolved fluorescence anisotropy study," *Biochimica et Biophysica Acta (BBA) - Biomembranes*, vol. 1768, no. 3, pp. 467–478, Mar. 2007, doi: 10.1016/j.bbamem.2006.10.011.

[37] K. Harlos and H. Eibl, "Hexagonal phases in phospholipids with saturated chains: phosphatidylethanolamines and phosphatidic acids," *Biochemistry*, vol. 20, no. 10, pp. 2888–2892, May 1981, doi: 10.1021/bi00513a027.

[38] A. J. Verkleij, R. de Maagd, J. Leunissen-Bijvelt, and B. de Kruijff, "Divalent cations and chlorpromazine can induce non-bilayer structures in phosphatidic acid-containing model membranes," *Biochimica et Biophysica Acta (BBA) - Biomembranes*, vol. 684, no. 2, pp. 255–262, 1982, doi: 10.1016/0005-2736(82)90014-1.

[39] C. Balch, R. Morris, E. Brooks, and R. G. Sleight, "The use of N-(7-nitrobenz-2-oxa-1,3-diazole-4-yl)-labeled lipids in determining transmembrane lipid distribution," *Chem Phys Lipids*, vol. 70, no. 2, pp. 205–212, Apr. 1994, doi: 10.1016/0009-3084(94)90088-4.

[40] J. K. Mills and D. Needham, "Lysolipid incorporation in dipalmitoylphosphatidylcholine bilayer membranes enhances the ion permeability and drug release rates at the membrane phase transition," *Biochimica et Biophysica Acta (BBA) - Biomembranes*, vol. 1716, no. 2, pp. 77–96, Oct. 2005, doi: 10.1016/j.bbamem.2005.08.007.

[41] S. Mukherjee, T. T. Soe, and F. R. Maxfield, "Endocytic Sorting of Lipid Analogues Differing Solely in the Chemistry of Their Hydrophobic Tails," *Journal of Cell Biology*, vol. 144, no. 6, pp. 1271–1284, Mar. 1999, doi: 10.1083/jcb.144.6.1271.

[42] P. R. Cullis and B. de Kruijff, "Lipid polymorphism and the functional roles of lipids in biological membranes," *Biochimica et Biophysica Acta (BBA) - Reviews on Biomembranes*, vol. 559, no. 4, pp. 399–420, Dec. 1979, doi: 10.1016/0304-4157(79)90012-1.

Chapter Five: Conclusions and Future Directions

5.1: Conclusions

PLD1 has an essential role in multiple membrane fusion processes. In this work we temporally resolved the localization of PLD1 and its product, PA during two types of exocytosis. PLD1 produces PA at sites of VAMP2 exocytosis, but also slowly during docking. Both of these aspects are PLD1-dependent, as inhibition of PLD1 specifically reduces PA production during both phases. PLD1 is also responsible for production of PA during docking at sites of MVEs. Interestingly, however, PLD1 is not responsible for the localization of PA to sites of MVE *fusion*, as PLD inhibition does not appear to alter PASS recruitment to sites of fusion. Therefore, there must be an alternate pathway for production or recruitment of PA during exosome secretion. Mobility of secretory vesicles was also affected by PLD1. However, PLD1 has no role in mobility of MVEs, but does affect the fate of late endosomes. Together, PLD1 is a necessary component of intracellular mobility of vesicles, late endosome fate, and for exocytosis.

We also showed that tubulated supported lipid bilayers can be used as a method to probe curvature preference of lipids. PA stabilizes the formation of tubules in these bilayers, indicating a preference for curvature. It also localizes to the inner, negatively curved leaflet of liposomes. Therefore, PA stabilizes negative curvature. In conjunction with the results from the PLD studies, production of PA by PLD1 appears to be necessary

due to its inherent alteration of lipid geometry and stabilization of negative curvature during the exocytic process.

5.2: Phospholipase D2

We have indirectly probed PLD2 activity during these events by inhibiting PLD1 specifically and then PLD1 and PLD2, but a more thorough study of this enzyme in the MVE pathway should be explored. While PLD1 has been known to be involved in exosome *secretion* [2], [35], [36]. PLD2 is involved in MVE budding and exosome production [2], [45], [46]. While PLD1 is present on exosomes, PLD2 is present to a higher extent, particularly when cells are treated with ionomycin [46], [47]. Signaling pathways and activation of PLD1 and PLD2 differ, and this could also be explored. Both are activated by protein kinases C, particularly protein kinase C α, but PLD1 specifically is activated by RhoA, Rac1, Cdc42Hs, Arf1 and probably Arf6 [48]. Arf-based activation of PLD2 has been suggested, particularly Arf1 [49], but other results conflict with this finding [50], [51]. Investigating activation pathways of PLD may also be interesting to explore.

5.3: Diacylglycerol Kinase

Diacylglycerol Kinases (DGK) are another class of lipid-modifying enzymes that produce PA, using diacylglycerol instead of PC [52]–[55]. Both DGKα [56] and DGKζ [57] localize to endosomes, with DGKα specifically localizing to MVEs [58]. DGKs, particularly DGKα, have been implicated in exosome secretion in T lymphocytes [58]–[62]. Not unlike PLD1, there is limited temporal data regarding DGKα in the MVE

pathway. Future experiments exploring localization of DGKα to MVEs, DGKα-production of PA in this pathway with DGKα inhibition with or without PLD inhibition, and PASS localization during these inhibition experiments similar to Chapter 3 would be an interesting path to explore. Ritanserin, R59022 and R59949 are inhibitors of DGKα that could be used [63].

5.4: Alternate PA Labeling Methods

In this work, the PA binding protein, PASS, was used to identify PA localization to sites of fusion. While we were able to show a difference in PA localization with an average of many events, it is difficult to observe on single secretory vesicle or MVEs at any stage due to a high signal-to-noise ratio. Therefore, it would be interesting to explore other options to identify PA presence. One such method is the IMPACT method described by the Baskin lab [64], [65], which takes advantage of the promiscuity of PLD to use primary alcohols instead of water and produce a fluorescent marker at sites of PLD activity specifically. A light-activated PLD has also been produced, which could be activated near specific organelles to observe PLD activity specifically at MVEs [65], [66]. A photoswitchable PA analog has additionally been developed, which can be switched via light to act like saturated or unsaturated PA, specifically, which can affect its role [65], [67], although there appears to be no dependence on saturation for syntaxin clusters when it comes to lipids in general, which may translate to PA [68]. Alternatively, while these techniques would lack temporal resolution, DGK-derived PA on small EVs could be radiolabeled in cells treated with ^{32}P [69], while PLD-derived PA can be measured by

production of phosphatidylbutanol in cells treated with 1-butanol and then measured with

thin-layer chromatography [70], [71].

General References

[1]   Y. R. Yang, H.-J. Jang, S. H. Ryu, and P.-G. Suh, "Phospholipases in Health and Disease," in *Phospholipases in Health and Disease*, New York, NY: Springer New York, 2014, pp. 3–38. doi: 10.1007/978-1-4939-0464-8_1.

[2]   A. Wolf, E. Tanguy, Q. Wang, S. Gasman, and N. Vitale, "Phospholipase D and cancer metastasis: A focus on exosomes," *Adv Biol Regul*, vol. 87, p. 100924, Jan. 2023, doi: 10.1016/J.JBIOR.2022.100924.

[3]   Y. Chen, Y. Zheng, and D. A. Foster, "Phospholipase D confers rapamycin resistance in human breast cancer cells," *Oncogene*, vol. 22, no. 25, pp. 3937–3942, Jun. 2003, doi: 10.1038/sj.onc.1206565.

[4]   J. H. Cho *et al.*, "Overexpression of phospholipase D suppresses taxotere-induced cell death in stomach cancer cells," *Biochimica et Biophysica Acta (BBA) - Molecular Cell Research*, vol. 1783, no. 5, pp. 912–923, May 2008, doi: 10.1016/j.bbamcr.2007.11.019.

[5]   Y. Wang *et al.*, "Blockade of PLD1 potentiates the antitumor effects of bortezomib in multiple myeloma cells by inhibiting the mTOR/NF-κB signal pathway," *Hematology*, vol. 25, no. 1, pp. 424–432, Jan. 2020, doi: 10.1080/16078454.2020.1845501.

[6]   D. W. Kang *et al.*, "Triptolide-induced suppression of phospholipase D expression inhibits proliferation of MDA-MB-231 breast cancer cells," *Exp Mol Med*, vol. 41, no. 9, p. 678, 2009, doi: 10.3858/emm.2009.41.9.074.

[7]   Y.-C. Chang *et al.*, "Aldolase A and Phospholipase D1 Synergistically Resist Alkylating Agents and Radiation in Lung Cancer," *Front Oncol*, vol. 11, Jan. 2022, doi: 10.3389/fonc.2021.811635.

[8]   A. R. Noble, N. J. Maitland, D. M. Berney, and M. G. Rumsby, "Phospholipase D inhibitors reduce human prostate cancer cell proliferation and colony formation," *Br J Cancer*, vol. 118, no. 2, pp. 189–199, Jan. 2018, doi: 10.1038/bjc.2017.391.

[9]   Q. Chen *et al.*, "Key Roles for the Lipid Signaling Enzyme Phospholipase D1 in the Tumor Microenvironment During Tumor Angiogenesis and Metastasis," *Sci Signal*, vol. 5, no. 249, Nov. 2012, doi: 10.1126/scisignal.2003257.

[10]   Q. Zhang *et al.*, "PLD1-dependent PKCγ activation downstream to Src is essential for the development of pathologic retinal neovascularization," *Blood*, vol. 116, no. 8, pp. 1377–1385, Aug. 2010, doi: 10.1182/blood-2010-02-271478.

[11]   Y. Zhang and M. A. Frohman, "Cellular and Physiological Roles for Phospholipase D1 in Cancer," *Journal of Biological Chemistry*, vol. 289, no. 33, pp. 22567–22574, Aug. 2014, doi: 10.1074/jbc.R114.576876.

[12]   G. M. Jenkins and M. A. Frohman, "Phospholipase D: a lipid centric review," *Cell Mol Life Sci*, vol. 62, no. 19–20, pp. 2305–2316, Oct. 2005, doi: 10.1007/s00018-005-5195-z.

[13]   X. Peng and M. A. Frohman, "Mammalian phospholipase D physiological and pathological roles," *Acta Physiologica*, vol. 204, no. 2, pp. 219–226, Feb. 2012, doi: 10.1111/j.1748-1716.2011.02298.x.

[14]   M.-F. Bader and N. Vitale, "Phospholipase D in calcium-regulated exocytosis: Lessons from chromaffin cells," *Biochimica et Biophysica Acta (BBA) - Molecular and Cell Biology of Lipids*, vol. 1791, no. 9, pp. 936–941, Sep. 2009, doi: 10.1016/j.bbalip.2009.02.016.

[15]   M. Zeniou-Meyer *et al.*, "Phospholipase D1 Production of Phosphatidic Acid at the Plasma Membrane Promotes Exocytosis of Large Dense-core Granules at a Late Stage," *Journal of Biological Chemistry*, vol. 282, no. 30, pp. 21746–21757, 2007, doi: 10.1074/jbc.M702968200.

[16]   C. Riebeling, A. J. Morris, and D. Shields, "Phospholipase D in the Golgi apparatus," *Biochimica et Biophysica Acta (BBA) - Molecular and Cell Biology of Lipids*, vol. 1791, no. 9, pp. 876–880, Sep. 2009, doi: 10.1016/J.BBALIP.2009.04.003.

[17]   R. Phillips, J. Kondev, J. Theriot, H. G. Garcia, and N. Orme, *Physical Biology of the Cell*. Garland Science, 2012. doi: 10.1201/9781134111589.

[18]   Y. Humeau *et al.*, "A role for phospholipase D1 in neurotransmitter release," *Proceedings of the National Academy of Sciences*, vol. 98, no. 26, p. 15300, Dec. 2001, doi: 10.1073/pnas.261358698.

[19]   S. Cockcroft, G. Way, N. O'Luanaigh, R. Pardo, E. Sarri, and A. Fensome, "Signalling role for ARF and phospholipase D in mast cell exocytosis stimulated by crosslinking of the high affinity FcεR1 receptor," *Mol Immunol*, vol. 38, no. 16–18, pp. 1277–1282, Sep. 2002, doi: 10.1016/S0161-5890(02)00075-5.

[20]   W. E. Hughes, Z. Elgundi, P. Huang, M. A. Frohman, and T. J. Biden, "Phospholipase D1 Regulates Secretagogue-stimulated Insulin Release in Pancreatic β-Cells," *Journal of Biological Chemistry*, vol. 279, no. 26, pp. 27534–27541, 2004, doi: 10.1074/jbc.M403012200.

[21] N. Vitale *et al.*, "Phospholipase D1: a key factor for the exocytotic machinery in neuroendocrine cells," *EMBO J*, vol. 20, no. 10, pp. 2424–2434, May 2001, doi: 10.1093/emboj/20.10.2424.

[22] A. D. Lam, P. Tryoen-Toth, B. Tsai, N. Vitale, and E. L. Stuenkel, "SNARE-catalyzed fusion events are regulated by Syntaxin1A-lipid interactions," *Mol Biol Cell*, vol. 19, no. 2, pp. 485–497, Feb. 2008, doi: 10.1091/mbc.e07-02-0148.

[23] R. Mendonsa and J. Engebrecht, "Phosphatidylinositol-4,5-Bisphosphate and Phospholipase D-Generated Phosphatidic Acid Specify SNARE-Mediated Vesicle Fusion for Prospore Membrane Formation," *Eukaryot Cell*, vol. 8, no. 8, pp. 1094–1105, Aug. 2009, doi: 10.1128/EC.00076-09.

[24] V. Hyenne *et al.*, "Studying the Fate of Tumor Extracellular Vesicles at High Spatiotemporal Resolution Using the Zebrafish Embryo," *Dev Cell*, vol. 48, no. 4, pp. 554-572.e7, Feb. 2019, doi: 10.1016/j.devcel.2019.01.014.

[25] T. B. Steinbichler, J. Dudás, H. Riechelmann, and I.-I. Skvortsova, "The role of exosomes in cancer metastasis," *Semin Cancer Biol*, vol. 44, pp. 170–181, Jun. 2017, doi: 10.1016/j.semcancer.2017.02.006.

[26] C. Kahlert and R. Kalluri, "Exosomes in tumor microenvironment influence cancer progression and metastasis," *J Mol Med*, vol. 91, no. 4, pp. 431–437, Apr. 2013, doi: 10.1007/s00109-013-1020-6.

[27] W. Feng, D. C. Dean, F. J. Hornicek, H. Shi, and Z. Duan, "Exosomes promote pre-metastatic niche formation in ovarian cancer," *Mol Cancer*, vol. 18, no. 1, p. 124, Dec. 2019, doi: 10.1186/s12943-019-1049-4.

[28] F. D. Brown *et al.*, "Phospholipase D1 localises to secretory granules and lysosomes and is plasma-membrane translocated on cellular stimulation," *Current Biology*, vol. 8, no. 14, pp. 835–838, Jul. 1998, doi: 10.1016/S0960-9822(98)70326-4.

[29] Z. Freyberg, D. Sweeney, A. Siddhanta, S. Bourgoin, M. Frohman, and D. Shields, "Intracellular Localization of Phospholipase D1 in Mammalian Cells," *Mol Biol Cell*, vol. 12, no. 4, pp. 943–955, Apr. 2001, doi: 10.1091/mbc.12.4.943.

[30] G. Du *et al.*, "Regulation of phospholipase D1 subcellular cycling through coordination of multiple membrane association motifs," *Journal of Cell Biology*, vol. 162, no. 2, pp. 305–315, Jul. 2003, doi: 10.1083/jcb.200302033.

[31] K. Toda, M. Nogami, K. Murakami, Y. Kanaho, and K. Nakayama, "Colocalization of phospholipase D1 and GTP-binding-defective mutant of ADP-ribosylation factor 6 to endosomes and lysosomes," *FEBS Lett*, vol. 442, no. 2–3, pp. 221–225, Jan. 1999, doi: 10.1016/S0014-5793(98)01646-9.

[32]   Y. H. Jang and D. S. Min, "The hydrophobic amino acids involved in the
        interdomain association of phospholipase D1 regulate the shuttling of
        phospholipase D1 from vesicular organelles into the nucleus," *Exp Mol Med*, vol.
        44, no. 10, p. 571, 2012, doi: 10.3858/emm.2012.44.10.065.

[33]   L. S. Arneson, J. Kunz, R. A. Anderson, and L. M. Traub, "Coupled Inositide
        Phosphorylation and Phospholipase D Activation Initiates Clathrin-coat Assembly
        on Lysosomes," *Journal of Biological Chemistry*, vol. 274, no. 25, pp. 17794–
        17805, Jun. 1999, doi: 10.1074/jbc.274.25.17794.

[34]   V. Muralidharan-Chari *et al.*, "ARF6-Regulated Shedding of Tumor Cell-Derived
        Plasma Membrane Microvesicles," *Current Biology*, vol. 19, no. 22, pp. 1875–
        1885, Dec. 2009, doi: 10.1016/j.cub.2009.09.059.

[35]   S. Ghoroghi *et al.*, "Ral GTPases promote breast cancer metastasis by controlling
        biogenesis and organ targeting of exosomes," *Elife*, vol. 10, Jan. 2021, doi:
        10.7554/eLife.61539.

[36]   H. Onallah, S. T. Mannully, B. Davidson, and R. Reich, "Exosome Secretion and
        Epithelial-Mesenchymal Transition in Ovarian Cancer Are Regulated by
        Phospholipase D," *Int J Mol Sci*, vol. 23, no. 21, p. 13286, Oct. 2022, doi:
        10.3390/ijms232113286.

[37]   H. T. McMahon and J. L. Gallop, "Membrane curvature and mechanisms of
        dynamic cell membrane remodelling," *Nature*, vol. 438, no. 7068, pp. 590–596,
        Dec. 2005, doi: 10.1038/nature04396.

[38]   P. P. Cheney, A. W. Weisgerber, A. M. Feuerbach, and M. K. Knowles, "Single
        Lipid Molecule Dynamics on Supported Lipid Bilayers with Membrane
        Curvature," *Membranes (Basel)*, vol. 7, no. 1, p. 15, 2017, doi:
        10.3390/membranes7010015.

[39]   E. E. Kooijman, V. Chupin, B. de Kruijff, and K. N. J. Burger, "Modulation of
        Membrane Curvature by Phosphatidic Acid and Lysophosphatidic Acid," *Traffic*,
        vol. 4, no. 3, pp. 162–174, Mar. 2003, doi: 10.1034/j.1600-0854.2003.00086.x.

[40]   N. S. Hatzakis *et al.*, "How curved membranes recruit amphipathic helices and
        protein anchoring motifs," *Nat Chem Biol*, vol. 5, no. 11, pp. 835–841, 2009, doi:
        10.1038/nchembio.213.

[41]   E. Atilgan and S. X. Sun, "Shape transitions in lipid membranes and protein
        mediated vesicle fusion and fission," *J Chem Phys*, vol. 126, no. 9, p. 095102,
        Mar. 2007, doi: 10.1063/1.2483862.

[42]   O. Carmon *et al.*, "Chromogranin A preferential interaction with Golgi
        phosphatidic acid induces membrane deformation and contributes to secretory

granule biogenesis," *The FASEB Journal*, vol. 34, no. 5, pp. 6769–6790, May 2020, doi: 10.1096/fj.202000074R.

[43]   E. E. Kooijman *et al.*, "Spontaneous Curvature of Phosphatidic Acid and Lysophosphatidic Acid," *Biochemistry*, vol. 44, no. 6, pp. 2097–2102, Feb. 2005, doi: 10.1021/bi0478502.

[44]   B. Nuscher *et al.*, "α-Synuclein Has a High Affinity for Packing Defects in a Bilayer Membrane," *Journal of Biological Chemistry*, vol. 279, no. 21, pp. 21966–21975, May 2004, doi: 10.1074/jbc.M401076200.

[45]   R. Ghossoub *et al.*, "Syntenin-ALIX exosome biogenesis and budding into multivesicular bodies are controlled by ARF6 and PLD2," *Nat Commun*, vol. 5, no. 1, p. 3477, Mar. 2014, doi: 10.1038/ncomms4477.

[46]   K. Laulagnier *et al.*, "PLD2 is enriched on exosomes and its activity is correlated to the release of exosomes," *FEBS Lett*, vol. 572, no. 1–3, pp. 11–14, Aug. 2004, doi: 10.1016/j.febslet.2004.06.082.

[47]   C. Subra *et al.*, "Exosomes account for vesicle-mediated transcellular transport of activatable phospholipases and prostaglandins," *J Lipid Res*, vol. 51, no. 8, pp. 2105–2120, Aug. 2010, doi: 10.1194/jlr.M003657.

[48]   J. H. Exton, "Regulation of phospholipase D," *FEBS Lett*, vol. 531, no. 1, pp. 58–61, Oct. 2002, doi: 10.1016/S0014-5793(02)03405-1.

[49]   T. Koch, L.-O. Brandenburg, S. Schulz, Y. Liang, J. Klein, and V. Höllt, "ADP-ribosylation Factor-dependent Phospholipase D2 Activation Is Required for Agonist-induced μ-Opioid Receptor Endocytosis," *Journal of Biological Chemistry*, vol. 278, no. 11, pp. 9979–9985, Mar. 2003, doi: 10.1074/jbc.M206709200.

[50]   W. C. Colley *et al.*, "Phospholipase D2, a distinct phospholipase D isoform with novel regulatory properties that provokes cytoskeletal reorganization," *Current Biology*, vol. 7, no. 3, pp. 191–201, Mar. 1997, doi: 10.1016/S0960-9822(97)70090-3.

[51]   T.-C. Sung, Y. M. Altshuller, A. J. Morris, and M. A. Frohman, "Molecular Analysis of Mammalian Phospholipase D2," *Journal of Biological Chemistry*, vol. 274, no. 1, pp. 494–502, Jan. 1999, doi: 10.1074/jbc.274.1.494.

[52]   K. Goto, Y. Hozumi, and H. Kondo, "Diacylglycerol, phosphatidic acid, and the converting enzyme, diacylglycerol kinase, in the nucleus," *Biochimica et Biophysica Acta (BBA) - Molecular and Cell Biology of Lipids*, vol. 1761, no. 5–6, pp. 535–541, May 2006, doi: 10.1016/j.bbalip.2006.04.001.

[53] I. Mérida, A. Ávila-Flores, and E. Merino, "Diacylglycerol kinases: at the hub of cell signalling," *Biochemical Journal*, vol. 409, no. 1, pp. 1–18, Jan. 2008, doi: 10.1042/BJ20071040.

[54] F. Sakane, S. Imai, M. Kai, S. Yasuda, and H. Kanoh, "Diacylglycerol kinases: Why so many of them?," *Biochimica et Biophysica Acta (BBA) - Molecular and Cell Biology of Lipids*, vol. 1771, no. 7, pp. 793–806, Jul. 2007, doi: 10.1016/j.bbalip.2007.04.006.

[55] F. Sakane, S. Mizuno, D. Takahashi, and H. Sakai, "Where do substrates of diacylglycerol kinases come from? Diacylglycerol kinases utilize diacylglycerol species supplied from phosphatidylinositol turnover-independent pathways," *Adv Biol Regul*, vol. 67, pp. 101–108, Jan. 2018, doi: 10.1016/j.jbior.2017.09.003.

[56] S. Xie, N. Naslavsky, and S. Caplan, "Diacylglycerol Kinase α Regulates Tubular Recycling Endosome Biogenesis and Major Histocompatibility Complex Class I Recycling," *Journal of Biological Chemistry*, vol. 289, no. 46, pp. 31914–31926, Nov. 2014, doi: 10.1074/jbc.M114.594291.

[57] E. Rincón *et al.*, "Proteomics Identification of Sorting Nexin 27 as a Diacylglycerol Kinase ζ-associated Protein," *Molecular & Cellular Proteomics*, vol. 6, no. 6, pp. 1073–1087, Jun. 2007, doi: 10.1074/mcp.M700047-MCP200.

[58] R. Alonso, C. Mazzeo, I. Mérida, and M. Izquierdo, "A new role of diacylglycerol kinase α on the secretion of lethal exosomes bearing Fas ligand during activation-induced cell death of T lymphocytes," *Biochimie*, vol. 89, no. 2, pp. 213–221, Feb. 2007, doi: 10.1016/j.biochi.2006.07.018.

[59] R. Alonso *et al.*, "Diacylglycerol kinase α regulates the formation and polarisation of mature multivesicular bodies involved in the secretion of Fas ligand-containing exosomes in T lymphocytes," *Cell Death Differ*, vol. 18, no. 7, pp. 1161–1173, Jul. 2011, doi: 10.1038/cdd.2010.184.

[60] G. Bossi and G. M. Griffiths, "Degranulation plays an essential part in regulating cell surface expression of Fas ligand in T cells and natural killer cells," *Nat Med*, vol. 5, no. 1, pp. 90–96, Jan. 1999, doi: 10.1038/4779.

[61] M. Izquierdo, M. C. Ruiz-Ruiz, and A. López-Rivas, "Stimulation of phosphatidylinositol turnover is a key event for Fas-dependent, activation-induced apoptosis in human T lymphocytes.," *Journal of Immunology*, vol. 157, no. 1, pp. 21–28, Jul. 1996, doi: 10.4049/jimmunol.157.1.21.

[62] E. J. Quann, E. Merino, T. Furuta, and M. Huse, "Localized diacylglycerol drives the polarization of the microtubule-organizing center in T cells," *Nat Immunol*, vol. 10, no. 6, pp. 627–635, Jun. 2009, doi: 10.1038/ni.1734.

[63] L. Fu *et al.*, "DGKA Mediates Resistance to PD-1 Blockade," *Cancer Immunol Res*, vol. 9, no. 4, pp. 371–385, Apr. 2021, doi: 10.1158/2326-6066.CIR-20-0216.

[64] T. W. Bumpus and J. M. Baskin, "Clickable Substrate Mimics Enable Imaging of Phospholipase D Activity," *ACS Cent Sci*, vol. 3, no. 10, pp. 1070–1077, Oct. 2017, doi: 10.1021/acscentsci.7b00222.

[65] R. Tei and J. M. Baskin, "Click chemistry and optogenetic approaches to visualize and manipulate phosphatidic acid signaling," *Journal of Biological Chemistry*, vol. 298, no. 4, p. 101810, Apr. 2022, doi: 10.1016/j.jbc.2022.101810.

[66] R. Tei and J. M. Baskin, "Spatiotemporal control of phosphatidic acid signaling with optogenetic, engineered phospholipase Ds," *Journal of Cell Biology*, vol. 219, no. 3, Mar. 2020, doi: 10.1083/jcb.201907013.

[67] R. Tei, J. Morstein, A. Shemet, D. Trauner, and J. M. Baskin, "Optical Control of Phosphatidic Acid Signaling," *ACS Cent Sci*, vol. 7, no. 7, pp. 1205–1215, Jul. 2021, doi: 10.1021/acscentsci.1c00444.

[68] D. H. Murray and L. K. Tamm, "Clustering of Syntaxin-1A in Model Membranes Is Modulated by Phosphatidylinositol 4,5-Bisphosphate and Cholesterol," *Biochemistry*, vol. 48, no. 21, pp. 4617–4625, Jun. 2009, doi: 10.1021/bi9003217.

[69] M. L. MacDonald, K. F. Mack, C. N. Richardson, and J. A. Glomset, "Regulation of diacylglycerol kinase reaction in Swiss 3T3 cells. Increased phosphorylation of endogenous diacylglycerol and decreased phosphorylation of didecanoylglycerol in response to platelet-derived growth factor.," *J Biol Chem*, vol. 263, no. 3, pp. 1575–83, Jan. 1988.

[70] T. Munnik and A. M. Laxalt, "Measuring PLD Activity In Vivo," 2013, pp. 219–231. doi: 10.1007/978-1-62703-401-2_20.

[71] H. A. Brown, L. G. Henage, A. M. Preininger, Y. Xiang, and J. H. Exton, "Biochemical Analysis of Phospholipase D," 2007, pp. 49–87. doi: 10.1016/S0076-6879(07)34004-4.